OSTEOCONDUCTION OF CALCIUM PHOSPHATE THIN FILM ON POROUS-SURFACED IMPLANTS IN RABBIT TIBIAE

by

Hung Quoc Nguyen

A thesis submitted in conformity with the requirements
for the degree of Master of Science
Graduate Department of Faculty of Dentistry
University of Toronto

National Library of Canada
Acquisitions and Bibliographic Services
395 Wellington Street
Ottawa ON K1A 0N4
Canada

Bibliothèque nationale du Canada
Acquisitions et services bibliographiques
395, rue Wellington
Ottawa ON K1A 0N4
Canada

Your file Votre référence

Our file Notre référence

0-612-34047-3

Canada

ACKNOWLEDGEMENTS

The completion of this Master of Science thesis was not possible without the academic, technical and emotional support of a number of individuals. I would like to thank my supervisors, Dr. DA Deporter and Dr. RM Pilliar, for their support, guidance, insightful comments and suggestions as well as their ability to bring a different and practical perspective to my project. A very special indebtedness to Dr. DA Deporter for the many hours spent revising this manuscript. I am additionally grateful to Dr. MJ Filiaggi for his explanation of the sol-gel process.

For their invaluable technical and academic support, I wish to further acknowledge the contributions of the following: Mr. Dave Abdulla for preparing the porous-surfaced implants; Mrs. Raisa Yakubovich for the application of the sol-gel Ca-P coating onto the porous-surfaced implants; Mrs. Nancy Valiquette for preparation of the histological specimens; Mr. Robert Chernecky for his assistance on the SEM, for the wonderful freeze-fractured SEM photomicrographs and the many hours in the darkroom; Ms. Dianna Lindsay for caring of the animals; Dr. Wayne Maillet and Mrs. Thuy Nguyen for their valuable help with instrument sterilization and clinical assistance during implant surgery procedures; Miss Kinh Tung Nguyen for the many late evenings spent at the digital image analyzer; Mrs. Rita Bauer and Mr. Steve Bruany for photography assistance. A special thank to Professor A. Csima for her expertise and assistance in the statistical ananysis utilized in the preparation of this thesis.

The loaning or use of equipment was also an integral part of the completion of this project. I would like to extend my gratitude to Mr. Robert Chernecky for literally

giving me full access to the SEM room and the darkroom; and to Dr. JE Davies for providing unlimited access to the Bioquant image analyzer.

I am additionally grateful to Dr. Shimon Friedman and Dr. Calvin Torneck of the Endodontic department for allowing the opportunity to pursue a research interest outside of the Endodontic department.

To my wife, Thuy, who literally became a single mother of three young children and still superbly managed the additional burden of keeping law and order. Thuy had supported me throughout the entire process and understood why I needed to pursue such professional and academic goal.

And to my young children, Charles, Michelle and Emily, who will always be my greatest treasured accomplishment, I would like to thank them for the love and support they have given me in the last several years and for knowing when to stay out of my way! For this, I dedicate this thesis to my three children.

TABLE OF CONTENT

List of Figures **Page**

Page

List of Tables: **Page**

ABSTRACT

The purpose of this study was to compare the healing responses, after two weeks of implantation, between porous-surfaced Ti-6Al-4V implants as controls and the same implant design with a submicron (0.3-0.5 μm) layer of calcium phosphate (Ca-P) applied to the implant surface using the sol-gel technique. Seventeen rabbits were used in three experiments. In Experiment I ,the proximal end of the right tibia in 10 rabbits received two transcortical implants, one Ca-P-coated and one control. In Experiment II, one of each implant type was placed into either the right or left tibia of 6 rabbits. Only 1 rabbit was used in Experiment III where one Ca-P-coated implant was installed in each of the left and right tibiae. Backscattered scanning electron microscopy and a Bioquant Image Analysis computer software package were used to analyze absolute bone contact length (ACL), contact length fraction (CLF), straight line endosteal bone growth (SLBG), absolute bone ingrowth area (ABIA), and bone ingrowth fraction (BIF). The results were submitted to Repeated Measures ANOVA. In Experiment I, ACL, CLF, & ABIA for Ca-P-coated implants were significantly greater than for control implants ($p<0.05$); however, SLBG & BIF differences were not significantly different ($p>0.05$). In Experiment II, ACL, CLF & SLBG for the Ca-P-coated group were significantly greater than for the control group and there were no significant differences in the ABIA & BIF values. When both group I & II were combined, the results were similar to that of group II. Freeze-fractured SEM investigation of the specimens in Experiment III (35X to 20,000X) revealed woven bone closely adapted to the neck regions between interconnecting spherical particles of the sintered porous surface zone for the Ca-P-coated implant with the "cement layer" clearly visible. The sol-gel Ca-P layer was often about 1 μm thick on

the implant surface and thicker in the neck regions (in excess of 1.5 μm). This Ca-P layer, being thicker than the intended 0.3 μm, often resulted in surface cracking and delamination in the neck regions. When the extent of bone ingrowth into the neck regions of both implant types in Experiments I & II were investigated, the Ca-P-coated implants exhibited significantly ($p < 0.0001$) greater bone ingrowth into these neck regions than the control implants suggesting a superior three-dimensional bone / implant interlock. The slight differences between group I & II suggest the need for further investigation including a thorough characterization of the sol-gel coating. Nevertheless, the results indicate that an ultrathin layer of Ca-P may be capable of promoting osteoconduction and the sol-gel technique of Ca-P application is suitable for porous-surfaced implant without occluding the pores.

I) INTRODUCTION

Bone-interfacing implants made from titanium alloy (Ti-6Al-4V) or other metals, and having a porous surface geometry comprised of a multilayer of spherical particles of the same metal have been used successfully to replace both damaged joint structures and lost tooth roots (Pilliar 1987, 1990 b; Deporter *et al.* 1996). If the particle size range is appropriate (45 to 150 μm) the resulting surface coat is characterized by a 35% volume porosity with "pores", or spaces between adjacent particles, in the size range 50 μm to 200 μm, a condition favouring bone ingrowth (Bobyn *et al.* 1980). As a consequence of this bone ingrowth, the implant becomes securely fixed or "osseointegrated" by means of a 3-dimensional mechanical interlocking of bone within the porous surface zone (Deporter *et al.* 1990; Pilliar *et al.* 1991 a). Another advantage of the surface configuration of this porous surface-structured implant is that it promotes osteoconductivity when compared to implants with an electropolished surface (Dziedzic *et al.* 1994) and therefore, at least in the case of dental implants, favoured shorter initial healing intervals (e.g. 4 months in the maxilla as opposed to the recommended 6 months for threaded implants with a machined surface finish) and successful implant installation in bone of low density as often occurs in the maxilla (i.e. Type III & IV after Lekholm and Zarb, 1985).

Other investigators have reported that bone-interfacing metal implants coated with a calcium phosphate surface layer such as hydroxyapatite also display osteoconductivity (Ducheyne *et al.* 1980; Geesink *et al.* 1987; De Groot *et al.* 1987; Rivero *et al.* 1988; Osborn 1989; Jansen *et al.* 1993), accelerated initial healing (Ducheyne *et al.* 1990 a, b; Manley 1993) and in addition increased resistance to torsional

and pull-out forces once the implant has become osseointegrated (Cook *et al.* 1987, 1992 b; Thomas *et al.* 1987; Rivero *et al.* 1988; Block *et al.* 1990). There are, however, problems with dental implant designs that rely primarily on a calcium phosphate surface layer for implant fixation. These surface coatings are generally applied by the technique of plasma-spraying and result in rather thick surface layers of 30 to 100 μm that are retained essentially by friction to an underlying grit-blasted metal substrate core. They have a tendency to delaminate or separate at the calcium phosphate-metal substrate interface, and this may lead to loss of osseointegration (Filiaggi *et al.* 1991; Whitehead *et al.* 1992; Delecrin *et al.* 1991; De Groot *et al.* 1987, 1990; Pilliar *et al.* 1991 b; Radin & Ducheyne 1992; Klein *et al.* 1989). Another common disadvantage of Ca-P coating (as in plasma-sprayed Ca-P) is the formation of amorphous Ca-P which readily undergoes dissolution and eventually leads to loss of coating thickness with time (Radin & Ducheyne 1992). As well, if the calcium phosphate coating becomes exposed to the oral environment because of crestal bone loss adjacent to a dental implant, it is likely that a bacterial-induced peri-implant infection will develop leading to implant failure. This mechanism of failure, i.e. infection-driven, appears to be related to poor patient homecare and the resultant peri-implant gingivitis (Teixeira *et al.* 1997), and is a late complication resulting in increased implant loss beginning at times ranging from two to five years of clinical function depending on the implant source (Wheeler 1996). Thus, it would appear that while the application of a calcium phosphate surface layer to a bone-interfacing implant may offer advantages in accelerating initial bone healing by promoting osteoconduction, using this layer as the main mechanism of long-term implant retention is not appropriate.

Recently a number of techniques have been developed for the production of very thin (i.e. submicron in thickness) surface layers of calcium phosphate onto metal substrates (see Pilliar and Filiaggi 1993 b for a review). The advantage of this approach is that a calcium phosphate surface coat may be added as a means of accelerating bony healing in relation to some other surface topography intended to act as the primary means of long-term implant retention. One such technique is the use of ultrathin (100 to 500 nm) sol-gel films formed by dipping the metal implant into a colloidal suspension of inorganic particles of the necessary reagents, slowly withdrawing the coated implants vertically in a controlled manner, allowing the coating to dry and then annealing it at 400 to 1000 ° C (Qiu *et al.* 1993). These investigators have found that this technique can be used to apply fairly uniform submicron thin surface layers of calcium phosphate to a porous-surfaced dental implant without obliterating the 3-dimensional porous surface geometry intended for primary and long-term implant fixation. In the present study the intent was to determine whether the addition of this calcium phosphate layer offered any improvement in osteoconductivity and bone ingrowth to that already inherent in the porous surface metal coat itself, the hypothesis being that if this were to be the case, the initial healing interval required for integration of porous-surfaced implants might be further shortened.

II) LITERATURE REVIEW

The replacement of missing teeth with root-form endosseous dental implants has become a well accepted treatment modality in the rehabilitation of both partial and complete edentulism. The term "osseointegration" was coined to describe the biological process whereby during wound healing following installation of a dental implant, bone tissue becomes intimately apposed to an implant surface thereby securing the implant to surrounding jawbone (Branemark *et al.* 1977). There are numerous dental implant designs currently available commercially, the majority being either threaded screws or "press-fit" , parallel-sided cylinders. The original threaded endosseous design was devised by Branemark and co-workers (Branemark *et al.* 1969, 1977, 1985) and had a machined surface finish which allowed for some micromechanical bone-to-implant interlock due to the presence of machining lines. Others have since modified this design concept by altering the surface finish either by means of plasma-spraying with Ti, Ti alloy as in the ITI ™ system (Schroeder *et al.* 1981, 1991) or with hydroxyapatite (de Groot *et al.* 1987; Thomas *et al.* 1987; Block *et al.* 1987, 1989), or more recently by etching the machined surface with HCl / H_2SO_4 acid (Cochran *et al.* 1996, 3I ™). All of these modifications are intended to increase surface roughness and area at the bone-to-implant interface thus hopefully producing a more secure osseointegration through mechanical interlock of the apposing bone to the metal substrate and resisting vertical shear forces. Cylindrical press-fit designs again rely on a plasma-sprayed metal or hydroxyapatite surface to achieve fixation to bone (Babbush *et al.* 1986; Buser *et al.* 1990, 1991 a, b).

All of these designs have some clinical disadvantages. For example, the original Branemark design (with a machined surface finish) relies primarily on friction for osseointegration or what has been called "two-dimensional mechanical bone-implant adhesion" , along the plane of the threads (Pilliar 1990 a), because it lacked surface undercuts to resist torsional (unscrewing) forces (Carr *et al.* 1995, 1997). Therefore, machined threaded implant designs must be used in fairly long implant lengths and must be initially secured by means of bicortical stabilization, i.e. the implant must engage cortical bone both crestally and apically (Adell *et al.* 1990). It has been recommended that this implant device should be used in lengths of at least 10 mm in the mandible and 13 mm in the maxilla in order to promote successful integration and continued implant health (van Steenberghe *et al.* 1990). Branemark implants range in length from 7 to 20 mm , and as such are the longest root-form endosseous implants currently in use. This means that many edentulous sites which may have benefited from the placement of implants have insufficient bone height to receive this implant system without first being subjected to various procedures such as Guided Bone Regeneration (Buser *et al.* 1994), sinus elevation procedures (Boyne & James 1980; Wood & Moore 1988; Kent & Block 1989), or in the case of the posterior mandible, nerve repositioning (Jensen & Nock 1987; Friberg *et al.* 1992). Altering the design by plasma-spraying with Ti , such as has been done with the ITI Bone-fit implant (Schroeder *et al.* 1981, 1991) allows for somewhat shorter (8 to 18 mm) threaded implants to be used, but again it is generally recommended that where possible implant lengths of at least 10 mm be used.

With cylindrical press-fit designs, implant lengths are normally in the range of 8 to 16 mm thus presenting basically the same clinical limitation as threaded designs. However, these designs also appear to have a less favourable long-term prognosis,

because of continued significant crestal bone loss and subsequent contamination of the plasma-sprayed metal or hydroxyapatite surface with bacterial plaque leading to implant failure (Quirynen *et al.* 1992; Spiekermann *et al.* 1995; Block *et al.* 1996; Haas *et al.* 1996; Wheeler, 1996).

Since 1983 work has been conducted at the University of Toronto on the design and testing of a new and unique dental implant system now called the Endopore™ implant system. The Endopore™ implant system incorporates a tapered implant shape (to simulate a tooth root) machined from Ti alloy (Ti-6Al-4V) and subsequently coated with a porous surface zone over the intended bone-interfacing surface (Pilliar 1990 b) . The idea for using a porous-surfaced dental implant came from earlier work in orthopedics. For example, a so-called porous-surfaced Co-Cr-Mo implant device was developed in 1969 as a cementless orthopaedic hip prosthesis (Pilliar *et al.* 1975) to overcome the unfavourable biological and mechanical properties of bone cements commonly used at the time to secure such joint prostheses. Fabrication of a porous-surfaced bone-interfacing implant device is achieved by sintering (at 1,250 °C and in a high vacuum) spherical particles of metal (Ti alloy in the case of the Endopore™ implant) of a known size range (diameter 45 to 150 μm) onto a solid implant core . This produces a pore size (i.e. spaces between adjacent particles) in the range 50 to 200 μm which is known to allow bone ingrowth (Bobyn *et al.* 1980; Pilliar 1987). The pores themselves occupy about 35 % to 40 % by volume of the total porous surface region (Pilliar 1991 a). For the Endopore™ dental implant design, three layers of Ti-6Al-4V particles of this size range (overall thickness of the coat being about 0.3 mm) can be sintered onto the implant core while still maintaining overall implant dimensions (i.e. diameter) suitable for use in the typical residual alveolar ridge (5 mm or more in

buccolingual width), while still allowing for sufficient bulk in the implant core to facilitate the attachment of the prosthetic components . Larger particle sizes (up to 500 μm, and hence greater porosity) have been successfully used in orthopaedic applications of porous-surfaced implants (Bobyn *et al.* 1980), but these larger particles if used in a multilayer form would not be appropriate for dental implant application given the size limitations.

A porous surface-structured endosseous dental implant device appears to offer a number of clinical advantages (Deporter *et al.* 1996). Thus, because the sintering treatment results in a surface area of at least three times that of a threaded implant with a machined surface , porous surface-structured implants can be used with predictable success in shorter lengths than the conventional threaded implant design (Deporter *et al.* 1990, 1992, 1996). Other possible advantages include faster osseointegration because of the fact that the porous surface topography is osteoconductive (Dziedzic and Davies 1994) and hence shorter initial healing times; greater tolerance to early micromovements than other implant designs (Maniatopoulos *et al.* 1986); and greater resistance to loosening due to functional forces including torquing forces because of the 3-dimensional bone ingrowth (Deporter *et al.* 1986 a, 1988, 1990; Pilliar 1990 a). A further advantage of porous-surfaced implant designs is that once osseointegrated they have been shown to provide high implant-to-bone interface shear strength. Porous-structured implants had the highest resistance to shearing forces followed by plasma sprayed, screw threaded designs with textured and machined surface finish while cylindrical "press-fit" implant designs with machined surface finish having the lowest shear strength (see Kohn 1992 for a review). The animal and human clinical trial results supporting these claims are reviewed below.

A) Background Information on Porous Surface-Structured Dental Implants

Early studies that provided background information for the development of the Endopore™ dental implant included the work of Maniatopoulos *et al.* (1986) using a dog model to study various designs of endosseous endodontic pin implants (i.e. implants inserted into bone through existing tooth structure via the pulpal canals). The implants studied included smooth-surfaced rods , threaded pins with a smooth (i.e. machined) surface, and sintered porous-surfaced designs. All implants were made functional shortly after placement (i.e. within 3 days the dogs were placed on a hard food diet), the level of movement being limited by the periodontal ligament of the implant-supporting teeth. Following at least three months of implantation / function , the porous-surfaced endodontic pins became rigidly fixed by bone ingrowth , while the smooth and threaded implants progressively loosened with histologic evidence of the development of fibrous encapsulation . This observed difference in sensitivity to early micro-movement suggested that a porous surface-structured dental implant design, formed by sintering metal particles to form the porous surface region, may allow a shorter initial healing / integration period than threaded designs (Maniatopoulos *et al.* 1986; Deporter *et al.* 1990; Pilliar *et al.* 1993 a, 1995).

Following this work by Maniatopoulos *et al.*, a porous-surfaced titanium alloy root-form dental implant design was initially tested using a beagle dog model and a standard two-stage surgical protocol (Deporter *et al.* 1986 a, b, 1988). This implant had a tapered, truncated-cone shape and was self-seating, thereby allowing for a tight initial press-fit. Histomorphometric measurements in a first study in which the implants remained submerged and non-functional revealed that initial healing and bone ingrowth

had reached a plateau by 4 weeks with no significant difference in bone ingrowth observed with implants allowed to heal for 8 weeks (Deporter *et al.* 1986 a). In a second experiment (Deporter *et al.* 1988), implants were placed and allowed to heal for 4 or 8 weeks in either the left or the right side of the mandible respectively. Following the 4 or 8 week healing period, a transgingival collar with a porous surface region over the apical third was introduced at a second stage surgery. The porous surface of this transgingival collar was intended to encourage gingival connective tissue ingrowth and attachment. However, in the majority of implants (22 out of 32), the porous surface region of the transgingival collar provided an excellent milieu for bacterial contamination introduced presumably at or following the second stage surgical procedure leading to complications (Deporter *et al.* 1988). Thus, 22 of 32 of the implants showed signs of failure within eight months of function with progressive peri-implant bone loss associated with large subgingival bacterial plaque deposits. Subsequently, the collar design was changed to eliminate the porous surface zone leaving the whole transgingival collar with a machined surface (Deporter *et al.* 1990, 1992, 1996; Al-Sayyed *et al.* 1994; Levy *et al.* 1996). As well, the implant root component was modified so that the coronal-most 2 mm had a machined surface, while the remainder of the implant root component was coated with titanium alloy particles and sintered to form the porous surface structure. The implant was designated as being partially porous-coated (PPC). These modifications worked extremely well provided that the porous surface region of the implant root segment was initially fully submerged in bone (Deporter *et al.* 1990). Bone loss during subsequent implant function was limited to the machined coronal segment and this was argued to be due to a stress-shielding effect (Pilliar *et al.* 1991 a). Once the alveolar crest approached the machined surface-to-porous surface junction, a state of dynamic equilibrium was

established. This was attributed to effective stress transfer from implant to bone across the bone-ingrown porous surface of the submerged implant root (Vaillancourt 1994). Furthermore, by altering the length of the coronal machined surface zone (and hence the position of the smooth-to-porous surface junction) it was possible to predictably control the extent of crestal bone resorption (Al-Sayyed *et al.* 1994).

In another line of investigation , Pilliar and co-workers (1991 b) studied the effect on crestal bone resorption of coating the transgingival collar of the implant system with a plasma-sprayed hydroxyapatite layer. In this study, the investigators compared crestal bone loss between two implant designs, one with a machined transgingival collar, as previously described, and the other with the collar sand-blasted and then plasma-sprayed with calcium hydroxyapatite (HA). The plasma-sprayed HA coating (20 to 50 μm thick) of the implant collar resulted in significantly greater bone height retention next to the implants as compared with non-HA-coated implants of otherwise similar design. Examination after sacrifice indicated that most of the thickness of the HA was lost through dissolution and resorption by the end of the 18 month functional period. The authors speculated that the osteoconductive effect of the HA coating itself as well as the increased surface roughness resulted in the increased bone height retention. In situations where the HA underwent resorption or dissolution, the underlying sand-blasted surface of the collar beneath the plasma-sprayed coating may have provided sufficient surface roughness to allow enough stress transfer to retain more of the crestal bone adjacent to the implant than was the case with the strictly machined surface.

Deporter *et al.* (1990) compared the modified, partially porous-coated (PPC) titanium alloy implant design with a threaded implant design made from commercially pure (CP) titanium. During an 18 month functional period, the sintered porous-surfaced

implants performed as well as the threaded controls. However, morphometric assessments of bone-to-implant contact revealed a higher bone-to-implant surface contact per unit length of implant with the porous-surfaced design, suggesting that shorter implant lengths could be used with this design. This was later verified in humans (Deporter *et al.* 1992, 1996). This interesting observation is believed to be due to two factors: i) the available surface area of the porous-surfaced dental implant is at least three times that of the surface area of a threaded implant of a similar overall length and with a machined surface finish and ii) the healing response within the 3-dimensional interconnected openings provided by the porous surface region (Pilliar 1990 b & personal communication).

Using the same animal model and similar porous-surfaced implant designs , Levy *et al.* (1996) compared the traditional two-stage surgical approach with a single-stage (non-submerged) technique. On one side of the mandible of each of 4 dogs the traditional two-stage implant placement surgery with a porous surface-structured implant root design (PPC) and a 0.75 mm coronal machined collar (Al-Sayyed *et al.* 1994) were used. On the contralateral side of each animal a single-stage surgical approach was employed and for this the implant root component was modified further to have a 3 mm (rather than a 0.75 mm) coronal machined collar permitting it to be exposed to the oral cavity from the outset. Histological and histomorphometric analyses conducted at six weeks following implantation revealed that both implant designs became osseointegrated except with one animal where there were post-surgical complications. The bone-to-implant contact (absolute bone contact length and contact length fraction) was significantly greater for the traditional two-stage (submerged) approach, suggesting that bone healing may have been delayed with the one-stage (non-submerged) technique. However, as both methods of

implant placement resulted in osseointegration after six weeks of initial healing (in beagle dogs) the authors concluded that one-stage placement was a possibility with porous-surfaced implant designs provided that extreme care is taken during surgery with soft tissue manipulation and primary wound closure.

B) Background on Calcium Phosphate Coatings for Use with Bone-Interfacing Implants

Calcium phosphate coatings for bone-interfacing implant devices have been investigated for orthopaedic and dental applications since the early 1970's (Hulbert *et al.* 1987). An original intention for such coating was to improve the long-term biocompatibility of metallic implants , especially Co-Cr and stainless steel-based systems, by establishing a barrier coating to inhibit corrosion and associated metal ion release by the metallic substrate in vivo (Brossa *et al.* 1987; Buchanan *et al.* 1987; Wisbey *et al.* 1987; Sella *et al.* 1991; Shirkhanzadeh 1992).

Calcium phosphate (Ca-P) is a general term used for synthetic bioactive ceramics of various calcium and phosphate ratios and of various crystalline structures approaching that of the natural hydroxyapatite of bone with the chemical composition $Ca_{10}(PO_4)_6(OH)_2$. The term Ca-P includes, but is not limited to, hydroxyapatite (HA), amorphous Ca-P, tricalcium phosphate (TCP) and monocalcium phosphate (MCP). These materials are said to be "bioactive" because they are thought to have the ability to facilitate the formation of a direct physicochemical bond between healing bone matrix and implant surfaces (Hench *et al.* 1971, Driskell *et al.* 1973; Ricci *et al.* 1989, 1991; Ducheyne *et al.* 1992; Williams *et al.* 1992). The bonding zone between a synthetic Ca-P layer and bone is thought to contain a calcium-and-phosphate-rich proteinacious layer

which subsequently mineralizes into hydroxyapatite and mediates the bonding of the implant to bone (Jarcho 1981; Cormack 1987). The formation of this bonding zone is generally believed to involve a partial degradation of the hydroxyapatite surface, followed by secondary nucleation, epitaxial crystal growth and / or reprecipitation (Daculsi *et al.* 1990 a; LeGeros *et al.* 1991, 1992; Bonfield *et al.* 1991). Jarcho *et al.* (1977, 1981) were the first to describe an amorphous bonding zone, approximately 0.2 μm wide, at the interface between bone tissue and a dense hydroxyapatite ceramic. Other investigators have since demonstrated a similar amorphous or granular zone, collagen-free electron dense layer interposed between the bone tissue and hydroxyapatite ranging from submicron (0.2 to 0.5 μm) thickness (van Blitterswijk *et al.* 1985, 1986; Ganeles *et al.* 1985; de Lange *et al.* 1987, 1989, 1990) to 1μm wide (Denissen *et al.* 1980; Frank *et al.* 1991). This "cement layer" as the means for Ca-P and bone tissue integration via a chemical bonding mechanism (ionic or covalent) is still controversial however, as it is also thought that collagen interdigitation with a mineralized matrix arising from the coating as well as the biological interactions sufficiently describes a type of micro-mechanical interlock which accounts for the high interfacial shear strengths between these Ca-P-based surface coatings and the surrounding bone (Kasemo & Lausmaa 1991; Davies *et al.* 1990 a, 1991 a, b; Orr *et al.* 1992).

Plasma-Spraying

In the past, Ca-P coatings generally have been applied by plasma-spraying to the surface of a bone-interfacing implant resulting in a surface coat of 30 to 100 μm thickness. Such coatings have been reported to promote faster fixation of implant to bone,

i.e. "osseointegration", as compared to non-Ca-P-coated implants and this has been attributed to the property of Ca-P to act as an osteoconductive substrate (Ducheyne *et al.* 1980; Geesink *et al.* 1987; De Groot *et al.* 1987; Rivero *et al.* 1988; Osborn 1989; Jansen *et al.* 1993). "Osteoconduction" is defined as the function or ability of a biomaterial, either natural or synthetic, to promote the migration of osteoprogenitor cells along its surface (Jarcho 1981; Ricci 1989; Manley 1993). Hence an osteoconductive material has the ability to promote faster bone growth in an area where bone cells are the normal resident cells. Ca-P has also been shown to increase the implant-to-bone interface shear strength by two to eight times that observed with non- Ca-P-coated implants where osseointegration has been achieved (Cook *et al.* 1987; Thomas *et al.* 1987; Rivero *et al.* 1988; and Block *et al.* 1990); however, such observed improvements may have not taken into consideration any differences in surface roughness.

Cook *et al.* (1987, 1992 b) demonstrated using a canine transcortical pushout model that after 6 weeks of implantation, HA-coated implants had an average torsional resistance of 1.77 to at least two times greater than grit-blasted controls without HA. Qualitatively, HA-coated implants appeared to develop superior osseointegration, with fewer areas of fibrous tissue interposition. The HA-coating was largely intact at the end of the 6-week study period. Interface failures occurred primarily at the HA/implant interface ("adhesive" failures), although cohesive failures through the HA coatings and occasionally failures at the bone / HA interface were also observed. The authors concluded that the bond between bone and HA was stronger than the bond between HA and metal substrate. HA-coated implants have also been shown by others (Thomas *et al.* 1987; Rivero *et al.* 1988; Block *et al.* 1990) to similarly increase the implant-bone interface shear strength by two to eight that of non-HA-coated implants.

Plasma spraying is by far the most popular commercial method for forming the desired Ca-P coatings on metal implants. The literature is replete with studies demonstrating enhanced and accelerated bony ingrowth and implant fixation through direct bone bonding with implants coated with plasma-sprayed Ca-P (Geesink *et al.* 1987; Cook *et al.* 1988, 1992 a, b; De Groot *et al.* 1987; de Lange & Donath 1989; Manley 1993). However, concerns related to the coating such as long-term integrity given their poor mechanical properties (Filiaggi *et al.* 1991; Whitehead *et al.* 1992; Delecrin *et al.* 1991) and potentially significant coating resorption and the consequences of such coating degradation (de Groot *et al.* 1987, 1990; Klein *et al.* 1989; Pilliar *et al.* 1991 b; Radin & Ducheyne 1992) have not been satisfactorily resolved.

Plasma-spraying is achieved by introducing HA particles into a very high temperature plasma flame where they are partially or fully melted. The melted particles are accelerated by the plasma flame (ionized gas), acted on by an electric potential, and deposited onto a prepared metal substrate surface positioned normal to the particle beam. This process utilizes a plasma gun consisting of a conical-shaped cathode surrounded by a cylindrical or ring- shaped water-cooled anode. An arc created across the gap between the electrodes ionizes inert gas fed through this space, and the electrons produced are accelerated toward the anode and the positive ions toward the cathode. Collisions between these moving particles and other neutral atoms or molecules which exist in the gas lead to dissociation of molecules and further ionization, "stretching" and transforming the gas in the arc into the characteristic plasma flame with temperature reaching in excess of 20,000K.

Ceramic powders are suspended in a carrier gas such as argon, and injected into the plasma flame. The ceramic particles are partially or fully melted and accelerated to

velocities on the order of hundreds of metres per second by viscous drag created by the mass flow rate of the plasma. They are impacted with the substrate surface. Molten particles arriving at the target flatten and spread out over surfaces that have been roughened to enhance the primary mode of mechanical interlock of the coating and substrate. Since the particles solidify within 10^{-7} to 10^{-6} seconds, the coating is built up particle by particle, with each particle solidifying before the arrival of the next, resulting in a characteristic lamellar structure with inherent porosity as well as unmelted or partially melted inclusions trapped within the layers. Macroscopic residual stress at the interface due to mismatch of thermal expansion coefficients of coating and substrate can lead to coating delamination while temperature gradients within the coating may create tensile stresses leading to cracking of the coating. Furthermore, the reagents used must be strictly controlled in regard to purity, composition and particle size in order to avoid the formation of excessive amounts of non-HA (amorphous calcium phosphate) end products (even with the best control, some non-HA products will result) with unpredictable properties, voids in the coating, and / or low crystallinity leading to degradation in situ (Kay *et al.* 1986).

Most Ca-P coatings deposited by plasma spraying are composed of multiple phases including HA and commonly some TCP and / or amorphous phases. The optimum thickness of a plasma sprayed HA coating is about 30 to 50 μm and the bond between metal substrate and Ca-P coating is mainly of a mechanical nature relying strictly on the surface roughness of the metal substrate surface for retention. Plasma sprayed Ca-P coatings do undergo significant degradation and delamination with time and these are thought to be the result of a number of factors including:

i) the heterogeneous composition and inherent macroscopic and microscopic defects that result from plasma spraying (Radin & Ducheyne 1992). Above approximately 1300 ° C, the HA undergoes irreversible phase changes because of dehydroxylation or decomposition. As the plasma flame temperature is well above the range of HA stability as predicted by equilibrium phase diagnosis, significant compositional and structural changes resulting in the presence of tetracalcium phosphate, α- and β-tricalcium phosphate, and oxyhydroxyapatite can occur. Although these HA derivatives are biocompatible, they appear to be less stable in physiological environments, thus affecting the lifetime of the coatings in vivo. In addition, some amorphous Ca-P will also form as a result of the rapid cooling rates encountered (10^{-6} to 10^{-7} C°/s). These will also contribute to coating instability. The degradation / dissolution of Ca-P resulted in a local increase in calcium and phosphate concentrations that eventually reprecipitate and become incorporated into the surrounding bone (Klein *et al.* 1983, 1989). Thus Ca-P degradation in these situations may be acceptable as the mode for achieving the desired osteoconductivity.

ii) the low coating-to-substrate bond strengths, reflecting primarily mechanical interlocking of the coating to the roughened metal substrate (Filiaggi *et al.* 1991). The modes of Ca-P-substrate bonding result in an interfacial tensile bond strength (TBS) of 5 to 18 MPa, and an interfacial shear bond strength of 10 to 20 MPa, both of which are considered to be very low. Hence, the Ca-P-to-metal substrate interface forms the weak link in the implant-bone complex (Pilliar & Filiaggi 1993 b).

Thus, while there may be biological advantages to the application of plasma sprayed Ca-P layers to a metal bone-interfacing implant, there would appear to be at least three major disadvantages to the types of coatings achievable with the technique of

plasma-spraying. First is the fact that this technique is a "line-of-sight" process and as such the undercut surfaces within sintered porous surface zones are not accessible and hence not coated by HA ; secondly, since the applied coatings are 30 to 50 μm or so in thickness, they are not suitable for application to a porous-surfaced implant with pores and openings of similar size range (such as the Endopore™ implant); and, thirdly, the layers are subject to delamination because of weak adhesion between the coating and the underlying implant substrate.

There are however other methods for application of Ca-P to metal substrates as reviewed by Pilliar & Filiaggi (1993 b). These include dip coating, slip casting and electrophoretic deposition as alternative methods for forming thick Ca-P coatings while electrochemical deposition, sputtering deposition, laser ablation, and sol-gel dip-coating are methods for forming thin Ca-P coatings. A thorough review of each of these different methods of Ca-P application is beyond the scope of this literature review.

Sol-Gel Film Formation

The sol-gel film technique (Qiu *et al.* 1993) is essentially a spin-coating or dip-coating technique which generally results in coatings of less than 1 μm in thickness (100 to 500 nm). It is a low cost method of coating preparation utilizing a wet chemistry procedure that allows for precise chemical and microstructural control of the coatings (Dislich 1988; Klein 1991; Yi *et al.* 1991; Fabes *et al.* 1993). The reagents containing the desired components of the coating are mixed either as a colloidal suspension solution of inorganic particles or as metal alkoxides or other organic precursors which react at relatively low temperatures (usually at room air environment) to cause agglomeration of

fine oxide particles to form a film. Calcium phosphate sol-gel films are created by reacting calcium nitrate ($Ca(NO_3)_2$), ammonium dihydrogen phosphate ($NH_4H_2PO_4$) and concentrated ammonium hydroxide (NH_4OH). Afterwards, the layer is densified by annealing at temperatures in the range of 400 to 1000 ° C . The chemical reaction is as follows:

$$5Ca(NO_3)_2 + 3NH_4H_2PO_4 + 7NH_4OH \rightarrow Ca_5(OH)(PO_4)_3 + 10NH_4NO_3 + 6H_2O$$

X-ray diffraction analyses of these films indicate the formation of crystalline HA and a granular structure (with individual grains approximately 50 nm in diameter) within the film. These films have been shown to be resorbed by osteoclasts (in vitro) which may be of potential benefit in clinical applications (Davies *et al.* 1993).

This sol-gel Ca-P thin film is extremely dense, coherent and adheres strongly to the underlying substrate (Qiu *et al.* 1993, Filiaggi *et al.* 1996 a, b). With this technique, the substrate is dipped into the sol-gel solution and then gradually withdrawn vertically at a controlled rate of 20 to 200 mm/min. using a commercially available, vertically mounted screw-driven gliding unit (UniSlide, Velmex, Inc., East Bloomfield, NY). Rate of travel of the UniSlide, and hence selection of withdrawal speed, is controlled through a NF90 Series stepping motor controller using a PC and a customized software program. It is then allowed to dry in a laminar flow cabinet, followed by vacuum annealing in a programmable muffle furnace (Thermolyne Model # F48058, Dubuque, IA, USA) at 400 to 1100 ° C for anywhere from two minutes to two hours (Qiu *et al.* 1993) to bring about the desired densification and crystallization.

The annealing temperature and the duration of firing both affect the structure and surface morphology of the resulting Ca-P thin film. The high end of the temperature

range results in higher crystallinity than the lower temperatures. The grain size of the film is also increased with increasing temperature and annealing time.

Cell culture studies on sol-gel-formed Ca-P thin films have been demonstrated with SEM to result in the elaboration of extracellular matrix with the collagen fibres closest to the film completely buried in biologically produced mineral appearing to merge with the surface of the sol-gel film (Qiu *et al.* 1993). This biological interfacial matrix has been described as a cement line-like material (Davies *et al.* 1991 a, b). While the two layers are distinguishable at low SEM magnifications (~ 4,000X), they cannot be easily distinguished from each other at higher SEM magnifications (greater than 20,000X), especially when the grain size and the intergranular voids of the film are of the same order of magnitude as the biological calcium phosphate crystals (Qiu *et al.* 1993), demonstrating a chemical bonding process of bone matrix with Ca-P coating. Bone cells closest to the sol-gel film were more flattened and spread out as compared to the more rounded cells further away from the film surface, demonstrating the ability of the roughened, microporous sol-gel surface to promote cell spreading and hence cell migration (Qiu *et al.* 1993; Dziedzic *et al.* 1994). Interdigitation of the elaborated biological mineral matrix with the sol-gel Ca-P grains, intergranular voids and microporosity resulted in secondary micro-mechanical bone-to-thin film interlock.

III) RATIONALE FOR THE PRESENT EXPERIMENT

The Ca-P surface layers applied to implants by plasma spraying are typically 30 to 100 μm in thickness and when applied to porous-surfaced implants of the pore size range used by Deporter, Pilliar and co-workers would result in occlusion of the pores and thus negate the advantages of such a porous-surfaced design. This dictates that the porous surface be made with larger particles resulting in a pore size in the 500 μm size range. However, this larger pore size range is beyond the optimal (50 to 200 μm) pore size with respect to rate of bone ingrowth and strength of fixation development. The larger pore size range is not suitable for use in the 3.5 to 4 mm diameter limitation of most dental implant applications and will not allow sufficient room for the prosthetic hardwares (Bobyn *et al.* 1980; Pilliar 1987).

Given the accepted advantage of a Ca-P surface layer for increased osteoconductivity and in view of the recent development of the sol-gel coating technique, it was of interest to study whether or not the application of an ultrathin layer of Ca-P to a porous-surfaced implant design such as the Endopore™ dental implant would accelerate initial osseointegration during the early healing stage. The advantages of using the sol-gel approach are that the resulting thin Ca-P layer would not occlude the porous structure, may promote osteoconduction and therefore, provide greater resistance to forces applied early on (Rivero *et al.* 1988; Cook et al 1992 b) as more bone may form within the pore spaces sooner.

IV) OBJECTIVE OF THE PRESENT STUDY

The objective of this study was to compare the early healing responses in rabbit tibial sites (i.e. non-functional) of porous-surfaced Ti-6Al-4V implants with or without a submicron layer of calcium phosphate applied to its surface by the sol-gel technique. This was based on the hypothesis that the sol-gel Ca-P layer was osteoconductive.

V) MATERIALS AND METHODS

A) Implant Fabrication

Forty-two custom-made 3.5 mm x 8 mm porous-surfaced cylindrical-shaped Ti-6Al-4V implants were used. One end of the implant had an expanded flat head to facilitate implant placement and to control the depth of implantation (fig. 5.1). The core component of the implant was modified with a sintered porous surface coating using -100/+325 mesh Ti-6Al-4V powders ranging in diameter from 45 to 150 μm. These powders were sintered to the implant core at high temperature (1250 ° C for two hours) in a high-vacuum furnace (approximately 10^{-5} Torr at the sintering temperature) to form a 2 to 3 particle layer thick zone with approximately 35% volume of interconnected porosity. All implants used in this study were manufactured by Innova Corp. (Toronto, Canada).

Prior to sol-gel coating, the implants were cleaned in a laminar-flow sterile air cabinet using the following procedure (Deporter *et al.* 1986). They were washed in 2% Decon (BDH Chemicals, Toronto, CAN) in double-distilled, de-ionized water (DDDW) under sonication for one hour. This was followed by three washings (three minutes each) in DDDW alone under sonication. They were then treated in 28% nitric acid under sonication for one hour to form a passive surface-oxide layer (Solar *et al.* 1979), and washed five times (five minutes each) in DDDW again under sonication. Finally, they were soaked for one hour in 100% ultrapure ethanol, allowed to dry by evaporation and sterilized using gamma radiation.

B) Sol-gel Ca-P Coating

Twenty-two implants were further modified by receiving a calcium phosphate coating of 300-500 nm thickness using the sol-gel technique (Centre for Biomaterials, University of Toronto, Toronto, Canada). The necessary reagents, calcium nitrate ($Ca(NO_3)_2$), ammonium dihydrogen phosphate ($NH_4H_2PO_4$) and concentrated ammonium hydroxide (NH_4OH), were mixed to form a colloidal suspension solution (in water base) of inorganic particles which at relatively low temperatures (usually at room temperature) reacted to cause agglomeration of reaction products to form a film (Qiu *et al.* 1993) according to the following chemical reaction:

$$5Ca(NO_3)_2 + 3NH_4H_2PO_4 + 7NH_4OH \rightarrow Ca_5(OH)(PO_4)_3 + 10NH_4NO_3 + 6H_2O$$

The Ti-6Al-4V cylindrical implants were dipped into the sol-gel solution and then gradually withdrawn vertically at a controlled rate of 100 mm/min. using a commercially available, vertically mounted screw-driven gliding unit (UniSlide, Velmex, Inc., East Bloomfield, NY). Rate of travel of the UniSlide, and hence selection of withdrawal speed, was controlled through a NF90 Series stepping motor controller using a PC and a customized software program. The sol-gel Ca-P-coated implants were then allowed to dry and subsequently annealed in a programmable vacuum furnace (Thermolyne Model #F48058, Dubuque, IA) at 683 ° C for 15 minutes, followed by cooling in the furnace to bring about the desired film densification and crystallization (Qiu *et al.* 1993). The implants were re-sterilized with gamma radiation, and stored in sealed vials. Figure 6.1 shows an example of a visibly darker porous-surfaced implant coated with sol-gel Ca-P and a lighter untreated control implant.

C) Animal Model

Twenty-one white male New Zealand rabbits (weighing approximately 4.5 kg each) were used in this study. The animal experiment conformed to standards of the Animal Care Act and had been approved by the University of Toronto Animal Care Committee (protocol N^0 00312). Prior to implantation, the animals were induced with IM injections of Ketamine HCl (20 mg/kg) and Xylazine (2 mg/kg) and maintained in a surgical state of anesthesia with a mixture of Halothane 1-1.5% in N_2O + O_2 (2:1) via inhalation. In a pilot study, four rabbits were used each receiving one control and one sol-gel Ca-P-coated implant in the right tibia near its midshaft to ensure bicortical implant stabilization. The implants were placed 15 mm apart from centre to centre.

In Experiment I, ten rabbits were used each receiving one control and one sol-gel Ca-P-coated implant in the right tibia as in the pilot experiment; however, the implant positions were located towards the metaphyseal half of the tibia, while still maintaining bicortical stabilization. In five of these rabbits, the experimental implant was the more proximal implant and the more distal implant was the control. In the other five rabbits, the implant positions were reversed.

In Experiment II, both the right and left tibiae of six rabbits were similarly prepared to receive only one implant per tibia with the implant position being at the same distance from the proximal metaphysis to allow bicortical implant stabilization. Three of these rabbits received the Ca-P coated implant in the right tibia and the control in the left tibia. The remaining three rabbits received the control implant on the right and the experimental (sol-gel coated) on the left.

Experiment III consisted of only one rabbit in which one Ca-P-coated implant was placed in each tibia. This animal was used only for subjective observations of the implant / Ca-P / bone interface after freeze-fracturing the bone from the implant (see below).

D) Surgical / Implantation Procedure

Each animal was immobilized on its back, and using a sterile surgical technique, a longitudinal incision was made on the medial surface in the proximal diaphyseal region of the tibia. The soft tissues, muscles and periosteum were dissected and reflected to expose bone (figure 5.2), after which a series of burs (figure 5.3) rotating at about 8,000 to 10,000 rpm in an electric motor (NT Company, Chattanooga, Tenn., USA) and hand piece (figure 5.4) with copious saline irrigation, were used to drill through the medial cortex, medulla and lateral cortex of the tibia. The intent was to prepare an implant site that was slightly smaller in diameter than the implant to be inserted. A #6 round bur was used to make the initial penetration through the medial cortical bone (figure 5.5). A periodontal probe was then used to confirm that the depth was only 6 to 7 mm such that when the lateral cortical bone was penetrated, both cortices could be used to engage the implant. If the initial penetration before involving the lateral cortex was 7.5 mm or longer, then this hole was closed with bone wax and another hole drilled slightly distal to it. Once both cortices had been penetrated, a 2 mm twist drill bur, a 3 mm twist drill bur and finally a 3.4 mm double edged bur (Brasseler of Canada, Toronto, Canada) were used to prepare the recipient site (figure 5.6 a, b, c, d, e). This procedure ensured a tight initial transcortical fit or "press-fit" of the implant within the prepared site. A hemostat was utilized to hold each implant at the flattened head to avoid damage to the implant surface

(figure 5.7 a, b, c) as the implant was tapped into place with light hand pressure using rotational force delivered in both a clockwise and counter-clockwise manner. The implants in Experiment I were placed 15 mm apart (figure 5.7 c). Subsequently, the soft tissues were reapproximated in separate layers with 4-0 Vicryl suture material (Ethicon Sutures Ltd., Peterborough, Ontario) (figure 5.8 a, b, c). Buprenorphine HCl (0.3 mg/kg IM) was administered as required to control postoperative discomfort.

E) Specimen Collection and Preparation for Experiments I & II

At the end of the two week experimental period, all animals were sacrificed by injecting 2.5 ml of T-61 (Hoescht of Canada) into the marginal ear vein. Excess tibial soft tissues and muscle were excised. The proximal half of the tibiae containing the implant(s) was harvested using a Stryker saw, and placed into fixative (10% formaldehyde, methanol, and water at 1:1:1.5 ratio) for two weeks. Specimens were sectioned into separate blocks each containing one implant. Tissues were sequentially dehydrated in 30%, 50%, 70%, 95% alcohol and finally twice with 100% alcohol. These were processed and embedded in methylmethacrylate (Deporter *et al.* 1986 a). Non-demineralized sections containing bone and implant were cut using a Buehler Isomet Saw to achieve initial section thickness about 120 to 150 μm and then further reduced to approximately 40 μm thickness by petrographic grinding techniques (Deporter *et al.* 1986 a). The sections were stained using a mixture of Stevenel's blue and Van Gieson's picro-fuchsin (Maniatopoulos *et al.* 1986). This staining procedure allowed for clear distinction between bone, osteoid, and fibrous connective tissue, and provided good cellular detail at the light microscopic level.

Eight sections were obtained for each implant (figure 5.9 a, b). The first cut was a cross-sectional cut through the tibia and along the long axis of the implant to yield proximal and distal halves. The proximal half was then further sectioned along the long axis of the tibia to yield proximal anterior and proximal posterior quarters. The distal half was similarly cut to produce distal anterior and distal posterior quarters. Each of the cut surfaces of these quarters was further sectioned to yield proximal anterior cross-section (PAX), proximal anterior longitudinal (PAL); proximal posterior cross-section (PPX), proximal posterior longitudinal (PPL); distal anterior cross-section (DAX), distal anterior longitudinal (DAL); distal posterior cross-section (DPX), distal posterior longitudinal (DPL) sections respectively.

F) Analysis of Bone Growth and Ingrowth

Each section was examined and photographed by light microscopy (LM) and by backscattered scanning electron microscopy (SEM) and quantified using the Bioquant Image Analyzer (R & M Biometrics, TN, USA) for bone contact to estimate osteoconduction along the implant surface from each of the two cortices. To do this, black and white LM photomicrographs (figure 5.10 a) of each section at 10X magnification were acquired using a Wild Leitz Macro Zoom lens in order to include the whole implant in one print. Similarly, back scattered SEM photomicrographs (figure 5.10 b) at 15X magnification (15 to 20 KV) were taken for each section. The resultant LM and backscattered SEM photomicrographs had final magnifications of 23X and 34X respectively after the films were printed onto 8 inch X 10 inch photographic paper (Kodabrome II RC, Eastman Kodak Company, Rochester, NY, USA). Direct bone

contact with the outer surface of the implant beads was traced on each micrograph using a fine red marker, while those outer bead surfaces not in direct contact with bone were traced with a different coloured (green or blue) marker. This final red and green tracing formed a continuous curvilinear interface along the outer surfaces of the porous coat. A Bioquant Image Analyzer System IV software package (R & M Biometrics Inc., Nashville, TN, USA) was used to quantify these red and green markings from the endosteal cortical bone level to the furthest point of bone growth for each of the medial and lateral halves of each implant section as follows (figure 5.11 a, b, c):

1) the total length of direct bone contact was quantified to give the absolute contact length (ACL);
2) similarly, the total length of non-bone contact was quantified and added to ACL to yield the length of implant surface available for contact;
3) the straight line linear bone growth (SLBG) was measured as a straight line from the endosteal cortical bone level to the furthest point of bone growth;
4) the total bone ingrowth area was obtained by quantifying the areas of the bone tissue that had grown into the available pore spaces with the outer limit of the measurement being a line tangent to the outer-most bead surfaces (figure 5.12). This yielded the absolute bone ingrowth area (ABIA);
5) The total area available for bone ingrowth or the total area of the pore spaces was measured by subtracting the total area of the beads from the area of the rectangle bounded by: a) the inner level of the cortical bone, b) the furthest extent of medullary bone growth, c) the line represented by the surface of the implant inner core, d) the line parallel to the implant core and tangent to the outer surface of the outer-most porous bead (figure 5.12);

6) The depth of bone penetration represented by the perpendicular distance from the tangent line in (4) to the deepest level where bone growth had penetrated the pores;

7) Thickness of the porous surface zone was measured from the tangent line above to the implant core;

All measurements were made in millimetres. From the above histomorphometric measurements, the following calculations of bone ingrowth measurements were obtained (Deporter *et al.* 1986 a; Jasty et al 1992):

8) Contact length fraction (CLF) where

$$CLF = \frac{\text{Absolute length of bone in contact with implant (ACL)}}{\text{length of implant surface available for contact (see \# 2 above)}} \times 100$$

9) Bone Ingrowth Fraction (BIF) where

$$BIF = \frac{\text{Absolute bone ingrowth Area(ABIA)}}{\text{Area available for bone ingrowth or the area of the pores(\# 5)}} \times 100$$

10) Bone Penetration Fraction (BPF) where

$$BPF = \frac{\text{Depth of bone penetration (\# 6)}}{\text{Thickness of porous surface zone (\# 7)}} \times 100$$

ACL, CLF, SLBG, ABIA, BIF from experiments I & II were submitted to multiple factor analysis of variance (ANOVA) for repeated measures using the general linear models procedure of SAS. The ANOVA tested main effects and interactions between factors ($p < 0.05$). If significant main effects were found between factors tested (implant surface type, implant position, medial / lateral region of implant, implant type/position interaction, implant surface, implant type / surface interaction), the Duncan multiple-range test was used for pair-wise comparisons of the means ($p < 0.05$).

G) Freeze-Fracture SEM Analysis

The two specimens from the one animal in the third experiment were fixed and dehydrated in a manner similar to those from experiments I and II. The tibial blocks containing implants were then frozen with liquid CO_2 and freeze-fractured to permit separation of bone and implant surface using a knife and mallet. Each implant specimen with whatever bone remained attached to it and the fractured-off bone fragment were critical point dried by replacing the alcohol with liquid CO_2 and heated to 38 ° C under pressure at 1500 PSI. All recovered tissues and implants were mounted on aluminum studs and then sputter-coated with 3 nm of platinum. Specimens were viewed in the SEM at 10 KV using secondary electron imaging. Photomicrographs ranging in magnification from 50 X to 15,000 X were used to assess the relationships between bone and Ca-P coating.

H) Analysis of the Extent of Bone Ingrowth Pattern

The subjective findings of experiment III were related to the histological specimens of Experiment I and II to evaluate the extent of bone ingrowth. Each specimen section was re-examined using backscattered scanning electron microscopy to assess bone ingrowth in relation to the acute corners / tight neck regions (figure 5.13) of the porous surface structure. The neck region was determined as in the following sequence: i) a line through the centres of the two adjoining circles (spherical particles) was first drawn; ii) then a second line parallel to the first line and tangent to the smaller of the two circles was drawn. The area bounded by the second line and the two circles forms the

neck region (figure 5.13 a). That is, the bounded neck region always forms an isosceles triangle. To investigate the extent of bone ingrowth into the neck region, two SEM photomicrographs at 15 to 20 KV and 100X magnification were taken of each implant section and the films were printed onto 8 inch by 10 inch photographic paper (Kodabrome II RC). The first photomicrograph was of the medial aspect of the implant section to include only a small portion of the endosteal medial cortical bone (for orientation purpose) and as much of the new endosteal bone growth as possible . A line perpendicular to the implant core was constructed on the photomicrograph at the junction of the medullary space and the cortical bone. A similar second line was drawn at exactly 700 μm from the first line towards the medullary cavity (figure 5.13 c). Similarly, a second photomicrograph of the same section was taken for the lateral aspect of the implant section. From these photomicrographs, a non-parametric analysis of the neck regions (figure 5.13 b) of the spherical particles was carried out. Three nominal groups (figure 5.13 b) were assigned according to the amount of bone growth seen within each neck region: a) a category of "Group 1" was assigned to a neck region that had none to less than one-third of the area filled with bone; b) a category of "Group 2" was assigned to a neck region that had more than one-third and less than two-thirds of the area filled with bone; c) and a category of "Group 3" was assigned to a neck region that had from two-thirds to 100% of the area filled with bone. Within the confines of the 700 μm described above, the total number of neck regions corresponded to these criteria for each of the Group 1, 2 and 3 were counted and recorded. The above data were submitted for similar analysis of variance (ANOVA) using SAS at 5% level of significance.

Figure 5.1: The porous surfaced-structure implant used in the study. One end of the implant had an expanded flat head to facilitate implant placement and to control the depth of implantation. The implant dimension is 3.5 mm X 8 mm. The core component of the implant was prepared with a sintered porous surface using -100/+325 mesh Ti-6Al-4V powders ranging in diameter from 45 to 150 μm to form a 2 to 3 particle layer thick zone with approximately 35% volume of interconnected porosity.

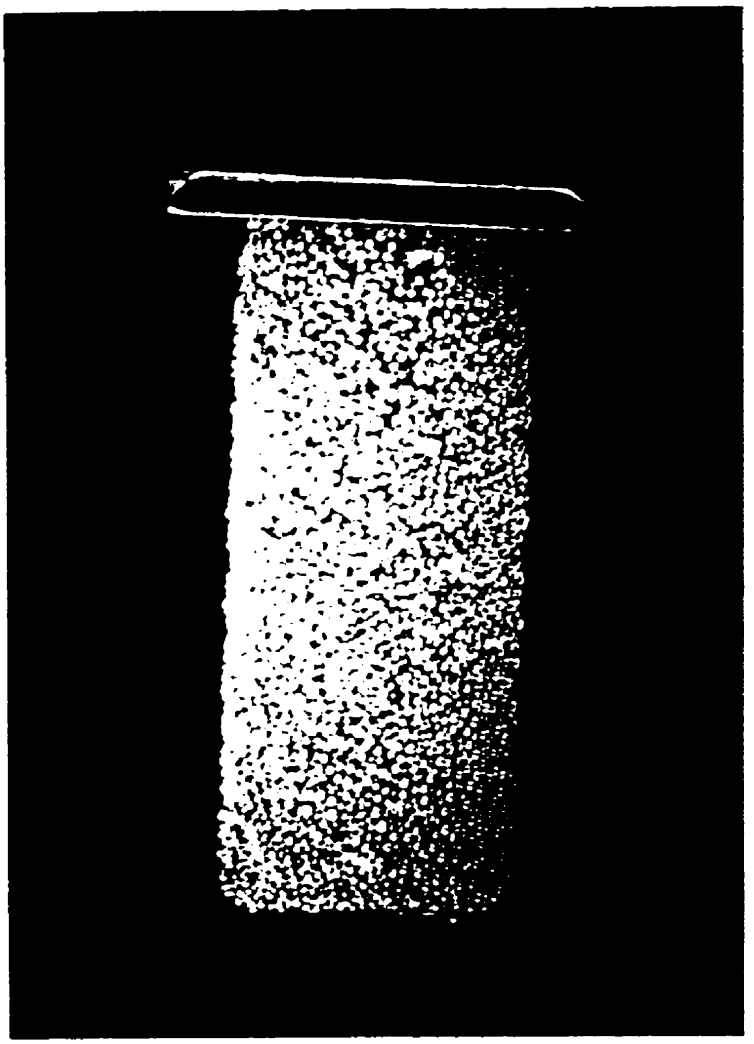

Figure 5.2: An incision was made on the medial aspect of the tibia. The soft tissues, muscles and periosteum were dissected and reflected to expose the underlying bone.

Figure 5.3: The sequence of burs used to prepare the implantation site. From left to right: # 6 round bur, 2 mm twist drill bur, 3 mm pilot drill bur, 3 mm twist drill bur, 3.4 mm double-edged bur.

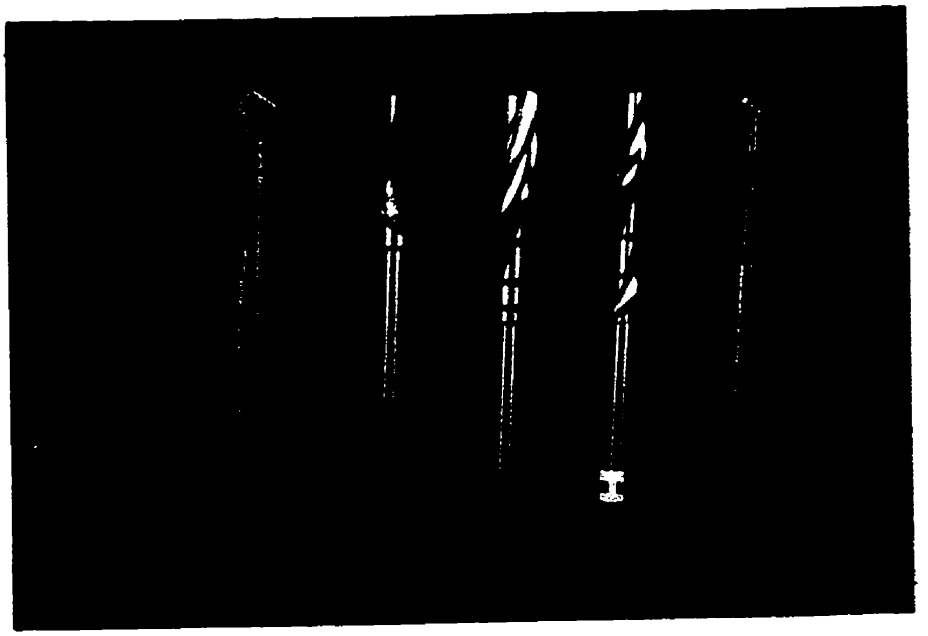

Figure 5.4: Electric motor with handpiece speed setting at about 8,000 to 10,000 rpm.

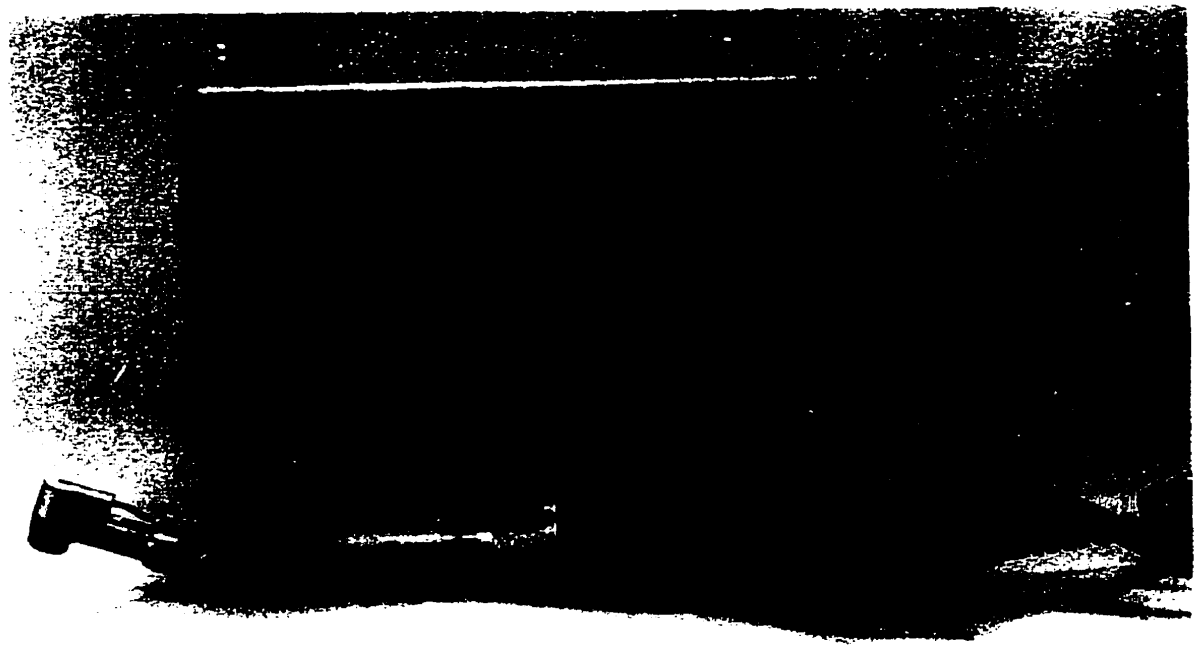

Figure 5.5: A # 6 round bur was used to make the initial penetration through the medial cortical bone.

Figure 5.6: A 2 mm twist drill bur (a) , a 3 mm pilot drill bur (b), a 3 mm twist drill bur (c) and finally with 3.4 mm double-edged bur (d). The recipient sites for Experiment I as shown are ready for implant installation (e).

(a)

(b)

(c)

(d)

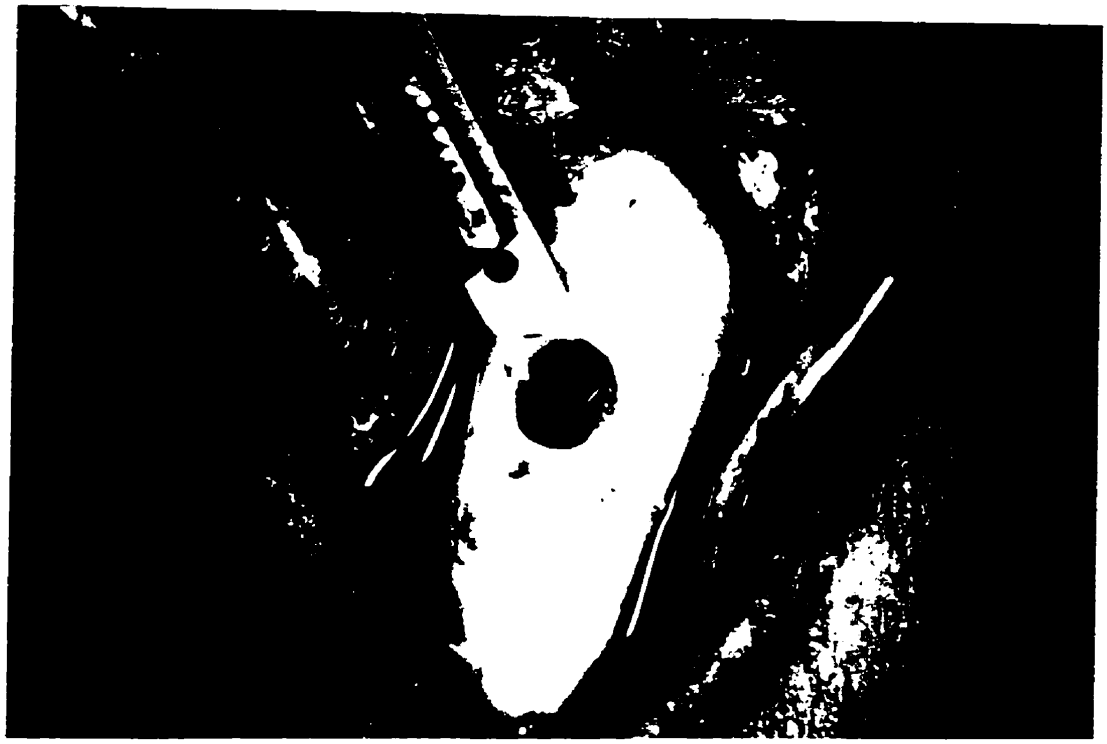

(e)

(c)

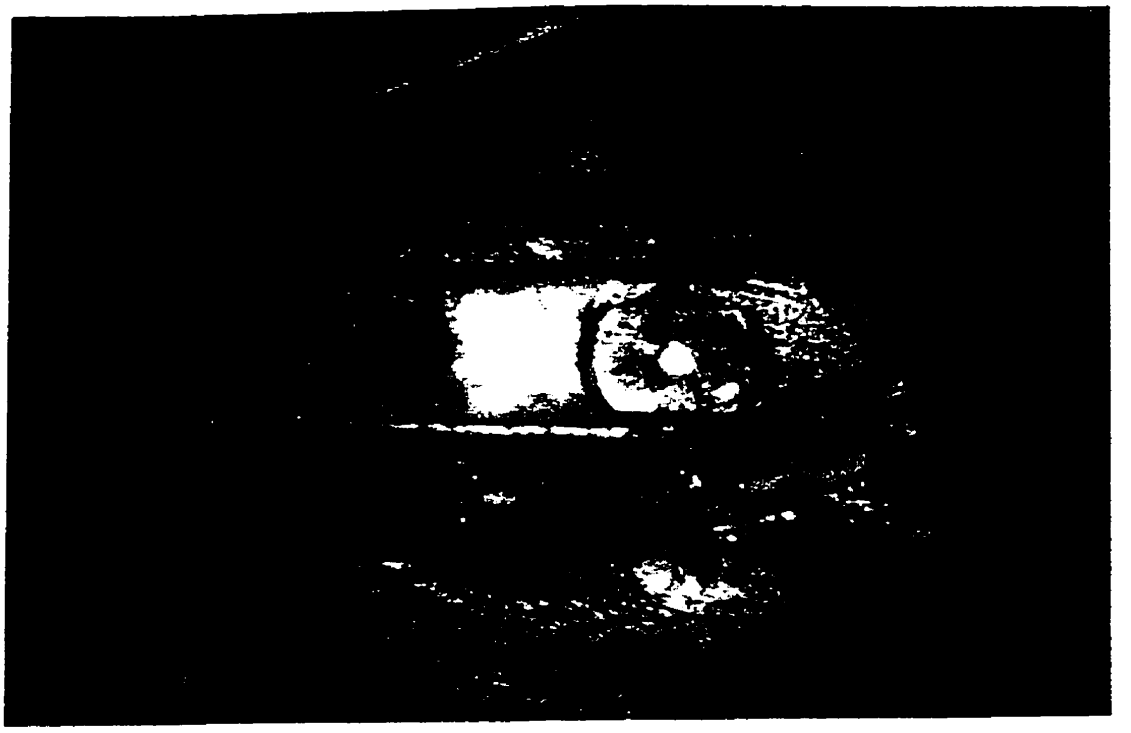

, muscle (a, b) and skin (c), were reapproximated in separate

material.

(c)

Figure 5.9: a) is a schematic drawing illustrating bicortical implant stabilization. b) is a schematic drawing demonstrating how eight histological sections were obtained for each implant. The first cut was a cross-sectional cut through the tibia and along the long axis of the implant to yield proximal and distal halves. The proximal half was then further sectioned along the long axis of the tibia to yield proximal anterior and proximal posterior quarters. The distal half was similarly cut to produce distal anterior and distal posterior quarters. Each of the cut surfaces of these quarters was further sectioned to yield proximal anterior cross-section (PAX), proximal posterior longitudinal (PPL); proximal posterior cross-section (PPX), proximal posterior longitudinal (PPL); distal anterior cross-section (DAX), distal anterior longitudinal (DAL); distal posterior cross-section (DPX), distal posterior longitudinal (DPL) respectively.

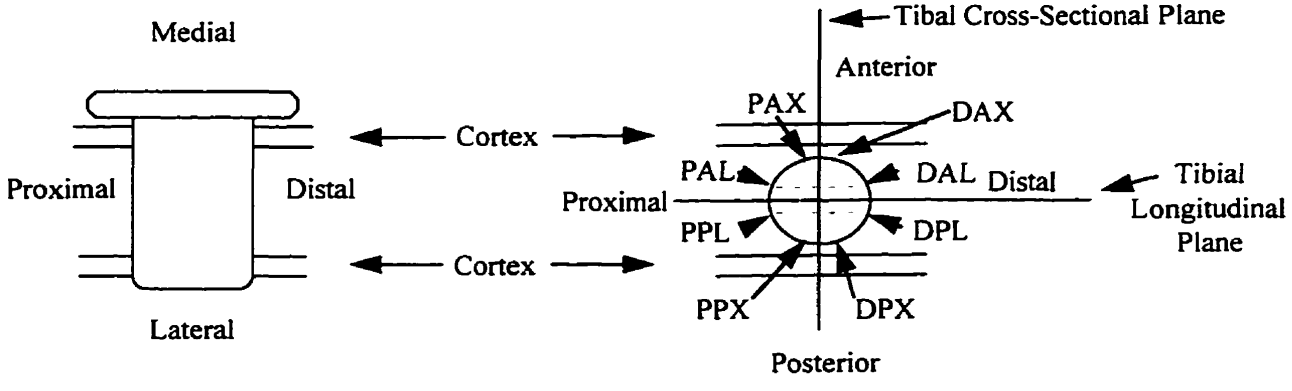

Figure 5.10: Typical LM photomicrographs (a, b) demonstrating the difficulties associated with identifying actual bone-to-implant contact. Typical backscattered SEM photomicrographs demonstrating distinct identification of bone-to-implant contact (c, d, e).

(a) (b)

Figure 5.11: (a) is a schematic drawing of bone-to-implant contact tracing. (b) is a pre-tracing SEM photomicrograph. (c) is a post-tracing SEM photomicrograph of the same section. Direct bone contact with the outer surface of the implant spherical particles was traced on each photomicrograph using a fine red marker, while those outer bead surfaces not in direct contact with bone were traced with a different coloured (green / blue) marker. The straight line linear bone growth (SLBG) was measured as a straight line from the endosteal cortical bone level to the point of maximal bone growth. (B = ACL, O = soft tissue contact, S = SLBG, A_T = total area of pores and spherical particles, A_h = area of spherical particles, A_B = ABIA).

(a)

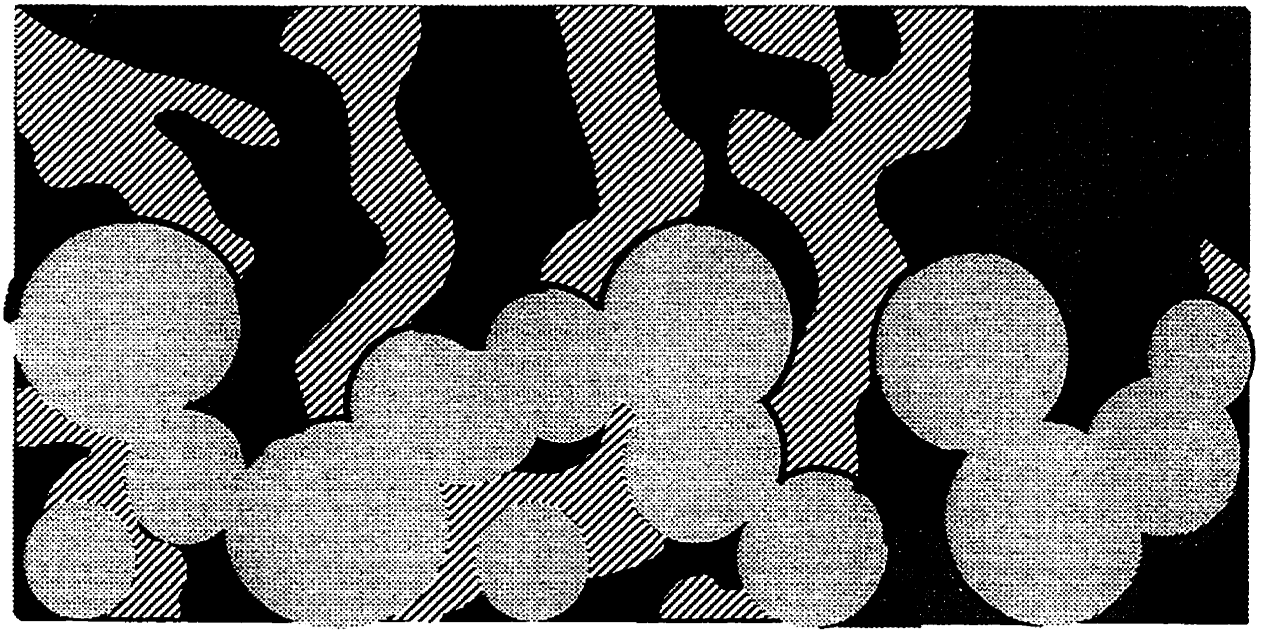

Figure 5.12: Schematic drawing illustrating the means used to quantitate the of absolute bone ingrowth area (ABIA) and bone ingrowth fraction (BIF). The sintered titanium alloy porous surface zone is shaded in black and bone is shaded with the hatches. The unmarked areas represent non-osseous tissue. The total area available for bone ingrowth or the total area of the pore spaces was measured by subtracting the total area of the beads from the area of the rectangle bounded by: (a-c) the inner level of the cortical bone, (b-d) the furthest extent of medullary bone growth, (c-d) the line represented by the surface of the implant inner core, (a-b) the line parallel to the implant core and tangent to the outer surface of the outer-most porous bead.

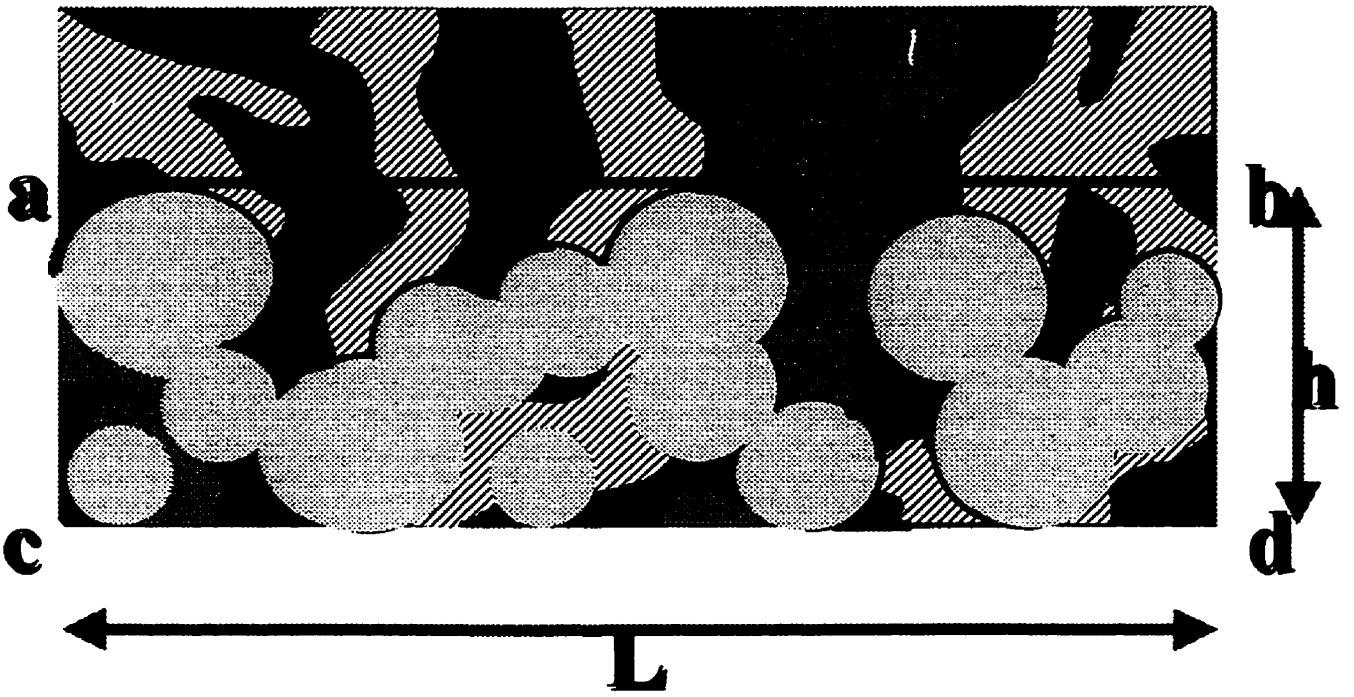

Figure 5.13: (a) is a schematic diagram illustrating how a neck region is determined. A line through the centre of two adjoining circles is first drawn, then a second line parallel to it and tangent to the smaller circle is drawn. The area bounded by the second line and the two circles forms the neck region. (b) is a schematic diagram illustrating the three different categories of the extent of bone ingrowth in the neck regions "Group 1" was assigned to a neck region that had none to less than one-third of the area filled with bone; "Group 2" was assigned to a neck region that had more than one-third and less than two-third of the area filled with bone; "Group 3" was assigned to a neck region that had from two-third to 100% of the area filled with bone. (c) is an SEM photomicrograph at 100X magnification showing bone ingrowth in relation to the acute corners / tight neck regions of the porous layer. A line perpendicular to the implant core was constructed on the photomicrograph at the junction of the medullary space and the cortical bone. A similar second line was drawn at exactly 700 μm from the first line towards the medullary cavity. Within the confines of this 700 μm , the total number of neck regions corresponded to each of the Group 1, 2 and 3 were counted and recorded.

(a)

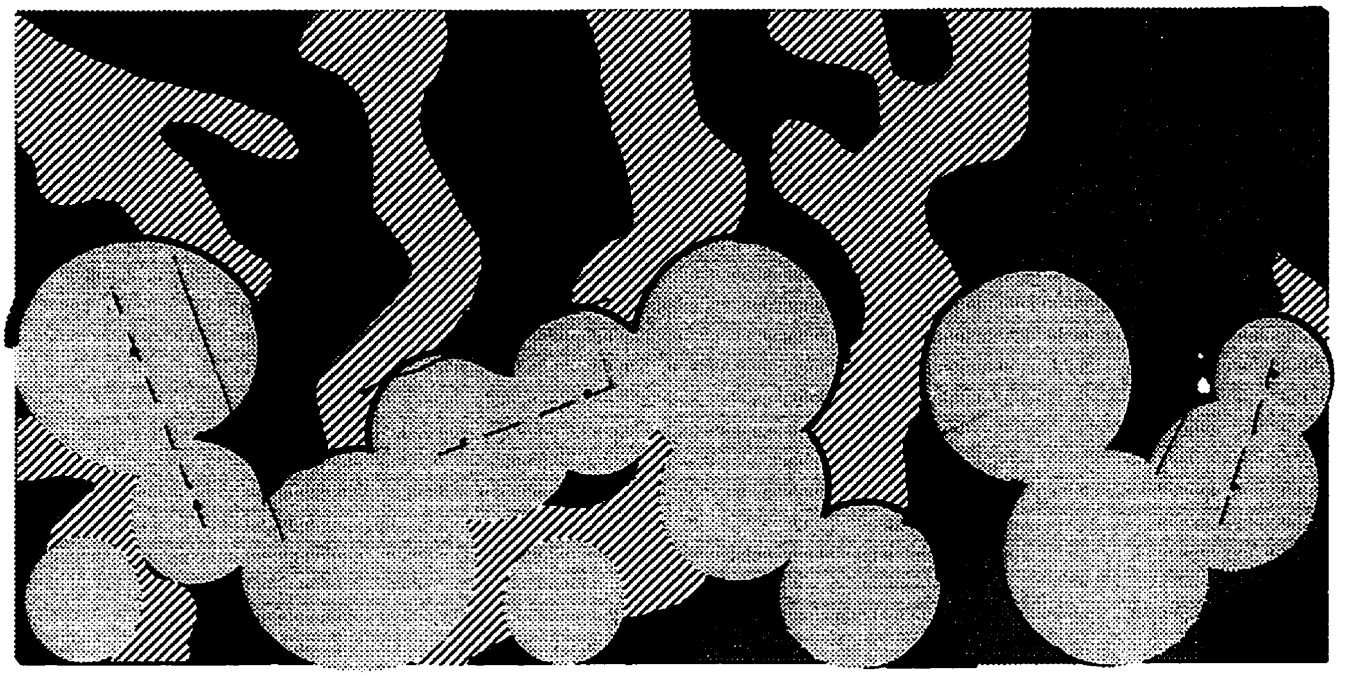

(b)

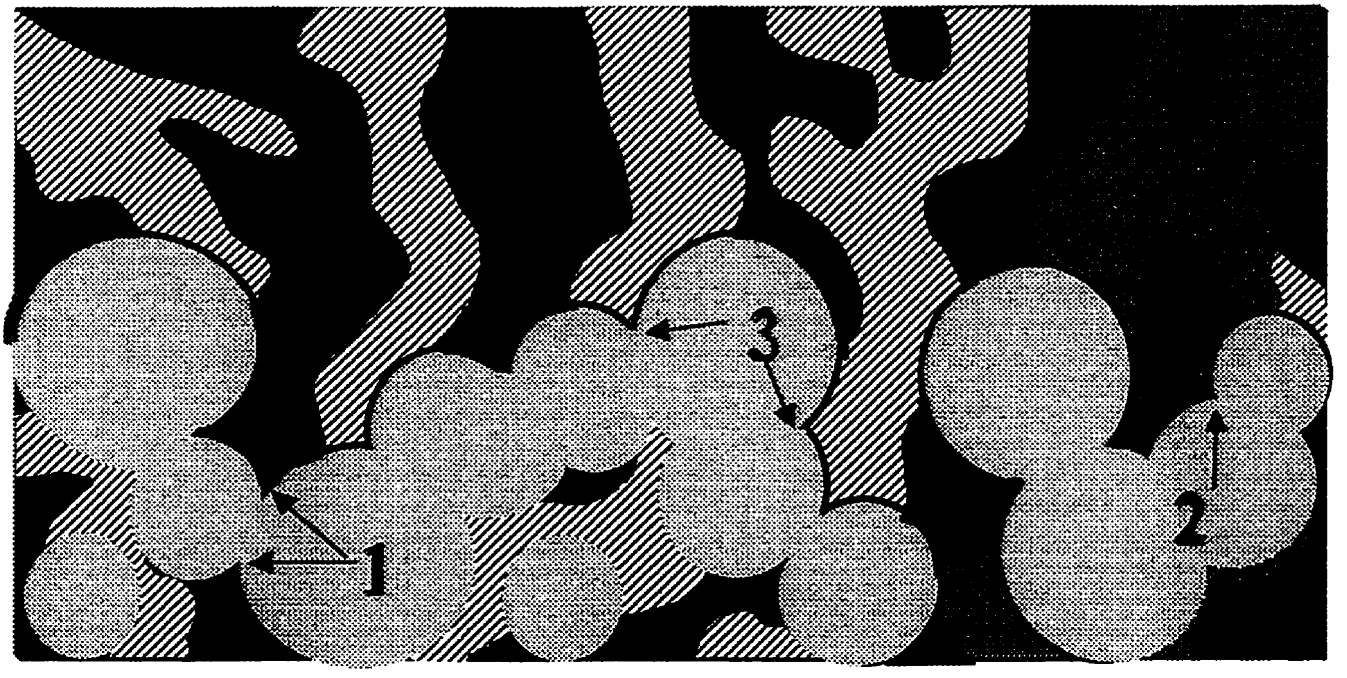

(c)

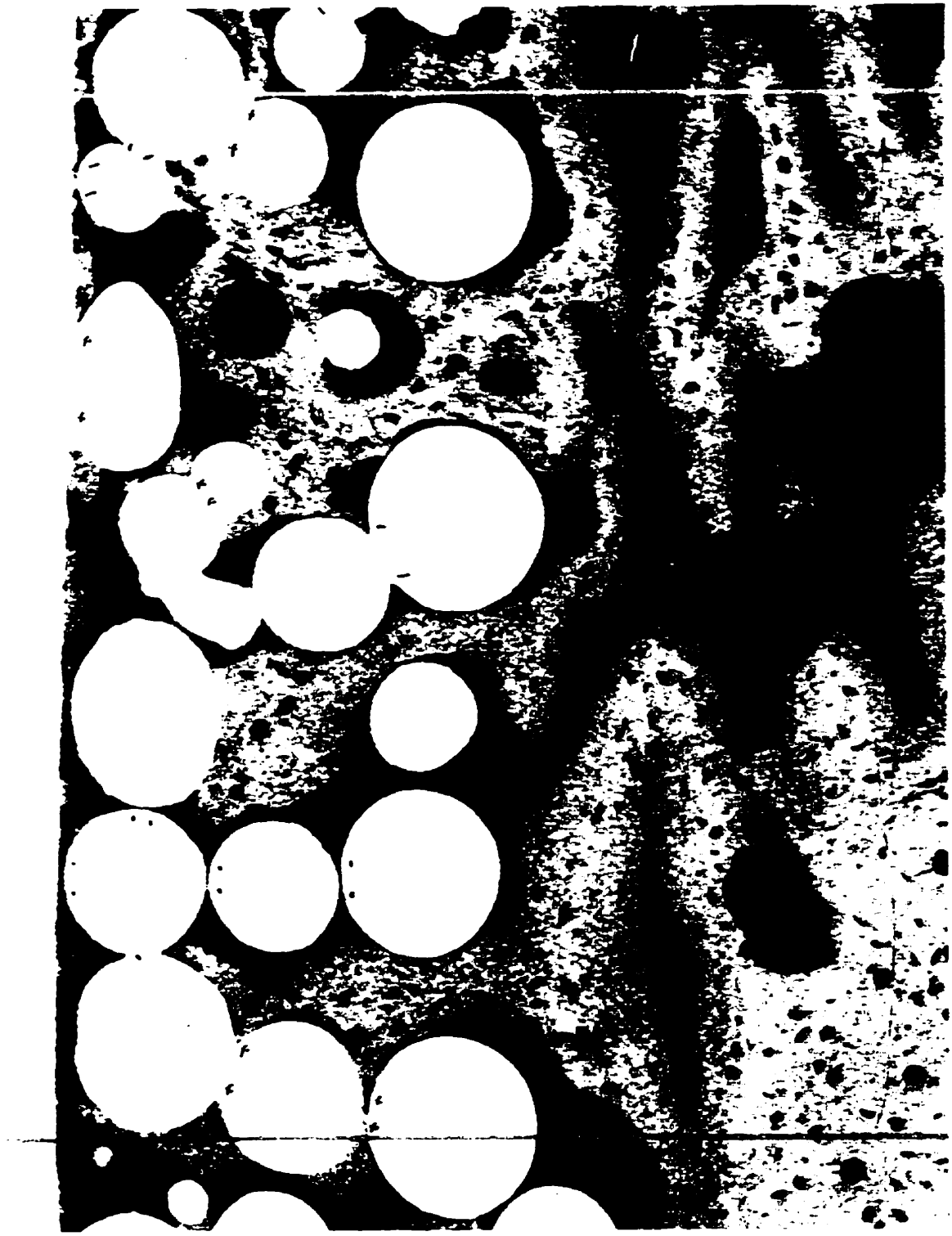

VI) RESULTS

A) Pilot Study for Experiment I

Three of the four rabbits used in the pilot study developed pathological fractures of the implanted tibiae at day three while the fourth rabbit showed a similar fracture at day five. All of these animals had to be sacrificed prematurely in advance of the two week experimental period, and led to revision of the experimental protocol. Thus, implant installation was subsequently conducted closer to the proximal tibial metaphysis in all animals.

B) Surface Topography of Sol-gel Ca-P-Coated Implant

Figure 6.1 shows the two implant types used in this study. The darker implant (figure 6.1a) is the sol-gel Ca-P-coated implant while the lighter colored implant (figure 6.1b) is the control. The thin Ca-P coating applied by the sol-gel technique appeared to have penetrated the full thickness of the porous surface zone which can be seen in figure 6.2. Figure 6.2 illustrates standard (secondary electron imaging, 300X & 500X) SEM photomicrographs showing surface topography of the control implant (figure 6.2 a) and the thin Ca-P film typically covering the spherical particles of the porous surface zone, and also verifies that the pores had not been occluded by this treatment (figure 6.2 b, c). The Ca-P film appeared somewhat rough and granular thus imparting an additional secondary micro-textured topography (see discussion) to the porous region. SEM photomicrographs (figure 6.3) at higher magnifications (2,000X & 5,000X) of part of the

field in figure 6.2 a & b showing typical examples of the Ca-P layer seen in the neck regions between adjacent spherical particles or between the deepest layer of spherical particles and the solid machined implant core. In these regions the film appeared thicker, and this subjective observation was confirmed using freeze-fracture technique (see below).

C) Qualitative Light Microscopic (LM) and SEM Observations on the Healing of the Implanted Sites

There were several qualitative differences between the proximal and distal implant positions in Experiment I. Bicortical stabilization was routinely achieved for the distal implants (figure 6.4) whereas 10% (one out of ten, either control or Ca-P implants) of the proximal implants did not achieve bicortical stabilization and these were called "floater" implants (figure 6.5 a, b, c). Only one implant did not osseointegrate and it was the "floater" control implant. In addition, 6.3% of the implant sections, either Ca-P-coated or control, showed incomplete engagement of lateral cortical bone (i.e. partial bicortical stabilization) in several histological sections (see Appendix A). This high incidence of implant with a "floating" surface was due to enlarging tibial diameter as well as inadequate implant length. As such, the "floating" surfaces were frequently the proximal sectioned surfaces of the more proximal implants (figure 6.6).

After two weeks of initial healing, the osseointegrated implants showed bone ingrowth into the porous surface region (figure 6.4, 6.7). The extent of this ingrowth, however, varied for both implant types between the cortical and medullary regions. Regions of all implants in contact with cortical bone always demonstrated abundant bone

ingrowth into the porous region. Porous surfaces that were within the medulla but in proximity to the cut endosteal surfaces of the cortex displayed considerable bone ingrowth but less than porous surfaces that were in direct contact with cortical bone. All of the observed new bone appeared woven in nature. In marked contrast, those implant surfaces situated toward the mid-medullary (i.e. distant from the endosteum) spaces were ingrown primarily with fibrous connective tissue. These observations suggest that the pattern of bone ingrowth in relation to those implant surfaces within the medulla and close to the endosteum (endosteal bone growth) resulted from osteoconduction, i.e. migration of bone cells or their precursors from the cortex and endosteum along the porous surface zone, rather than from invasion of medullary cells into the porous surface region and their subsequent differentiation into osteoblasts, although this is strictly speculation at this time. The origin and direction of endosteal bone growth could not be determined for several sections (about 9.4% of all available sections, see Appendix A) where the entire implant surface was in close proximity to the endosteum (figure 6.4 f, g) as most of the medullary space was filled with bone.

In the SEM and LM photomicrographs (figure 6.4, 6.5, 6.6, 6.7, 6.8) it can be seen that bone had penetrated to the entire depth of the porous surface zone regardless of the implant type. Thus, the bone penetration fraction (BPF) was 100% for all implants and this parameter was eliminated from the analysis.

D) Light Microscopic (LM) Examination and Morphometric Measurement

It was very difficult utilizing black and white LM photomicrographs to trace accurately bone contact with the implant surfaces under study (e.g. figure 6.7, 6.8)

because of difficulties in focusing arising from the thickness of the histological sections (about 40 μm), and because of poor contrast between bone and soft tissue. Attempts to quantify bone-to-implant contact using such photomicrographs needed to be routinely verified by direct light microscopic examination of each histological section. This made data collection difficult, time consuming and likely inaccurate so that early in the study this analytical approach was eliminated.

E) Scanning Electron Microscopic Examination and Morphometric Measurements

The morphometric measurements were submitted to an analysis of variance (ANOVA) which indicated that there were significant differences in several of the parameters used between the two implant treatment groups. Further study indicated that endosteal bone growth / ingrowth were not significantly different ($p > 0.5$) for the medial (figure 6.4 M) or lateral (figure 6.4 L) regions of the respective sections within each of the Ca-P and control implants. Hence, medial and lateral measurements could be combined for each of the Ca-P and control implants. Similarly, implant surface (PAX, DAX, DPX, PPX, PAL, DAL, DPL, PPL, see figure 5.10), proximal versus distal implant position (Experiment I), and Experiment I versus Experiment II did not result in significant differences ($p > 0.05$), suggesting that the differences observed were primarily due to treatment.

Subjective assessment suggested that there were readily apparent large variations in bone ingrowth among rabbits, and this was verified by morphometric measurement. Nevertheless, results from both Experiments I & II, when considered either individually

or together (Tables 1, 2, 3, 4), showed that the sol-gel Ca-P-coated implants consistently resulted in greater bone contact and ingrowth for each of the parameters studied.

Experiment I

The results of Experiment I are presented in Table I. Endosteal bone growth and ingrowth into the porous-surface zone (i.e. osteoconduction) in Experiment I (Table 1), where one of each implant type was placed in the right tibia, revealed that the mean absolute bone contact length (ACL) was 1.048 mm ($\pm$ 0.729 mm) for the sol-gel Ca-P-coated implants and, this value was statistically significantly higher ($p < 0.0001$) than ACL for the control implants (0.597 mm $\pm$ 0.610 mm). Likewise , contact length fraction (CLF) for Ca- P-coated implants at 42.23% ($\pm$ 17.77%) was statistically significantly greater ($p < 0.0001$) than CLF for the control implants (24.48% $\pm$ 18.00%).

The mean absolute bone ingrowth area (ABIA) for the Ca- P-coated implants was also statistically significantly greater ($p < 0.05$) than for the control implants, the values being 0.062 mm^2 ($\pm$ 0.045 mm^2) and 0.049 mm^2 ($\pm$ 0.048 mm^2) respectively. The bone ingrowth fraction (BIF), a ratio of ABIA to the total porous area available for ingrowth was not statistically significantly different ($p = 0.0766$) for the two implant types, although the mean BIF was higher for the Ca-P-coated implants. Likewise, while the mean straight line endosteal bone growth (SLBG) was higher for the Ca-P implants, the differences were not statistically significant.

Experiment II

The results of Experiment II (Table 2) in which each rabbit received one implant in each tibia were slightly different although supportive of the results of Experiment I. The mean ACL for the Ca-P-coated implants was 1.381 mm (± 0.678 mm) and for the control implants was 0.930 mm (± 0.636 mm), and these values were significantly different ($p < 0.0001$). The mean CLF for the Ca-P-coated implants was 37.38% (± 12.25%) and for the control implants was 30.30% (± 13.14%), values that again were significantly different ($p < 0.0006$) just as they were in Experiment I. The mean SLBG was 1.521 mm (± 0.631 mm) for the Ca-P-coated implants and 1.235 mm (± 0.548 mm) for the controls; however , unlike the outcome of Experiment I, these differences were significantly different ($p < 0.0005$). The mean ABIA and BIF were not statistically significantly different for the two implant types in Experiment II , although as in Experiment I, the Ca-P-coated implants always had higher values.

When the results from Experiments I and II were examined more closely, it became obvious that there were some differences between the two Experiments (Table 3). As indicated, in both Experiments the mean ACL figures were higher for the Ca-P-coated implants; however, ACL for both Ca-P and control implants in Experiment II were greater than their respective values in Experiment I. Similarly, the respective mean SLBG and ABIA values were higher in Experiment II than in Experiment I for both Ca-P-coated and control implants. As well, the control values for these two parameters in Experiment II were actually higher than for the Ca-P-coated implants in Experiment I. Because of these apparent differences between the results of the two Experiments, it was

decided to compare the two sets of results using ANOVA, and this revealed that in fact Experimental design, i.e. either two implants in right tibia (Experiment I) or one implant in each tibia (Experiment II), had no significant effect on any of the parameters used to measure endosteal bone growth or bone ingrowth. ANOVA also indicated that there were no interactions between the assessed factors with the parameters being studied. Thus the statistically significant differences in ACL, CLF, and ABIA in Experiment I and ACL, CLF and SLBG in Experiment II were interpreted to be due to the surface modification of the implant by the application of Ca-P which apparently favoured bone growth and ingrowth.

Since inter-animal variation in both Experiments was shown to be statistically independent, all of the animals from both Experiments were pooled to obtain combined mean values, and these are given in Tables 3 and 4.

The combined mean ACL was 1.177 mm ($\pm$ 0.727) mm for Ca-P-coated implants compared to 0.740 mm ($\pm$ 0.641 mm) for the control implants, and this difference was statistically significant ($p < 0.0001$). The combined means for CLF were 40.35% ($\pm$ 16.00%) versus 26.94% ($\pm$ 16.33%) for the Ca-P and control implants respectively and these differences again were statistically significant ($p < 0.0001$). The combined mean SLBG for the Ca-P-coated implants was 1.194 mm ($\pm$ 0.606 mm) and this was statistically significantly greater than that for the control implants at 1.038 mm ($\pm$ 0.615 mm) ($p < 0.001$). The combined mean ABIA was 0.074 mm^2 ($\pm$ 0.049 mm^2) for Ca-P-coated implants and this was greater than that of the control implants at 0.065 mm^2 ($\pm$ 0.079 mm^2), but the differences were not statistically significant. The combined mean

BIF at 34.695 % (± 15.71 %) for the Ca-P-coated implants almost achieved statistical significance ($p = 0.0635$) when compared to 31.021% ± 16.02% for the control implants.

Table 5 summarizes the statistical results from each individual Experiment and when the two Experiments were combined. It is important to note that only ACL and CLF were statistically significantly higher for the Ca-P-coated implants than the control implants in both Experiments I and II , and hence significantly higher for the Ca-P-coated implants in the combined data. In contrast, SLBG was not statistically significantly different for Ca-P and control implants in Experiment I, however, was highly significantly different in Experiment II (as previously noted), and this resulted in statistically significantly higher SLBG for the Ca-P-coated implants in the combined data. ABIA was statistically significantly higher at the 5% level for the Ca-P-coated implants in Experiment I but not in Experiment II. With the combined data there was no significant difference detected. BIF was higher for the Ca-P-coated implants in Experiment I and for the combined data with the respective differences almost achieving statistical significance. There were no significant differences in bone penetration fraction (BPF) for each group in each Experiment as bone penetrated equally well into the full depth of the two to three layers of spherical particles in the porous coat.

F) Freeze-Fracture SEM Observations

Figure 6.9 (a) is a photograph and figure 6.9 (b) is a composite SEM photomicrograph of a sol-gel Ca-P-coated implant recovered by freeze-fracturing the bone from the implant showing extensive bone growth from the endosteum along the

implant surface. Numerous bone spicules were observed attached to the implant surface in the medullary region.

SEM examination (250X to 1,000X) of this implant (figure 6.10) revealed that the thin Ca-P layer was well adapted to the metal substrate, bone was in direct contact with the Ca-P layer and numerous osteocytes were seen throughout the ingrown bone. At higher magnifications (figure 6.11, 1,500X to 20,000X), it was evident from several available cross-sectional freeze-fractured views that the thickness of the calcium phosphate layer was variable. Most of the surface of the spherical particles of the porous coat appeared to have a thickness of Ca-P in excess of the intended 0.3 μm (commonly seen thickness was about 1 μm). In the neck regions (figure 6.12, 1,000X to 10,000X) between contiguous spherical particles, however, the Ca-P layer was somewhat thicker (>= 1.5 μm).

At magnifications of 1,000X or greater where bone appeared to be bonded with the Ca-P layer there was an afibrillar layer possibly representing Ca-P layer dissolution and remineralization between the Ca-P and adjacent new bone (Jarcho *et al.* 1972, 1981; LeGeros *et al.* 1991). This afibrillar layer is separated from the bone matrix by a thin electron-dense line which resembled a cement line (Davies *et al.* 1990 a, 1991 a, b), contained numerous collagen fibrils connecting bone to the Ca-P layer (figure 6.10, 6.11, 6.12, 6.13). Also of interest was the observation that bone ingrowth into the neck regions appeared to be substantial , was in direct contact with the Ca-P layer and filled much of the porosity adjacent to the necks (figure 6.12), a finding which had not been seen in previous investigations (Deporter *et al.* 1986). It was, therefore, decided to re-examine all of the implant sections using higher magnification backscattered electron imaging

SEM micrographs to determine if there were detectable differences in bone ingrowth in relation to these neck regions between the two implant types.

G) Analysis of Extent of Bone Ingrowth in Relation to Neck Regions

Bone ingrowth into the neck regions observed in backscattered electron imaging SEM's was categorized into 3 groups (Groups 1, 2 & 3) depending on extent of bone fill. Neck regions with less than a third of the area filled with bone were assigned to Group "1". Neck regions with one third to two thirds filled with bone were labeled Group "2". Neck regions with at least two thirds to the entire neck area filled with bone were assigned to Group "3". Analysis of this data using ANOVA revealed that there was no effect of individual section (e.g. PAX, DAX), medial or lateral implant region, or implant position in either the Ca-P-coated or control implants.

This data suggested more extensive bone ingrowth and direct bone apposition in the neck regions of Ca-P-coated implants than control implants (figure 6.14, Table 6). Thus, the Ca-P-coated implants demonstrated similar (roughly one-third of the total) numbers of neck regions in each of the three Groups. There were significantly more ($p < 0.0001$) neck regions in Groups 2 and 3 with the Ca-P-coated implants than with the controls. In contrast, there were significantly less ($p < 0.0001$) neck regions in Group 1 of the Ca-P-coated implants than with the controls (Table 7). The control implants showed the majority of neck regions classified as Group 1 (50% to 70%). Only 15% to 30% of the neck regions of the control implants were classified as Group 2 and the remaining 10 to 15% as Group 3.

There were two (Experiment II) to three (Experiment I) times as many neck regions in Group 3 with the Ca-P-coated implants than with the control implants. As well, in Experiment I there were two times as many neck regions in Group 2 with the Ca-P-coated implants as with the controls, although this difference was not seen in Experiment II. These results were analyzed using ANOVA. For each of the Ca-P and control implants, the number of neck regions in Groups 1, 2 or 3 were in each case multiplied by the group number (i.e. 1, 2 or 3) indicating the extent of bone ingrowth , and these numbers were used to determine a weighted average for bone ingrowth into the neck regions for each implant type. This weighted average was 2.01 for the Ca-P sol-gel coated implant group and 1.47 for the control implant group, and the difference was statistically significant ($p < 0.0001$), demonstrating that the Ca-P-coated implants had significantly more extensive bone ingrowth into the neck regions than the control implants.

Figure 6.1: The two implant types used in the study. The sol-gel Ca-P-coated implant is the darker implant (a) while the lighter-colored implant is the control implant (b).

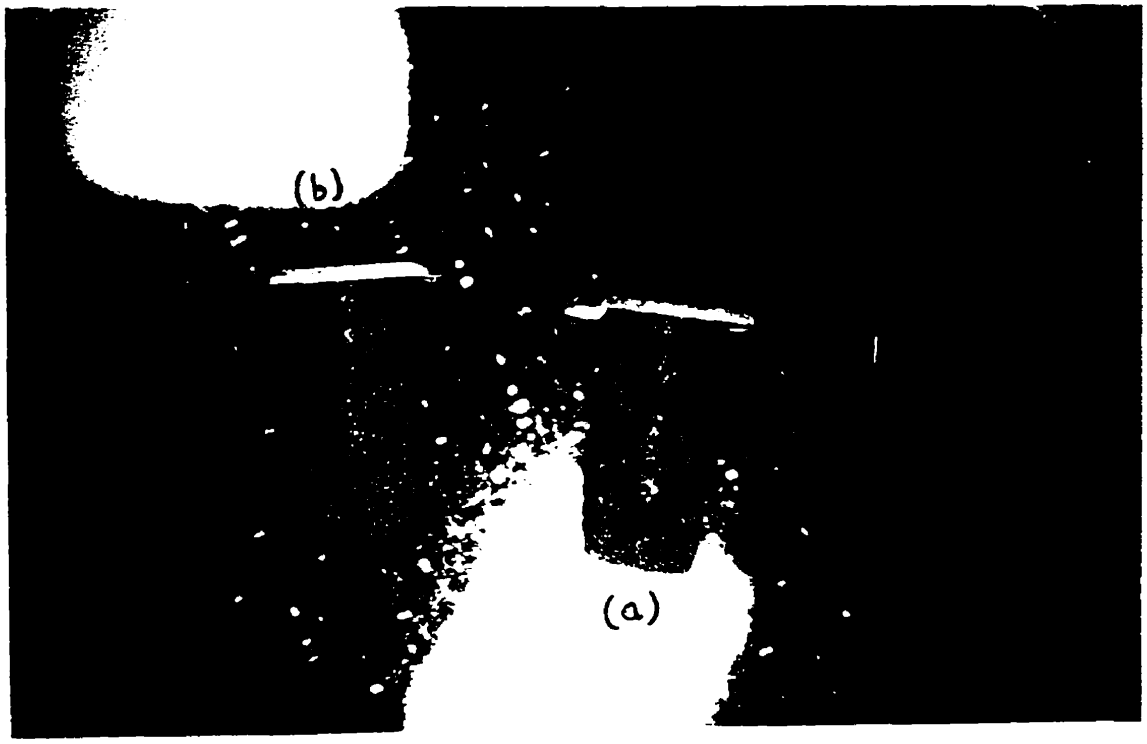

Figure 6.2: SEM photomicrographs showing surface topography of the control implant (a = 300X) and the thin Ca-P film (b = 300X & c = 500X) typically covering the spherical particles of the porous surface of an as-received, un-implanted sol-gel Ca-P-coated implant. This verifies that the pores had not been occluded by the sol-gel Ca-P treatment. The Ca-P film appeared somewhat rough and granular thus imparting an additional secondary microtextured topography to the porous surface.

(a)

(b)

(c)

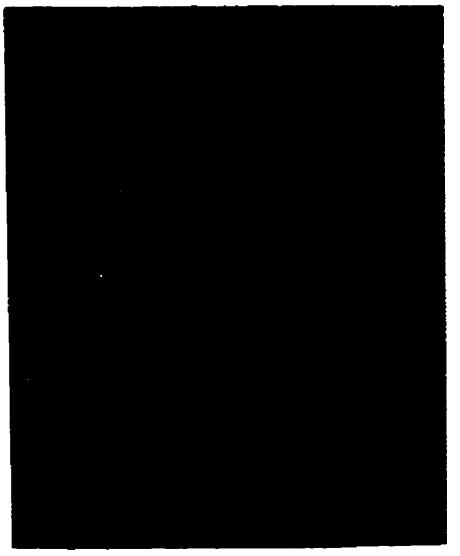

Figure 6.3: SEM photomicrographs of part of the field in figure 2 at higher magnifications (a & b = 2,000X ; c & d = 5,000X) showing a typical Ca-P layer in the neck regions between adjacent spherical particles or between the deepest layer of spherical particles and the solid machined implant core. In these regions the film appeared thicker and showed signs of surface cracking and delamination.

(a)

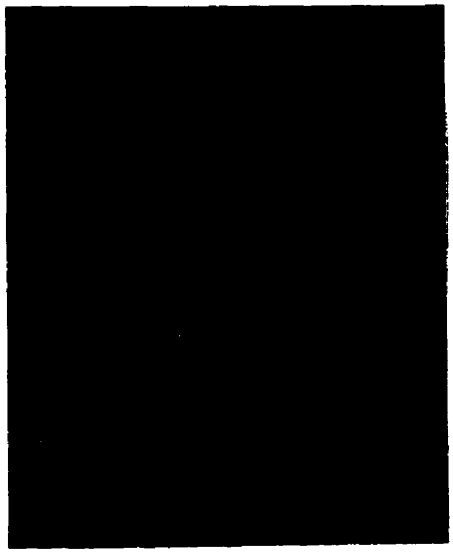

(b)

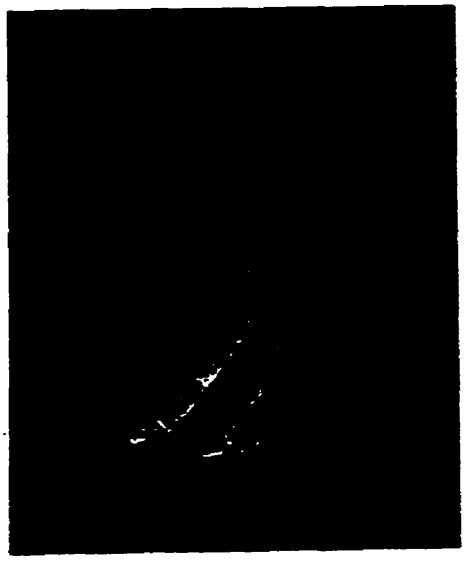

(c)

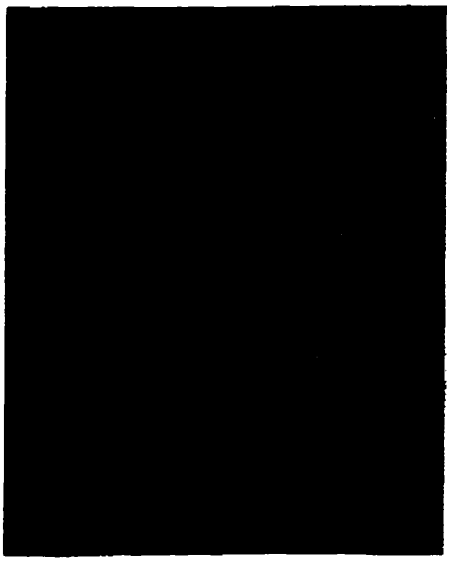

(d)

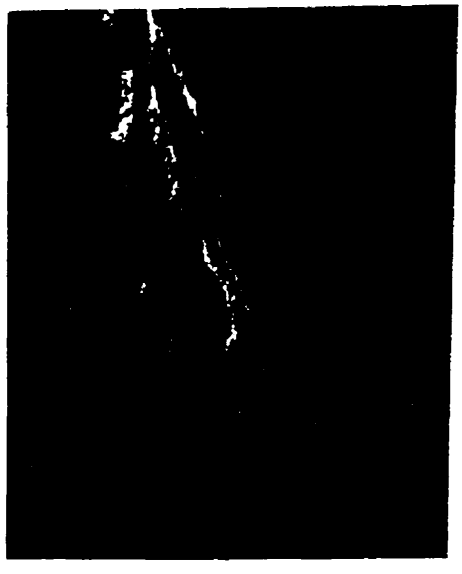

Figure 6.4: SEM photomicrographs (a, b, c, d) showing that bicortical stabilization or engagement by the implant was routinely achieved for the distal implants and in 90% of the proximal implants in Experiment I. Note that bone had penetrated to the entire depth of the porous surface as in the enlarged photomicrograph (e). The top right represents the medial (M) and the lower left represents the lateral (L) aspect of the implant in relation to the tibia. (f) & (g) illustrate implant sections situating too close to the endosteum along its entire length, hence it was not possible to determine the origin and direction of bone growth.

(a)

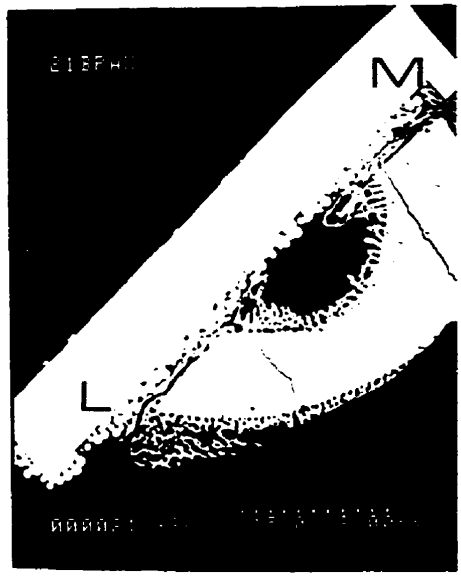

(b)

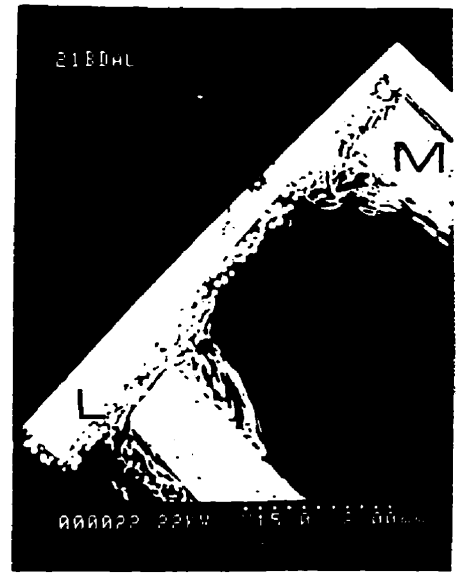

(c)

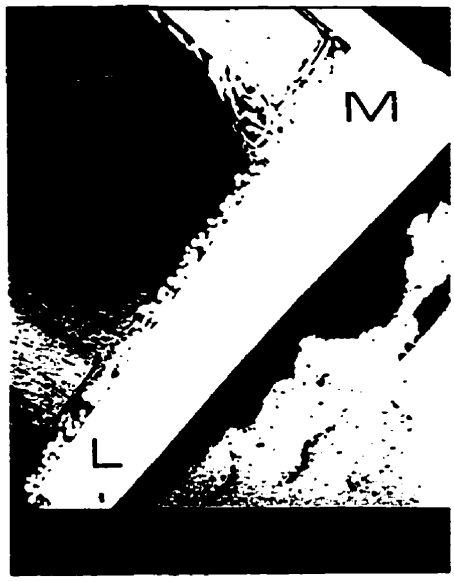

(d)

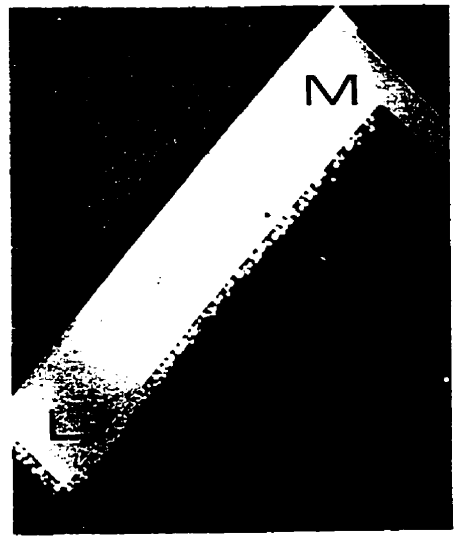

(e)

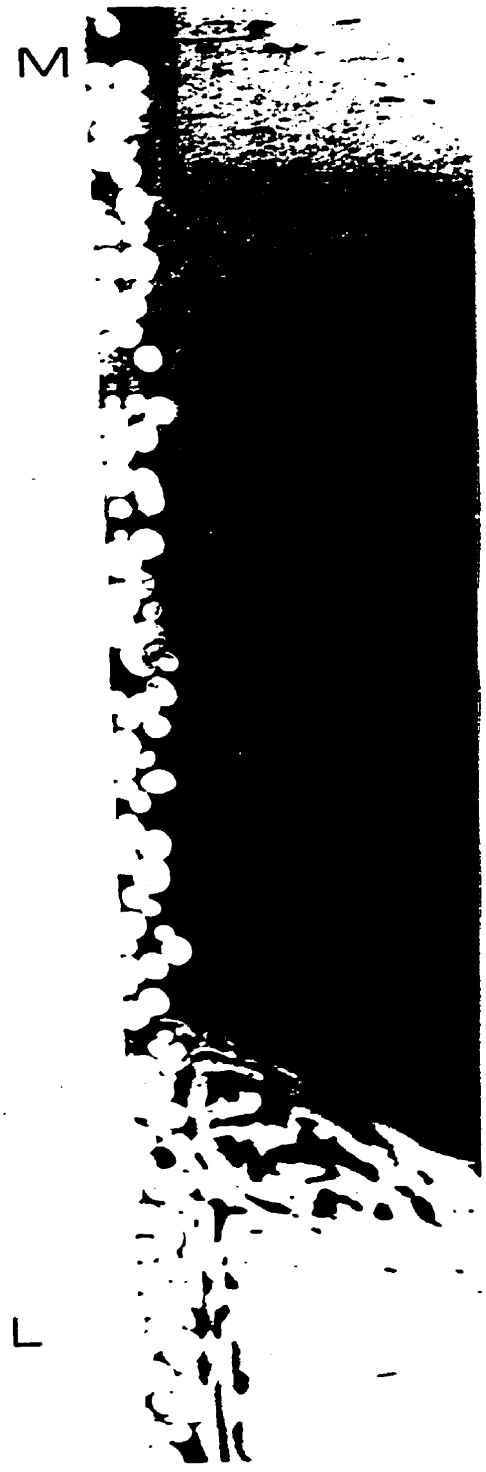

(f)

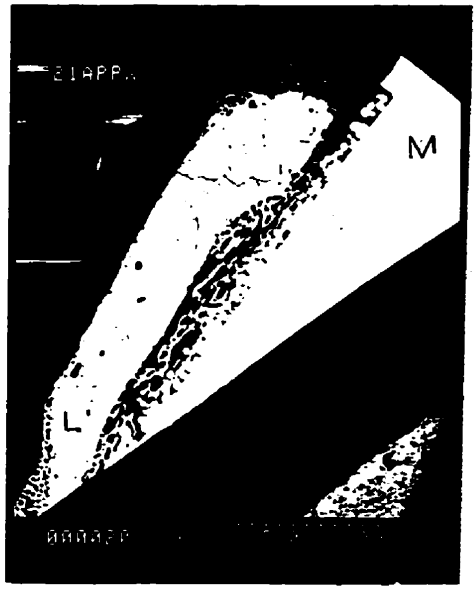

(g)

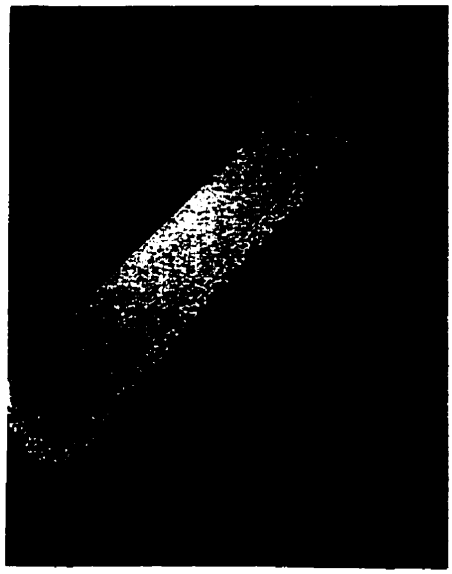

Figure 6.5: SEM photomicrographs (a, b, c) for Experiment I showing a proximal implant that did not achieve bicortical stabilization and was called "floater" implant.

(a)

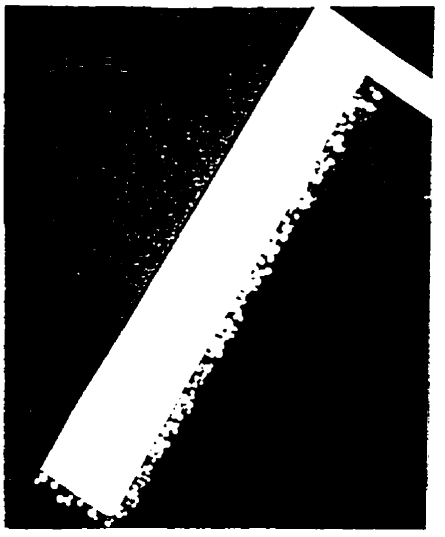

(b)

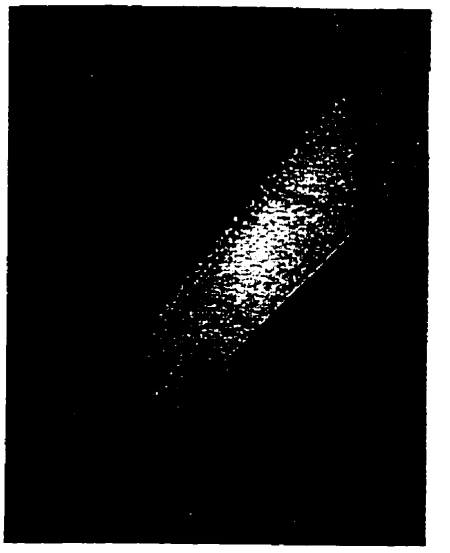

(c)

Figure 6.6: SEM photomicrograph of a section showing incomplete engagement of lateral cortical bone. This implant with a "floating" surface was due to enlarging tibial diameter as well as inadequate implant length. As such, the "floating" surfaces were frequently the proximal sectioned surfaces of the more proximal implants (PAX, PPX, PAL, PPL) in Experiment I.

Figure 6.7: Light microscopic photomicrographs showing bone ingrowth into the porous surface zone. The extent of this ingrowth, however, varied for both the Ca-P-coated implants (a) and the control implants (b) between the cortical and medullary regions. Porous surface zones that were within the medulla but in proximity to the cut endosteal surfaces of the cortex displayed considerable bone ingrowth but less than porous-surface zones that were in direct contact with cortical bone. All of the observed new bone appeared woven in nature. In contrast, those implant surfaces situated toward the mid-medullary (i.e. distant from the endosteum) spaces were ingrown primarily with fibrous connective tissue. Note that bone had penetrated to the entire depth of the porous coat regardless of the implant type.

(a)

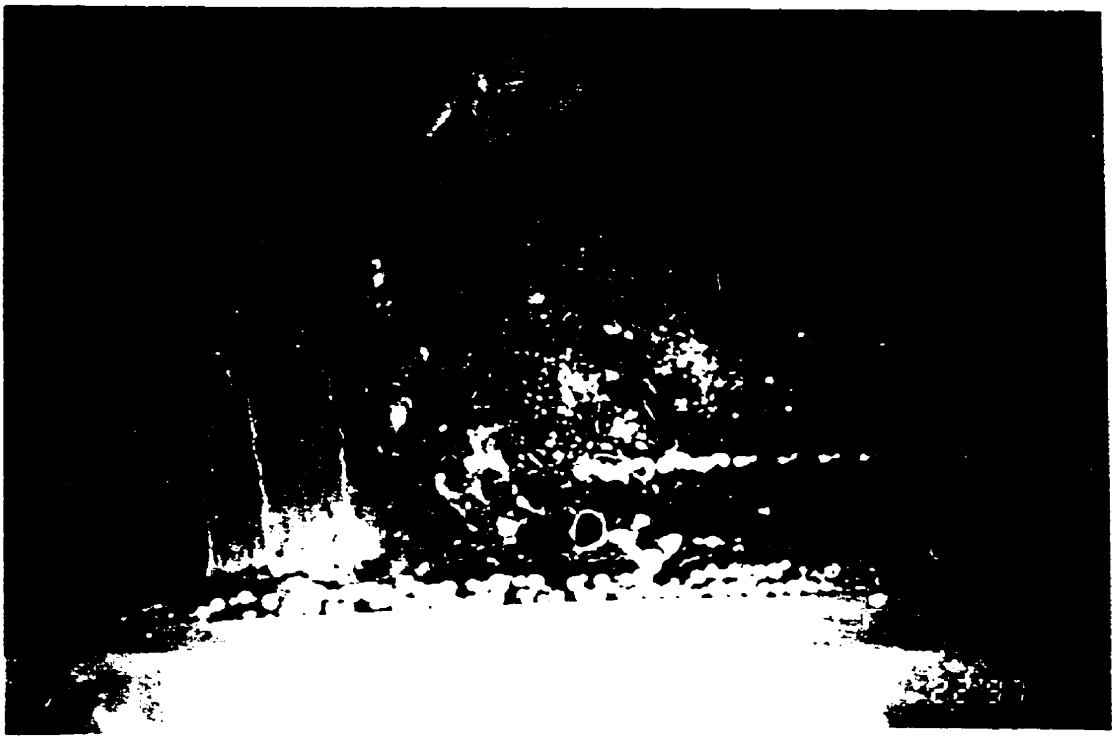

(a)

(b)

(b)

Figure 6.8: Black and white LM photomicrograph tracing of bone contact with the implant surfaces was inaccurate because of difficulties in focusing arising from the thickness of the histological sections (~ 40 μm), and because of poor contrast between bone and soft tissue. Attempts to quantify bone-to-implant contact using such photomicrographs needed to be routinely verified by direct light microscopic examination of each histological section.

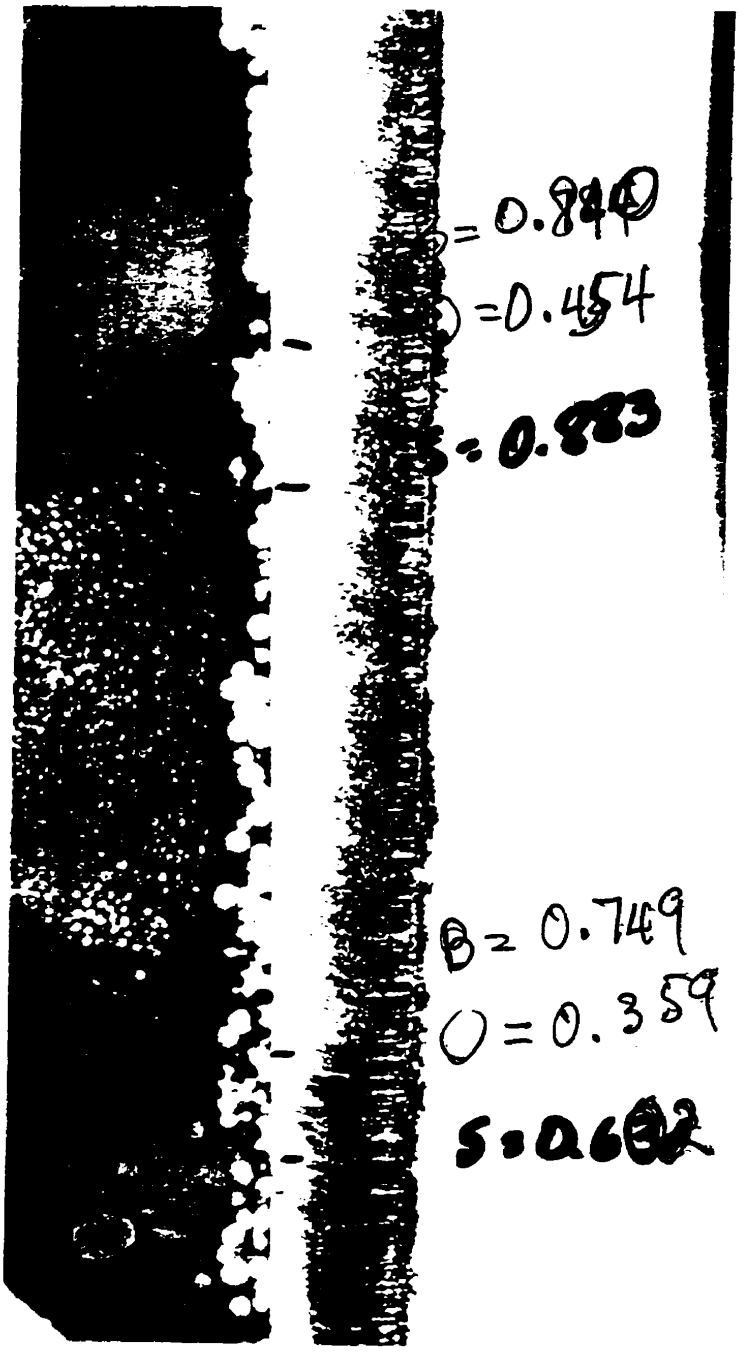

Figure 6.9: (a) is a photograph and (b) is a composite SEM photomicrograph of a sol-gel Ca-P-coated implant recovered by freeze-fracturing the bone from the implant showing extensive bone growth from the endosteum (E) along the implant surface. Numerous bone spicules were observed attached to the implant surface in the medullary (M) region.

(a)

(b)

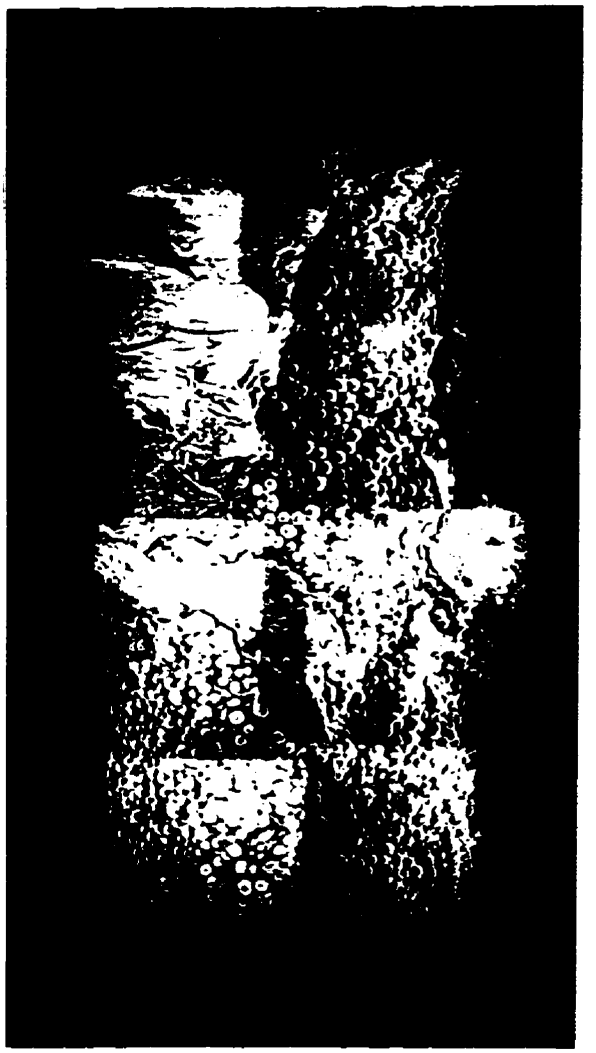

Figure 6.10: SEM photomicrographs (250X to 1,000X) of freeze-fractured implant revealed that the thin Ca-P layer was well adapted to the metal substrate, bone matrix was in direct contact with the Ca-P layer (a, b, c) and numerous osteocytes (Oc) were seen throughout the ingrown bone (d).

(a)

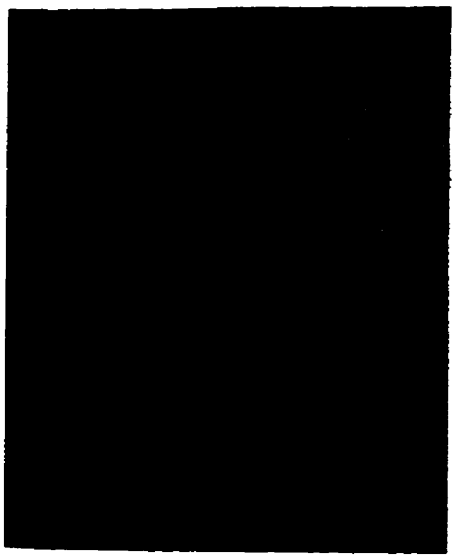

(b)

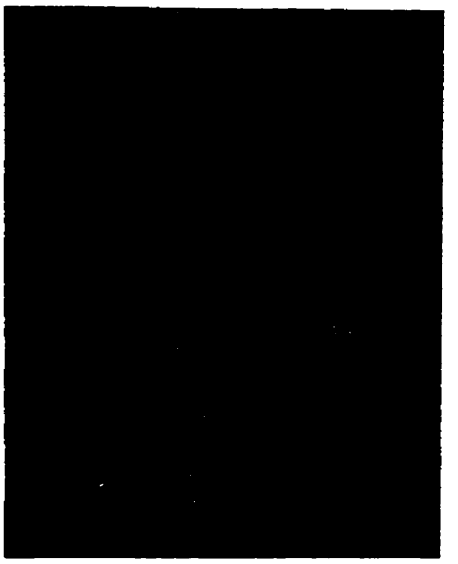

(c)

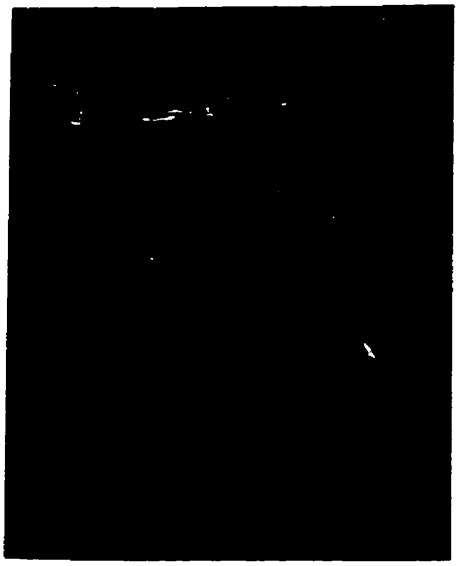

(d)

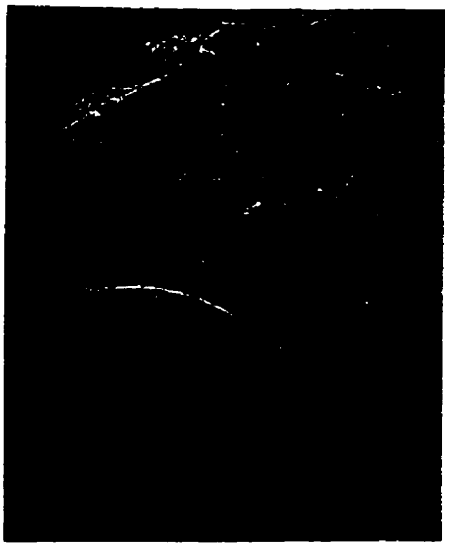

Figure 6.11: SEM photomicrographs of freeze-fractured implants at higher magnifications (1,500X to 20,000X), it was evident that the thickness of the calcium phosphate layer was variable. Most of the surface of the spherical particles of the porous surface zone exhibited a thickness of Ca-P in excess of the intended 0.3 μm (commonly seen thickness was about 1 μm).

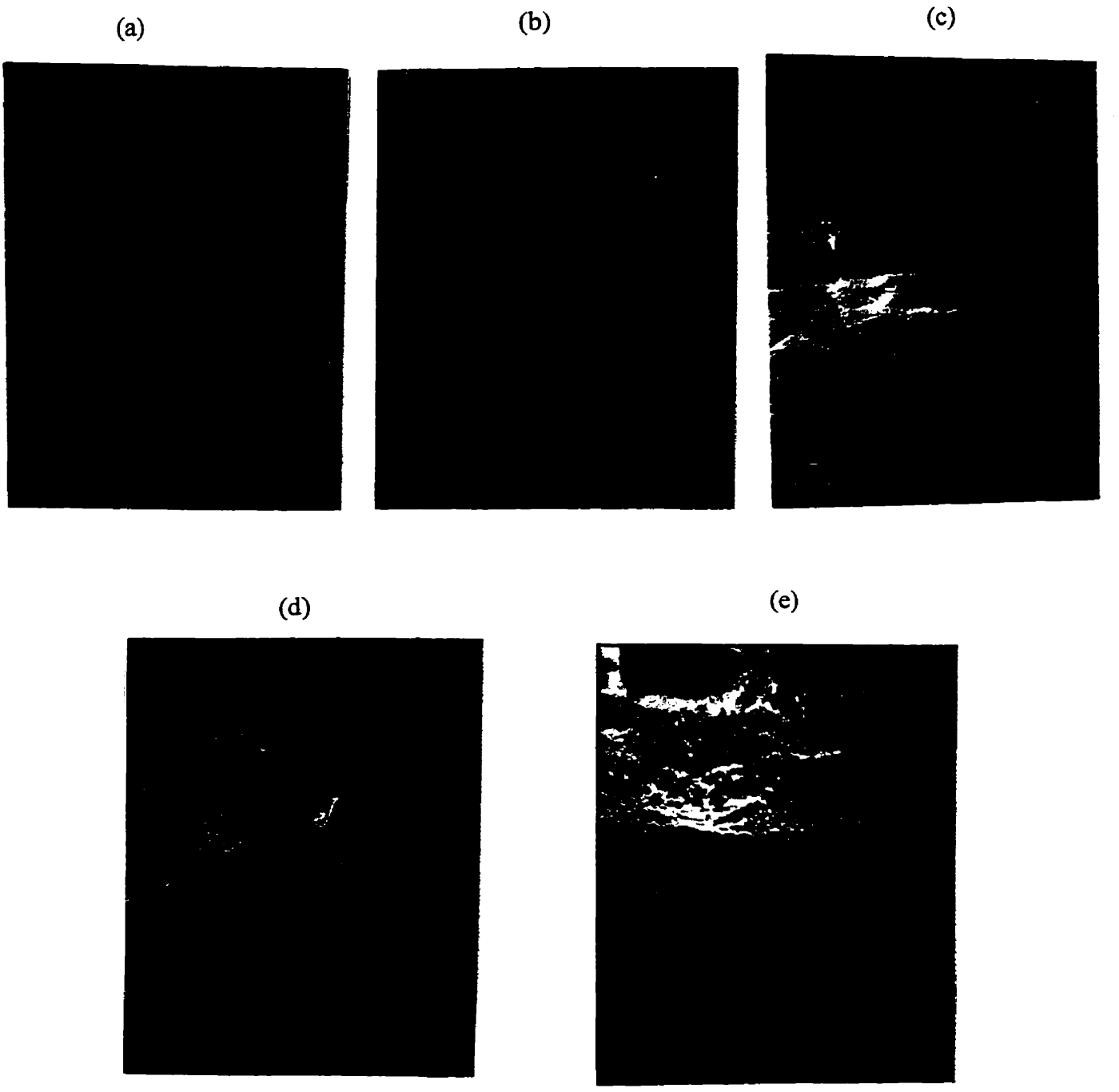

Figure 6.12: SEM photomicrographs of freeze-fractured implants at higher magnifications in the neck regions (1,000X & 10,000X) between contiguous spherical particles showing the Ca-P layer was somewhat thicker (>= 1.5 μm). These photomicrographs shows that even if the Ca-P layer may have been delaminated or exhibited areas devoid of it, bone appeared to grow between the Ca-P the titanium alloy or managed to bridge the segmented Ca-P layer respectively. Bone was in direct contact with the Ca-P layer and filled much of the porosity adjacent to the necks

(a)

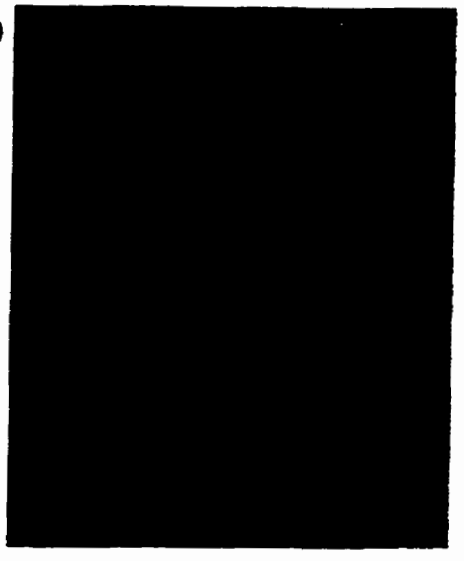

(b)

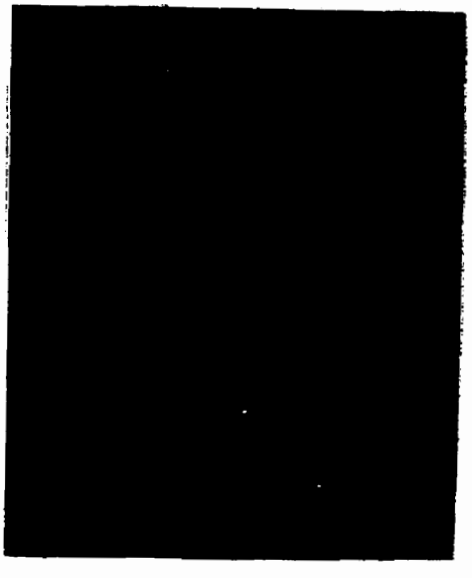

(b)

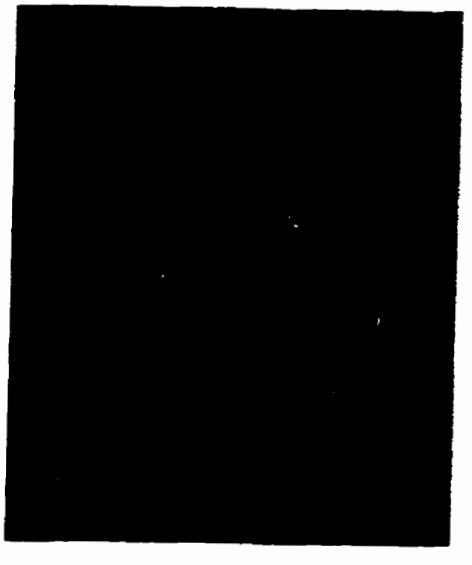

Figure 6.13: SEM photomicrographs (1,000X to 20,000X) illustrating an interposing layer bonding bone with the Ca-P layer. There appears to be an afibrillar layer (af) connecting the Ca-P layer to the adjacent new bone via this cement line-like structure (cm) by numerous collagen fibrils (cf).

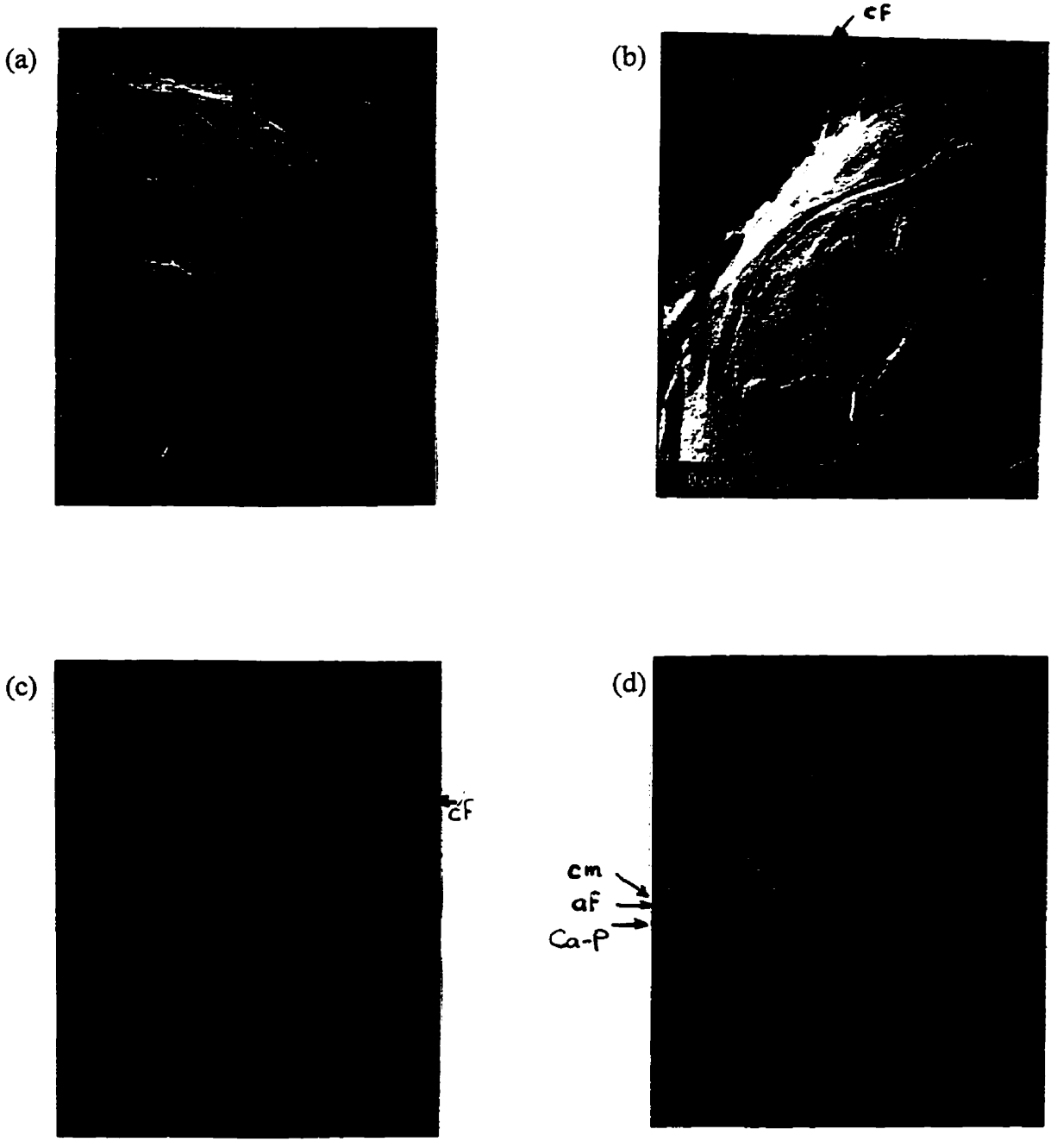

(e)

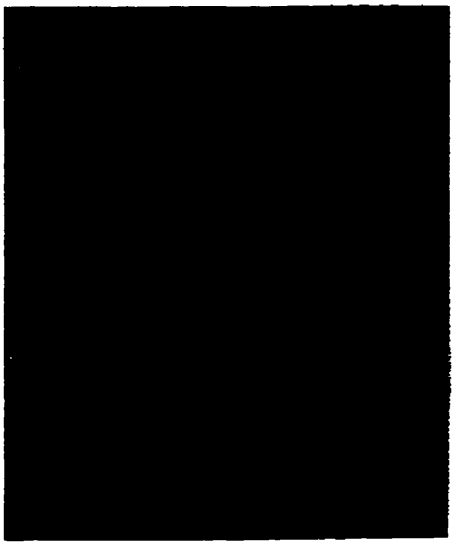

(f)

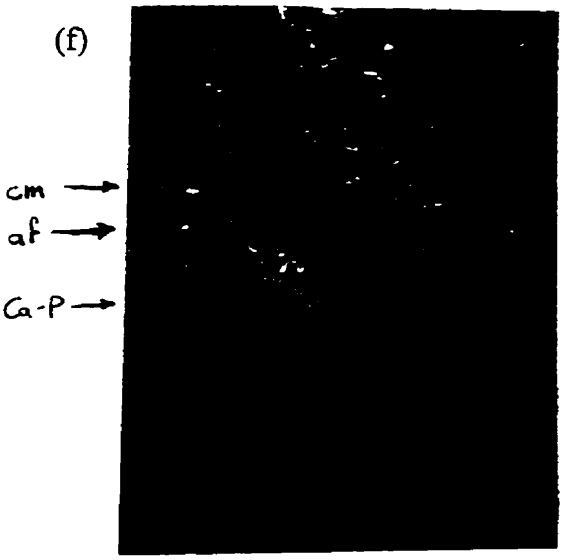

(g)

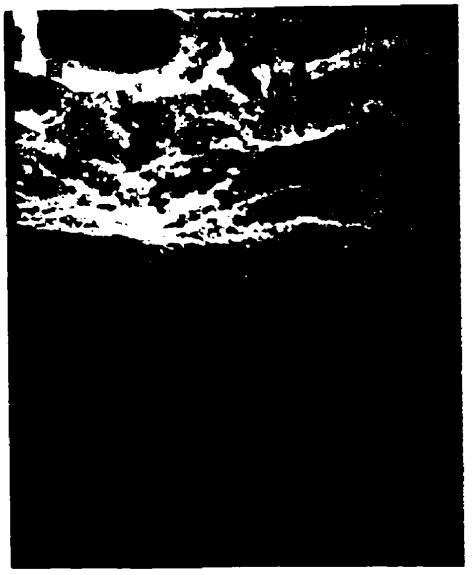

Figure 6.14: SEM photomicrographs showing that bone ingrowth into the neck regions of the Ca-P-treated implants appeared to be substantial (a) and was in direct contact with the Ca-P layer and filled much of the porosity adjacent to the necks. In contrast, bone ingrowth into the neck regions of control implants appeared to be less pronounced and did not fill much of the porosity adjacent to the necks (b).

(a)

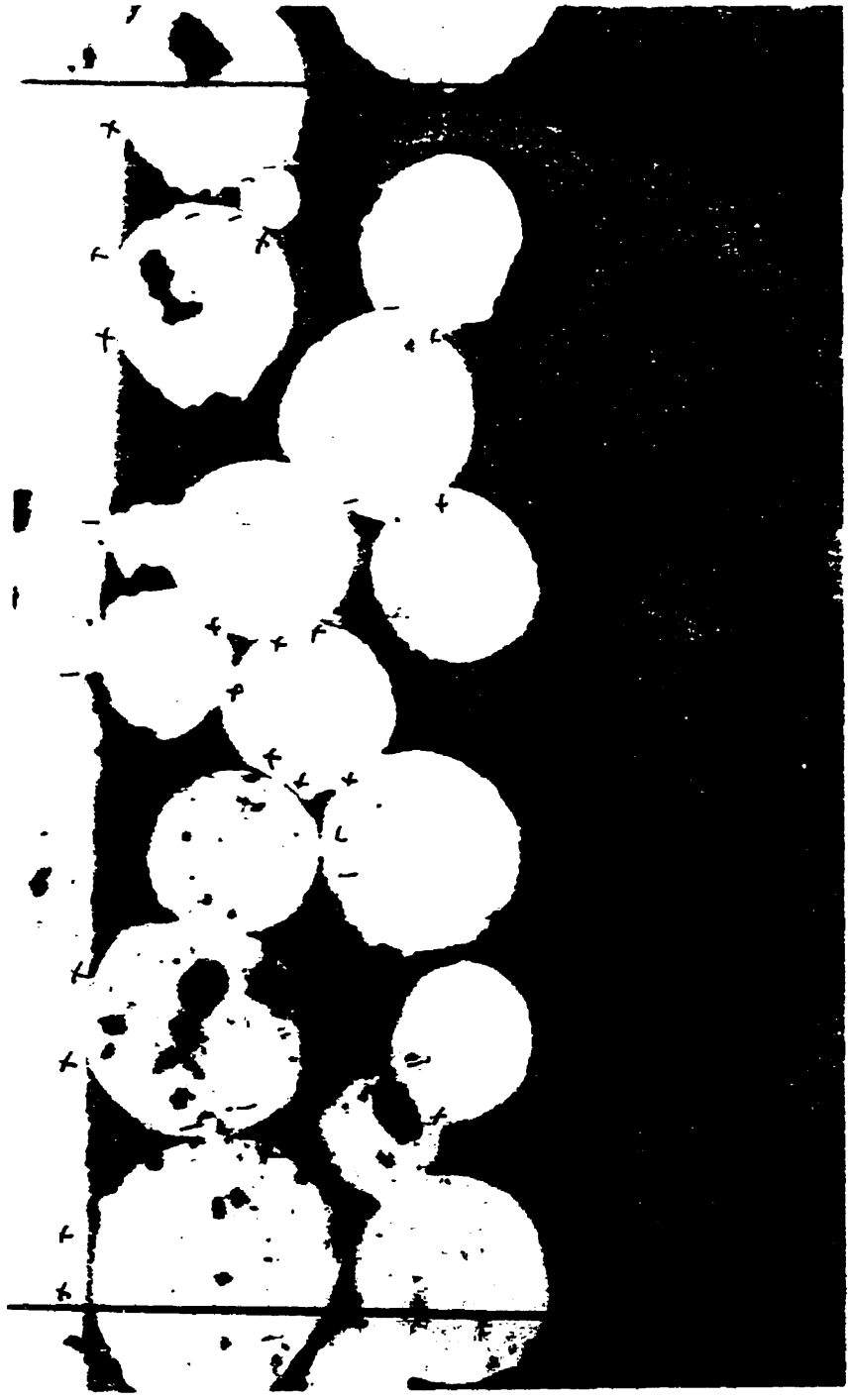

(b)

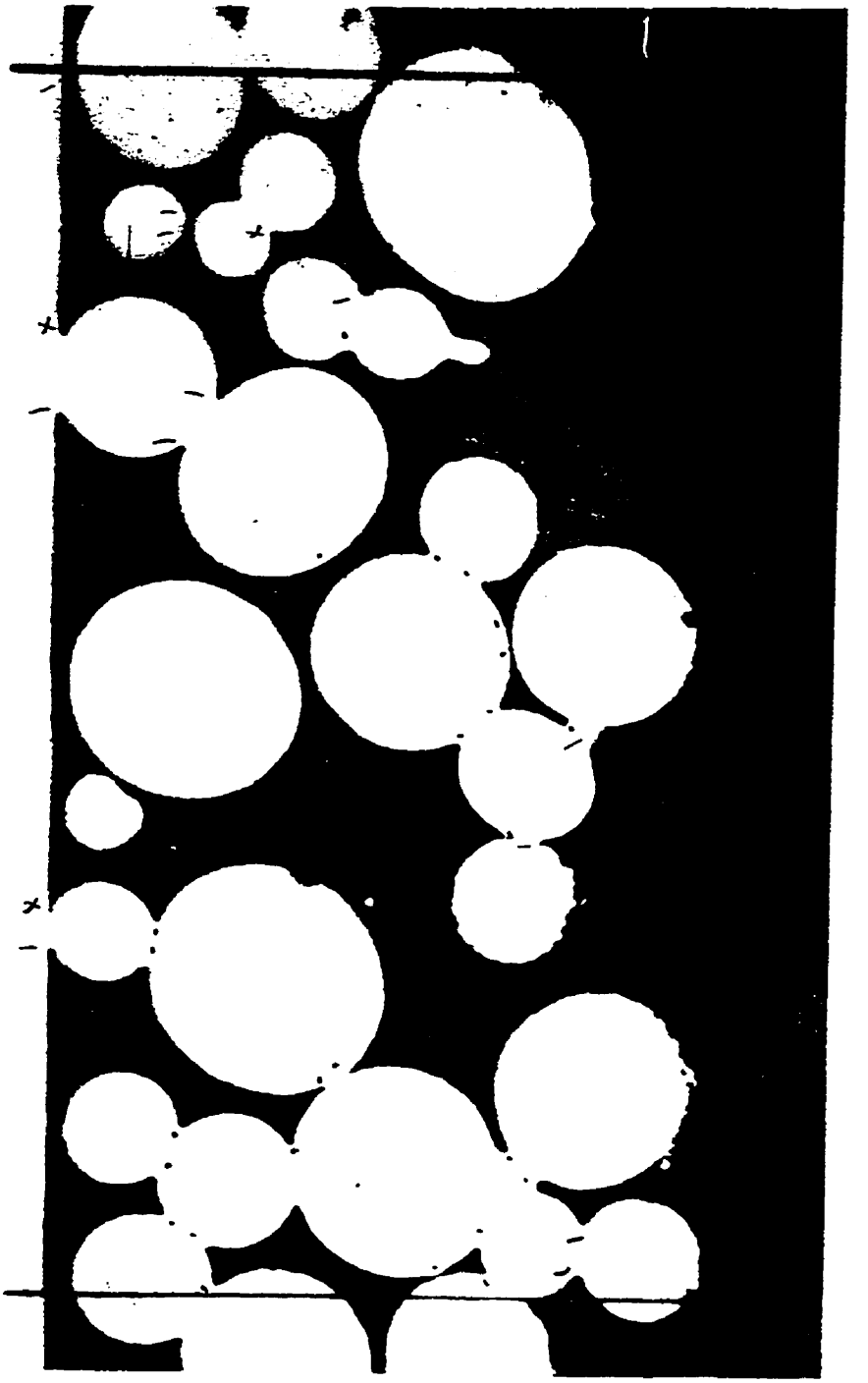

Table 1: Mean morphometric measurement and statistical analysis results for Experiment I in which one Ca-P-coated and one control implant was placed in the right rabbit tibia (pilot animals were excluded).

	Ca-P-coated implants n = 10	Control implants n = 10	STAT
Variable	Mean (±SD)	Mean (±SD)	
ACL (mm)	1.048 (±0.729)	0.597 (±0.610)	p = 0.0001
CLF (%)	42.23 (±17.77)	24.48 (±18.00)	p = 0.0001
SLBG (mm)	0.985 (±0.488)	0.891 (±0.624)	NS
ABIA (mm^2)	0.062 (±0.045)	0.049 (±0.048)	p = 0.0453
BIF (%)	34.63 (±17.41)	29.05 (±18.53)	p = 0.0766 NS
BPF (%)	100	100	NS

ACL: Absolute Bone Contact Length

CLF: Contact Length Fraction

SLBG: Straight Line Bone Growth

ABIA: Absolute Bone Ingrowth Area

BIF: Bone Ingrowth Fraction

BPF: Bone Penetration Fraction

Table 2: Mean morphometric measurements and statistical analysis results for Experiment II in which only one implant, either Ca-P-coated or control, was placed into each rabbit tibia.

	Ca-P-coated implants n = 6	Control implants n = 6	STAT
Variable	Mean (±SD)	Mean (±SD)	
ACL (mm)	1.381 (±0.678)	0.930 (±0.636)	p = 0.0001
CLF (%)	37.38 (±12.25)	30.30 (±13.14)	p = 0.0006
SLBG (mm)	1.521 (±0.631)	1.235 (± 0.548)	p = 0.0004
ABIA (mm^2)	0.092 (±0.049)	0.087 (±0.103)	NS
BIF (%)	34.80 (±12.69)	33.57 (±11.61)	NS
BPF (%)	100	100	NS

Table 3: Mean morphometric results for Experiments I, II and combined data from Experiments I & II.

	Experiment I n = 10		Experiment II n = 6		Experiment I & II n = 16	
	Ca-P	Control	Ca-P	Control	Ca-P	Control
ACL (mm)	1.048	0.597	1.381	0.930	1.177	0.740
CLF (%)	42.24	24.48	37.38	30.30	40.35	26.94
SLBG (mm)	0.985	0.891	1.521	1.235	1.194	1.038
ABIA (mm^2)	0.062	0.049	0.092	0.087	0.074	0.065
BIF (%)	34.63	29.05	34.80	33.57	34.70	31.02

Table 4: Mean morphometric and statistical results for the combined data from Experiments I & II.

	Ca-P-coated implants n = 16	Control implants n = 16	STAT
Variable	Mean (±SD)	Mean (±SD)	STAT
ACL (mm)	1.177 (±0.727)	0.740 (±0.641)	p = 0.0001
CLF (%)	40.350 (±16.00)	26.964 (±16.33)	p = 0.0001
SLBG (mm)	1.194 (±0.606)	1.038 (±0.615)	p = 0.0013
ABIA (mm^2)	0.074 (±0.049)	0.065 (±0.079)	NS
BIF (%)	34.695 (±15.712)	31.021 (±16.016)	p = 0.0635
BPF (%)	100	100	NS

Table 5: Summary of statistical results.

	Experiment I	Experiment II	Experiments I & II
ACL (mm)	p = 0.0001	p = 0.0001	p = 0.0001
CLF (%)	p = 0.0001	p = 0.0006	p = 0.0001
SLBG (mm)	NS	p = 0.0004	p = 0.0013
ABIA (mm^2)	p = 0.0453	NS	NS
BIF (%)	NS p = 0.0766	NS	NS p = 0.0635
BPF	NS	NS	NS

Table 6: Average number of neck regions exhibiting each of the different category of bone ingrowth (Group 1: no bone filled to less than one-third , Group 2: one-third to less than two-thirds bone filled, Group 3: at least two-thirds to completely filled with bone) in the medullary space within 700 μm from the endosteal cortical bone level.

	Ca-P-coated implants n = 16			Control implants n = 16		
	Group 1	Group 2	Group 3	Group 1	Group 2	Group 3
Experiment I	11.4	9.3	9.3	21.7	5.1	2.9
Experiment II	7.7	9.2	10.7	16.9	9.1	5.3
Experiments I & II	9.9	9.3	9.8	19.7	6.8	3.9

Table 7: Summary of statistical results of the pattern of bone ingrowth.

		Ca-P-coated implants		
	Extent of bone ingrowth	Group 1	Group 2	Group 3
Control implants	1	p = 0.0001		
	2		p = 0.0001	
	3			p = 0.0001

Appendix A

Breakdown of available histological sections into usable and unusable sections.

	Experiment I		Experiment II		Experiment I & II		Overall Total
	Ca-P	Control	Ca-P	Control	Ca-P	Control	Ca-P & Control
Rabbits (n)	10	10	6	6	16	16	16
Available sections	80	80	48	48	128	128	256
Too close to cortex sections	6 (7.5%)	8 (10%)	6 (12.5%)	4 (8.3%)	12 (9.4%)	12 (9.4%)	24 (9.4%)
Floater sections	8 (10%)	8 (10%)	0	0	8 (6.3%)	8 (6.3%)	16 (6.3%)
Usable sections	66 (82.5%)	64 (80%)	42 (87.5%)	44 (91.7%)	108 (84.4%)	108 (84.4%)	216 (84.4%)
Unusable sections	14 (17.5%)	16 (20%)	6 (12.5%)	4 (8.3%)	20 (15.6%)	20 (15.6%)	40 (15.6%)

VII) DISCUSSION

The purpose of this study was to investigate the effects of the application by sol-gel technique of an ultrathin layer of calcium phosphate (Ca-P) on the early healing responses to porous-surfaced dental implants. The hypothesis tested was that Ca-P would act as an osteoconductive substrate and thereby increase the rate and extent of bone growth and ingrowth in relation to porous-surfaced implants. The overall results supported this hypothesis with the sol-gel Ca-P-coated implants showing greater bone contact and ingrowth at 2 weeks of healing compared to the control implants. The differences in osteoconductivity were detected by histomorphometric analyses of bone growth / ingrowth in relation to the porous surface alone using several different parameters (ACL, CLF, SLBG, ABIA, BIF), and by the extent of bone ingrowth into the neck regions between adjoining spherical particles constituting the porous surface region.

The two implant types used in the present study could be easily distinguished from each other macroscopically because the sol-gel Ca-P layer imparted a grayish colour to the implant surface. At SEM magnifications of 2000X or greater , the Ca-P layer was shown to be well adapted to the metal substrate and to have penetrated the entire thickness of the porous zone. The thickness of this surface coat was greater than intended, being frequently in the 1μm range rather than in the intended range of 0.3 to 0.5 μm. However, this somewhat thicker film did not occlude the pores within the porous zone, and, therefore, did not appear to affect the overall surface geometry in an unfavourable way. The sol-gel-formed Ca-P coating was successful in improving the conditions for bone growth and ingrowth.

The technique used for sol-gel Ca-P thin film application employed in this investigation was a dip coating technique. The porous-surfaced implant was dipped into a solution containing the calcium and phosphate particulates, vertically withdrawn at a controlled rate of 100 mm per minute, allowed to dry, and finally vacuum-annealed at 683° C for 15 minutes. This type of processing should have resulted in a calcium phosphate layer 0.3 to 0.5 μm thick based on published data (Bautigam *et al.* 1989; Qiu *et al.* 1993; Filiaggi *et al.* 1996 a, b). The film thickness achieved was about 1 μm on the surfaces of the spherical particles of the porous zone but in excess of 1.5 μm in the neck regions between the particles of the porous zone. It has been reported that film thickness varies inversely with the square root of the withdrawal speed (Gugliemi *et al.* 1992). Hence, a faster rate of withdrawal is predicted to result in a thicker film than a slower rate of withdrawal (Strawbridge and James 1986; Bautigam *et al.* 1989). A dipping rate of about 200 mm per minute was shown to give a coating thickness of about 0.1 - 0.2 μm (Bautigam *et al.* 1989). The withdrawal speed used in the present study was slower (100 mm/min.) and should have resulted in a thinner or at least as thin a layer as that achieved by Bautigam *et al.* (i.e. 0.2 μm in thickness); however, this was not found to be the case. This difference in results may have been due to the fact that the metal substrate used in the present study consisted of a porous surface which possessed surface irregularities which might have affected the flow characteristics as well as the retention of the gel solution compared to a relatively smooth and flattened metal or quartz substrate as used by Bautigam *et al.* and others (Qiu *et al.* 1993; Nordstrom *et al.* 1994). The thicker Ca-P layer produced in the present study also may have been partially caused by high surface tension again arising from the irregularities of the porous surface region creating a capillary-like action and "trapping" the Ca-P solution. Two other possible explanations

for the thicker Ca-P layer despite the slower withdrawal speed should be considered. Firstly, the viscosity of the solutions used here may have differed significantly from those used by others. Secondly, the Ca-P solution used in the present study was unlikely to have been a true solution as it was prepared as a particulate (i.e. colloidal solution) and, therefore, may not have had the flow and adhesion characteristics of a true solution (Filiaggi 1995 Ph.D. thesis & personal communication). Since there were few freeze-fractured SEM views representative of true cross-sectional fracture through the Ca-P layer that would give an accurate measurement of the Ca-P layer thickness, further investigation into sol-gel Ca-P film thickness on porous-surfaced implant is required.

As the sol-gel Ca-P layer used here was thicker than intended, it was susceptible to surface cracking as has been reported for such coatings as thickness increases beyond 0.3 μm (Nordstrom *et al.* 1994). In the one as-received calcium phosphate-coated implant which was not implanted in the present investigation, but examined directly by SEM, surface cracking of the Ca-P coating was not observed regularly on the surfaces of the spherical particles of the porous surface zone away from the neck regions. However, it was regularly observed in the neck regions and sometimes in association with early signs of delamination of the Ca-P layer. The two implants which were freeze-fractured prior to examination similarly demonstrated this cracking of the Ca-P layer in the neck regions. This cracking phenomenon is likely attributable to the thicker Ca-P layer (greater than 1.5 μm) observed in the neck regions. Others have shown that when sol-gel film thickness exceeds 0.3 μm, cracking and flaking is more frequently observed (Nordstrom at al. 1994). These freeze-fractured specimens also showed delamination of the Ca-P layer from the outermost surfaces of particles of the porous surface zone away from the neck region. Thus, it was observed that during the freeze-fracturing procedure the Ca-P layer

separated from the metal substrate and remained attached to the adjacent bone surface. The following is proposed to explain this observation. The implants used in the present investigation were cylindrical in shape and were slightly larger in diameter than the surgical burs used to create the implant site. These "press-fit" implants were installed into the prepared sites using rotational force delivered in both a clockwise and counter-clockwise manner with a hemostat used to grip the flattened head of the implant. This installation process may have resulted in delamination and / or abrasion of the sol-gel Ca-P coating on the outermost surfaces of the porous surface region. This may have some clinical relevance as the intended benefit of the applied Ca-P layer may be lost on the outermost surfaces of the sol-gel coated implants during implant installation. However, in some instances where small areas of delamination had occurred, it was observed that new bone had been deposited onto the metal substrate beneath the delaminated Ca-P layer indicating that the intended Ca-P benefit was not affected by the delamination. Other possible reasons for delamination include; i) artifacts from the freeze-fracturing process as the metal and the Ca-P layer have different thermal co-efficients of expansion / contraction; ii) the Ca-P layer along with the attached bone, being on the outer surface and readily accessible to liquid CO_2 , may be well frozen while the underlying metal substrate , being much thicker, deeper and less accessible to liquid CO_2 , may not have reached the same temperature.

Several problems were encountered with the experimental design as originally proposed. In the pilot study using 4 animals, two implants were placed in the mid-shaft area of the right tibia. As it turned out this region of the tibia has the smallest overall diameter and, therefore, once the two implant sites had been prepared the remaining bone

volume was insufficient to withstand the forces associated with subsequent loading of the bone, with the result that these rabbits developed pathological tibial fractures at day-three to day-five following implantation and had to be sacrificed. To correct this problem, the experimental protocol was modified to place the two implants more proximally towards the metaphysis. This protocol was used in Experiment I and the outcome was that all but one of ten sol-gel Ca-P-treated implants and all but one of ten control implants achieved bicortical stabilization as intended, and none of the animals suffered tibial fractures. The two implants which did not engage both cortices were the more proximal of the two placed in each of the affected tibiae and were due to the fact that the overall diameter of the tibia at the site of implantation exceeded the implant length. These two implants were called "floaters", and the control "floater" implant did not appear to osseointegrate. In contrast, the sol-gel Ca-P-coated "floater" implant was well osseointegrated within the single cortex engaged. This observed difference may be due to the ability of the Ca-P layer to promote osseointegration, through enhanced "osteoconduction", when the implant site or condition was less than ideal. However, there are other factors that may have affected osseointegration of the one control "floater" such as overheating during surgery and excessive relative mobility of the implant and bone during early healing. Overheating of bone during surgery was unlikely in this study as copious saline irrigation was used during surgery. Excessive mobility also was not suspected since this implant, like all of the others, needed to be press-fitted under friction. However, it may have been that the forces exerted by the overlying muscles as the animal moved around in its cage resulted in some level of implant micromovement during initial healing. The importance of careful and atraumatic surgery coupled with perfect fitting of the implant is crucial to achieving osseointegration (Branemark 1969, 1977, 1985; Albrektsson *et al.* 1981). An

ill-fitting implant subjected to early loading by muscle forces resulting in excessive micromovement may result in fibrous connective tissue formation at the implant surface (Maniatopoulos *et al.* 1986), and as mentioned above, the application of a bioactive surface coating that is osteoconductive may be beneficial in these situations (Maxian *et al.* 1994).

Another problem with placing two implants in one tibia was that even where an implant contacted the second cortex this contact was often incomplete, again because of inadequate implant length. As a result, there tended to be fewer appropriate sections available for the proximal surface of the more proximal implant in each animal. Consequently in Experiment II to avoid these problems only one implant was placed per tibia and both tibiae in each animal were used. As a result in Experiment II it was possible to choose an implantation site that allowed for optimal bicortical engagement.

A final limitation of the surgical protocol in both Experiments I and II was that occasionally proximity of the implant to the endosteal surface of the cortical bone on the anterior or posterior aspect of the tibia (due to implant diameter relative to the diameter of the medullary cavity in the site where the implant was installed) resulted in a few sectioned surfaces that were unsuitable for histomorphometric analysis. In these sections it was impossible to determine the origin of new endosteal bone that had formed in contact with the porous implant surface. That is it was impossible to determine if new bone in contact with the porous surface had originated by osteoconduction from the cut endosteal bone surface at either end of the implant or had simply grown into the porous surface from the anterior or posterior endosteum where this had coincidentally been in close proximity to the implant. These sections were among those labeled as PAX, PPX, DAX, DPX (i.e. all were tibial cross sections). As a consequence, these few (about 5%)

affected surfaces were excluded from the analyses. This problem was not seen with the longitudinal sections and could have been avoided with the use of longer implant lengths allowing placement to be more proximal and towards the metaphysis where the tibial diameter and the medullary space are larger.

To study the potential osteoconductive advantages of the sol-gel Ca-P-treated porous-surfaced implants in comparison to the control implants, histomorphometric measurements and analyses were carried out using SEM photomicrographs of each of the eight histological sections available for each implant. CLF and BIF in this study, 26.94 to 40.35% and 31.02 to 34.70% respectively, were much lower than data reported in earlier studies of porous surface-structured dental implants placed in dog mandibles (Deporter *et al.* 1986 a, 1988) where CLF ranged from 45% to 60% and BIF from 60% to 72% . These observed differences between the present study and earlier porous-surfaced implant studies might be attributed to species differences and to the much longer implantation period (9 to 10 months with 8 months in function) in the previous dog studies as compared to the 2 weeks in the present study. Another possible explanation may be differences in the bones being implanted with more bone available for contact with the implant surface in dog mandible where much of the implant length was initially in contact with either cortical or cancellous bone. In contrast, in the present study attempts were made to have only the two ends of each implant initially in contact with cortical bone so as to be able to assess osteoconduction over the implant length transversing the medulla. Furthermore, CLF and BIF were determined only for new bone which had developed by osteoconduction from the endosteal surfaces of the cortical bone and not within the cortical bone region itself. This may be another reason for the lower values for these morphometric parameters in this study.

On the periosteal aspect of the cortices, where the implant sat proud of the medial tibial cortex or extended beyond the lateral tibial cortical surface, bone growth / ingrowth was extensive and surrounded the entire exposed extra-cortical portions of the implants. This periosteal bone growth / ingrowth appeared to result in the same type of endosteal bone reaction being investigated, i.e. promoted osteoconduction. This suggests future studies aimed at investigating the potential usefulness of sol-gel Ca-P-treated porous-surfaced implants in conjunction with barrier techniques to regenerate lost alveolar ridge bone height at the time of implant placement.

Although morphometric analysis (ACL, CLF, SLBG, ABIA, BIF) indicated that sol-gel Ca-P-treated implants were more osteoconductive than the control implants, the differences may not be clinically relevant. Comparing the two implant types, the Ca-P coated implants yielded the greater values. Differences between the two implant surface treatments were 0.437 mm (or 59% improvement over the control implants) for ACL, 13.41% (or 50% improvement over the controls) for CLF, 0.156 mm (or 15% improvement over the controls) for SLBG, 0.009 mm^2 (or 14% improvement over the controls) for ABIA, and 3.68% (or 12% improvement over the controls) for BIF. Thus, except possibly for ACL and CLF, the relatively small improvements in bone growth and ingrowth may not result in significant clinical advantages during early healing. However, the more extensive ingrowth of bone into the neck regions for the sol-gel Ca-P-treated implants may present a significant clinical advantage of thin sol-gel Ca-P layers. Clearly, more bone ingrowth into the neck regions would indicate that the implant was better osseointegrated (i.e. improved 3-dimensional bone-to-implant interlocking) and would be

of clinical benefit during the early healing stage (and likely later as well) helping with initial and long-term implant stabilization.

In the present study only one healing interval was examined, i.e. 2 weeks post-implantation, and there was a statistically significant difference detected between the two surface treatments. Using a similar model, others have shown that thicker calcium phosphate layers enhance osteoconduction at early time periods out to 6 weeks (de Groot *et al.* 1987; Cook *et al.* 1992 b), but that the observed differences in bone to implant contact are no longer detectable after longer healing intervals of 6 weeks to 12 weeks or longer. Thus, for example, Thomas *et al.* (1986 a, b, 1989) found that HA-coated and uncoated porous titanium alloy canine transcortical plugs demonstrated similar bone ingrowth after 6 weeks with no significant difference in shear strength after three, six and twelve weeks of implantation. It is generally believed that Ca-P coatings seem to promote faster initial bone growth into the implant but as healing continues to occur, the implant without bioactive coating eventually catches up to that of the Ca-P-coated implant with bone apposition and ingrowth being similar between the two groups (Gottlander & Albrektsson 1991). The present study was not designed to support or dispute this statement.

The nature of the interface between synthetic Ca-P, both surface-deposited and in block form, and bone newly deposited upon it has been investigated by several researchers, but remains in dispute (Kasemo & Lausmaa 1991, Davies *et al.* 1991 a, b; Orr *et al.* 1992). Many have reported a direct deposition of bone matrix onto Ca-P in vivo as observed by transmission electron microscopy, while others have disputed this

conclusion demonstrating an intervening electron dense afibrillar layer between the Ca-P and overlying bone. This intervening layer, or so called cement line-like layer, is thought to be rich in calcium and phosphate and free of collagen fibres (Jarcho *et al.* 1977, 1981; Denissen *et al.* 1980; Ganeles *et al.* 1985; van Blitterswijk *et al.* 1985, 1985, 1990 a; de Lange *et al.* 1987, 1990; Frank *et al.* 1991; Davies *et al.* 1991 a). The freeze-fractured implants examined in the present study did demonstrate a cement line-like interface layer between the sol-gel Ca-P coat and the newly deposited bone, thus supporting the latter claims. Little is known about the bonding mechanisms if any between the Ca-P layer and cement layer. However, it has been speculated that such bonds do exist and probably involve both micro-mechanical interlock (Ricci *et al.* 1991; Orr *et al.* 1992) and some form of chemical interaction (Hench *et al.* 1971; Ducheyne *et al.* 1992; Williams *et al.* 1992).

Both of the implant surface treatments used in the present study showed osteoconductive properties. The osteoconductive activity displayed by the non-sol gel-coated implants was ascribed to the effects of surface topography as earlier reported with similar experimental implants placed in rat femurs (Dziedzic & Davies 1994). Other surface modifications including surface micro-roughness produced by sandblasting, acid etching, titanium plasma-spraying and HA plasma-spraying similarly result in varying degrees of osteoconductive activity (Schroeder *et al.* 1981, 1991; Buser *et al.* 1991 b). The sol-gel Ca-P film used in the present study resulted in an implant surface that was significantly more osteoconductive than the un-coated implant , and this difference may be explained by differences in surface roughness as seen in the freeze-fractured implants and in SEM photomicrographs of the as-received sol-gel coated implant examined. It

seems likely that this increased micro-texture of the Ca-P-treated implants may have contributed to the observed improvement in osteoconductivity. However it was not possible to determine the extent to which the increased osteoconductivity was due to surface micro-texture as opposed to benefits resulting from the chemistry of the Ca-P layer. Further investigation into these questions will be required to determine the individual benefits arising from physical and chemical phenomena. Numerous studies have addressed the effect of Ca-P chemistry, crystallinity and stability on osseointegration (Caulier *et al.* 1995, 1997; de Groot *et al.* 1994; de Bruijn *et al.* 1993 a, b). It was suggested by these investigators that less crystalline plasma-sprayed Ca-P coatings containing a high amorphous component (about 40%) resulted in improved bone-implant contact and this advantage was thought to be due to the dissolution of the amorphous component leading to elevated local levels of calcium and phosphate ions and providing a microenvironment more conducive to new bone formation. It is also known that the crystallinity of sol-gel Ca-P layers may be affected by different sintering temperatures (Qiu *et al.* 1993). Whether or not any of these factors were influential in the results observed in the present study is not known as the chemistry and crystallinity of the sol-gel layers used was not investigated.

As indicated, the long-term fate of the ultrathin sol-gel Ca-P film as used in the present study is not known. Sol-gel Ca-P films appear to be much denser than other forms of Ca-P surface layers including plasma-sprayed layers (Qiu *et al.* 1993; Basle *et al.* 1993; Caulier *et al.* 1995, 1997), and this difference in density may affect the ability of osteoclasts to resorb the deposited Ca-P. Basle and co-workers (1993) and Caulier and co-workers (1995; 1997) have demonstrated that "macroporous" (i.e. less dense) calcium phosphate biomaterials having a porosity in the range of 400 to 600 μm elicited

the recruitment of multinucleated cells and resulted in resorptive activity. Osteoclast-like cells were not observed in the freeze-fracture SEM photomicrographs examined in the present study so whether or not the dense ultrathin Ca-P layers used here are subject to osteoclastic resorption is presently not known, although it has been shown that similar layers are resorbed in vitro (Davies *et al.* 1993).

One of the problems with thick Ca-P layers applied by plasma-spray techniques is that they very often delaminate (de Groot *et al.* 1987; Pilliar *et al.* 1991 b; Radin & Ducheyne 1992; Klein *et al.* 1989; de Groot *et al.* 1990; Filiaggi *et al.* 1991; Whitehead *et al.* 1992; Delecrin *et al.* 1991) and where the Ca-P surface coat is the primary means of implant fixation this may lead ultimately to implant failure (de Groot *et al.* 1987; Radin & Ducheyne 1992; Klein *et al.* 1989; de Groot *et al.* 1990). Some delamination of the sol-gel ultrathin films used in the present study was seen in the freeze-fractured SEM specimens, and this occurred more often in the "neck" regions where the coating thickness tended to be considerably greater than the optimum thickness of 0.3 μm, and on the outermost surfaces of the outer layer of spherical particles of the porous coat, the latter incidences likely being related to shearing forces occurring during the insertion of the press-fit implants. It seems likely, however, that this observation would have little clinical significance for two reasons. Firstly, these delaminated fragments from the coated necks became surrounded by bone and remained in very close proximity to the implant surface and within the porous coat region, and it seems likely that they would eventually become resorbed if left in situ for periods of time longer than the two week period used here (Davies *et al.* 1993). Secondly, the ultrathin layers used in this work were intended to accelerate initial osseointegration, rather than serving as the primary

means of implant fixation, the latter characteristic being the role of the porous titanium alloy surface zone.

The hypothesis for the present study was that the application of an ultrathin layer of Ca-P to a porous-surfaced endosseous implant would promote osteoconduction during the initial healing period. This hypothesis was confirmed. This finding may be of use clinically as the use of ultrathin Ca-P coatings on porous-surfaced implants may permit significantly shorter initial healing intervals, although this requires verification in a clinical trial. The healing intervals reported with porous-surfaced implants in humans (Deporter *et al.* 1996) are generally the shortest of any of the commercially available dental implant systems. However, any further shortening of the initial osseointegration period would likely be welcomed by both patients and clinicians alike. The finding that ultrathin Ca-P coating accelerates initial bone growth / ingrowth may also be of some benefit in the further development of porous surface-structured implants for use in a single-stage surgical approach (i.e. non-submerged implant procedure) or for use as immediate implants at the time of tooth extraction. There would appear to be a perceived need for one-stage endosseous dental implant devices as evidenced by a number of recent publications (Salama *et al.* 1996; Bijlani *et al.* 1996; Levy *et al.* 1996; Schnitman *et al.* 1997; Gomez-Roman *et al.* 1997; Tarnow *et al.* 1997; Piattelli *et al.* 1997; Becker *et al.* 1997). As well , using a dog model, Levy *et al.* (1996), have shown that porous-surfaced dental implants with surface designs similar to the non-Ca-P-coated implants investigated in the present study became osseointegrated when used as non-submerged implants; however, the non-submerged implants had lower CLF than the traditional two-stage procedure. The application of a sol-gel Ca-P layer to these implants may further benefit

this clinical approach. Further investigations in this direction will be required to assess the potential benefits of sol-gel Ca-P layer for one-stage non-submerged implants and for use as immediate dental implants.

VIII) SUGGESTIONS FOR FUTURE STUDIES

In view of the observed improved osteoconductivity of an ultrathin layer of sol-gel Ca-P coating on porous-surfaced implants, there are several suggestions for future investigations. These are outlined as follow:

The observed periosteal bone growth / ingrowth in relation to the exposed extra-cortical implant region was qualitatively similar to the type of endosteal bone reaction being investigated. This suggests future osteoconductive studies aimed at investigating the potential usefulness of sol-gel Ca-P-treated porous-surfaced implants in conjunction with barrier techniques to regenerate lost alveolar ridge bone height at the time of implant placement. In such a model porous-surfaced implants might be installed with a variable length of the sol-gel treated, porous-surfaced segment proud of the crestal bone and covered with a barrier to exclude gingival tissues which also might have the surface intended for contact with bone coated with an ultrathin layer of Ca-P. If the osteoconductive potential of an ultrathin sol-gel Ca-P layer will allow for this supra-crestal "guided bone regeneration", such an implant system may be useful in clinical situations where there is minimal alveolar bone height available, and where it would be otherwise necessary to do a separate ridge augmentation procedure, sinus lift operation, or nerve repositioning prior to or in conjunction with implant installation.

It would also be beneficial to study longer healing periods with sol-gel Ca-P-treated and control implants with porous surface zones formed by metal powder sintering to determine the long-term stability of thin Ca-P layers applied using sol-gel technique. Additionally, whether or not the differences in bone growth and ingrowth observed at 2

weeks are maintained over longer times could be investigated. Ongoing experiments are addressing these questions.

With the improved osteoconductivity, it seems appropriate to propose future investigations involving clinical situations utilizing a single-stage surgical (non-submerged) procedure or immediate implantation subsequent to tooth extraction. The application of an ultrathin sol-gel Ca-P coating to porous-surfaced dental implants or other implant designs such as plasma-sprayed titanium, threaded implant with either machined or polished surfaces and grit-blasted or acid etched systems may be beneficial and possibly making such clinical approaches more predictable on a routine basis.

IX) CONCLUSIONS AND FINAL RECOMMENDATIONS

From the results reported here it may be concluded that:

1) The sol-gel technique of calcium phosphate application used here is suitable for modification of porous surface-structured implants, formed by sintering titanium alloy particles to the surface of a titanium alloy core, as this sol-gel application did not result in occlusion of the porous structure.
2) Porous surface-structured endosseous implant devices with an ultrathin (potentially submicron in thickness) layer of calcium phosphate applied by the sol-gel technique demonstrated an enhanced osteoconductivity.
3) Analysis of the extent of bone ingrowth into the neck regions between adjacent spherical particles of the porous surface zone is an excellent and useful parameter to evaluate osteoconductivity and the degree of osseointegration. Neck regions present acute-angled junctions between adjoining spherical particles that often are not significantly ingrown with bone with the non-sol-gel calcium phosphate-coated implants. This parameter (the extent of bone ingrowth in the neck regions) was more sensitive as an indicator of osteoconduction than conventional morphometric parameters such as Contact Length Fraction and showed a clearly superior result with the sol-gel treated implants.
4) Although torquing and pull-out tests were not part of this study, the more extensive bone ingrowth into the neck regions with the sol-gel calcium phosphate-treated implants would be expected to provide superior three-dimensional bone / implant interlock which should result in better resistance to torquing and tensile forces.

5) The sol-gel calcium phosphate processing procedure used in this study may have resulted in film thickness in excess of 1 μm, and this led to some cracking and delamination of the film. It would be prudent in future investigations to determine what alterations in processing are required to ensure that the Ca-P film was of the optimal 0.3 μm thickness, for example, by possibly decreasing the solution viscosity and using a newer polymeric sol-gel calcium phosphate form rather than the particulate / colloidal form used in this study.

REFERENCES

ADELL R, ERIKSSON B, LEKHOLM U, BRANEMARK P-I, JEMT T. A long-term follow-up study of osseointegrated implants in the treatment of totally edentulous jaws. *Int J Oral Maxillofac Implants*. 1990; 5:347-359.

ALBREKTSSON T, BRANEMARK PI, HANSSON HA, LINDSTROM J. Osseointegrated titanium implants. Requirements for ensuring a long-lasting direct bone anchorage in man. *Acta Orthop Scand*. 1981; 52:155.

AL-SAYYED A, DEPORTER DA, PILLIAR RM, WATSON PA, PHAROAH M, BERHANE M, CARTER S. Predictable Crestal Bone Remodeling Around Two Porous-surfaced Titanium Alloy Dental Implant Designs: A Radiographic Study in Dogs. *Clin Oral Impl Res*. 1994; 5:131-141.

BABBUSH CA, KENT JN, MISIEK DL. Titanium plasma-sprayed (TPS) screw implants for the reconstruction of the edentulous mandible. *J of Oral Maxillofac Surg*. 1986; 44:274-282.

BASLE MF, CHAPPARD D, GRIZON F, FILMON R, DELECRIN J, DACULSI G, REBEL A. Osteoclastic Resorption of Ca-P Biomaterials Implanted in Rabbit. Bone. *Calcif Tissue Int*. 1993; 53:348-356.

BAUTIGAM U, BURGER H, VOGEL W. Some aspects of property tailoring of sol-gel derived thin SiO_2 films. *J Non-Cryst Solids*. 1989; 110:163.

BECKER W, BECKER BE, ISRAELSON H, LUCCHINI JP, HANDELSMAN M, AMMONS W, ROSENBERG E, ROSE L, TUCKER LM, LEKHOLM U. One-step surgical placement of Branemark implants: A prospective multicenter clinical study. *Int J Oral Maxillofac Implants*. 1997; 12:454-462.

BLOCK MS, KENT JN, KAY JF. Evaluation of hydroxylapatite-coated titanium dental implant in dogs. *J Oral Maxillofac Surg*. 1987; 45:601.

BLOCK MS, FINGER IM, FONTENOT MG, KENT JN. Loaded hydroxylapatite-coated and grit-blasted titanium implants in dogs. *Int J Oral Maxillofac Implants*. 1989; 4:219.

BLOCK MS, DELGADO A, FONTENOT MG. The Effect of Diameter and Length of Hydroxylapatite-coated Dental Implants on Ultimate Pullout Force in Dog Alveolar Bone. *J Oral Maxillofac Surg*. 1990; 48:174-178.

BLOCK MS, FINGER IM, MISIEK DJ. Histologic examination of hydroxyapatite-coated implant nine years after placement. *J Oral Maxillofac Surg*. 1996; 54(8):1023-1026.

BOBYN JD, PILLIAR RM, CAMERON HU, WEATHERLY GC. The Optimum Pore Size for the Fixation of Porous-surfaced Metal Implants by Ingrowth of Bone. *Clin Orthop Rel Res*. 1980; 150:263-270.

BONFIELD W, LUKLINSKA ZB. High-resolution electron microscopy of a bone implant interface. In: *The Bone-Biomaterial Interface*, Davies JE (Ed), University of Toronto Press, Toronto. 1991; 89-94.

BOYNE PJ, JAMES RA. Grafting of the maxillary sinus floor with autogenous marrow and bone. *J Oral Surg*. 1980; 38:613.

BRANEMARK P-I, BREINE U, ADELL R, HANSSON BO, LINDSTROM J, OLSSON A. Intra-osseous anchorage of dental prostheses. I. Experimental studies. *Scand J Plast Reconstr Surg*. 1969; 3:81.

BRANEMARK P-I, HANSSON BO, ADELL R, BREINE U, LINDSTROM J, HALLEN O, OMANN A. Osseo-integrated implants in the treatment of the edentulous jaw. Experience from a ten year period. *Scand J Plast Reconstr Surg.* 1977; 11(suppl 16).

BRANEMARK P-I, ZARB GA, ALBREKTSSON T (Eds). Tissue-Integrated Prostheses. Osseointegration in Clinical Dentistry. Chicago: Quintessence, 1985.

BROSSA F, LOOMAN B, PIETRA R, SABBIONI E, GALLORINI M, ORVINI E. The use of titania and alumina as protective coatings on metallic prosthesis to prevent metal ion release. In: *High Tech Ceramics*, Vincenzini P (Ed). Elsevier, Amsterdam. 1987, 99-109.

BUCHANAN RA, RIGNEY ED, GRIFFIN CD. Biocorrosion study of ultralow-temperature-isotropic carbon-coated porous titanium. In: *Quantitative Characterization and Performance of Porous Implants in Hard Tissue Applications, ASTM TP 953*, Lemons J (Ed). American Society for Testing and Materials, Philadelphia. 1987; 105-114.

BUSER D, WEBER HP, LANG NP. Tissue integration of non-submerged implants. 1-year results of a prospective study with 100 ITI hollow-cylinder and hollow-screw implants. *Clin Oral Impl Res.* 1990; 1:33-40.

BUSER D, WEBER HP, BRAGGER C. Tissue integration of one-stage ITI implants: 3-year results of a longitudinal study with hollow-cylinder and hollow-screw implants. *Int J Oral Maxillofac Implants.* 1991 a; 6:405-412.

BUSER D, SCHENK RK, STEINEMANN S, FIORELLINI JP, FOX CH, STICH H. Influence of surface characteristics on bone integration of titanium implants. A histomorphometric study in miniature pigs. *J Biomed Mater Res.* 1991 b; 25:889-902.

BUSER D, DAHLIN C, SCHENK RK (Eds). Guided Bone Regeneration in Implant Dentistry. Quintessence. 1994

CAMERON HU, MacNAB I, PILLIAR RM. Evaluation of biodegradable ceramic. *J Biomed Mater Res.* 1977; 11:179-186.

CARR BA, LARSEN PE, PAPAZOGLOU E, McGLUMP Y. Reverse torque failure of screw-shaped implants in Baboons: Baseline data for abutment torque application. *Int J Oral Maxillofac Implants* 1995; 10:167-174.

CARR BA, BEALS WD, LARSEN PE. Reverse-torque failure of screw-shaped implants in Baboons: After 6 months of healing. *Int J Oral Maxillofac Implants* 1997; 12:598-603.

CAULIER H, VAN DER WAERDEN JPCM, PAQUAY YCGJ, WOLKE JGC, WALK W, NAERT I, JANSEN JA. Effect of calcium phosphate (Ca-P) coatings on trabecular bone response: A histological study. *J Biomed Mater Res.* 1995; 29:1061-1069.

CAULIER H, VERCAIGNE S, NAERT I, VAN DER WAERDEN JPCM, WOLKE JGC, WALK W, JANSEN JA. The effect of Ca-P plasma-sprayed coatings on the initial bone healing of oral implants: An experimental study in the goat. *J Biomed Mater Res.* 1997; 34:121-128.

CHAE JC, COLLIER JP, MAYOR MB, SURPRENANT VA, DAUPHINAIS LA. Enhanced ingrowth of porous-surfaced CoCr implants plasma-sprayed with tricalcium phosphate. *J Biomed Mater Res.* 1992; 26:93-102

COCHRAN DL, NUMMIKOSKI PV, HIGGINBOTTOM FL, HERMANN JS, MAKINS SR, BUSER D. Evaluation of an endosseous titanium implant with a sandblasted and acid-etched surface in the canine mandible: radiographic results. *Clin Oral Impl Res.* 1996; 7:240-252.

COOK SD, WALSH K, HADDAD R. Interface mechanics and bone growth into porous Co-Cr-Mo alloy implants. *Clin Orthop.* 1985; 193:271.

COOK SD, THOMAS KA, KAY JF, JARCHO M. Interface Mechanics and Histology of Titanium and Hydroxylapatite-coated Titanium for Dental Implant Applications. *Int J Oral Maxillofac Implantol.* 1987; 2:15-22.

COOK SD, THOMAS KA, KAY JF, JARCHO MJ (1988): Hydroxyapatite-coated porous titanium for the use as an orthopedic biologic attachment system. *Clin Orthopaed Rel Res* 1988; 232, 225-243.

COOK SD, THOMAS KA, KAY JF, JARCHO MJ. Hydroxyapatite-coated titanium for orthopedic implant applications. *Clin Orthopaed Rel Res.* 1988; 230:303-311.

COOK SD. Hydroxyapatite-coated total hip replacement, *Dent Clin North Amer.* 1992 a; 36(1):235-238.

COOK SD, BAFFES GC, PALAFOX AJ, WOLFE MW, BURGESS A. Tortional Stability of HA-coated and Grit-blasted Titanium Dental Implants. *J Oral implantol.* 1992 b; 28:359-365.

CORMACK DH (Ed). In: *Ham's Histology ed. 9.* Philadelphia, PA: JB Lippincott Co.; 1987: 283-287.

DACULSI G, LEGEROS RZ, HEUGHEBAERT JC, BARBIEUX I. Formation of carbonate-apatite crystals after implantation of calcium phosphate ceramics. *Calcif Tissue Int.* 1990 a; 46:20-27.

DACULSI G, PASSUTI N, MARTIN S, DEUDON C, LEGEROS RZ, RAHER S. Macroporous calcium phosphate ceramic for long term surgery in humans and dogs. Clinical and histological study. *J Biomed Mater Res.* 1990 b; 24:379-396.

DACULSI G. Physico-chemical and ultrastructural analysis of bone/bioactive ceramics interface. In: *Trans. 9th ESB Conference on Biomaterials*, Chester, UK. 1991; p 122.

DAVIES JE. The use of cell and tissue culture to investigate bone cell reactions to bioactive materials. In: *CRC Handbook of Bioactive Ceramics*, Volume I. Yamamuro T, Hench LL, Wilson J (Eds), CRC Press, Boca Raton, FL, USA. 1990a; 1-65.

DAVIES JE, LOWENBERG BF, SHIGA A. The bone-titanium interface in vitro. *J Biomed Mater Res.* 1990 b; 24:1289-1306.

DAVIES JE, CHERNECKY R, LOWENBERG BF, SHIGA A. Deposition and resorption of calcified matrix *in vitro* by rat bone marrow cells. *Cells and Materials* 1991 a; 1:3-15.

DAVIES JE, OTTENSMEYER P, SHEN X, HASHIMOTO M, PEEL SAF. Early extracellular matrix synthesis by bone cells. In: *The Bone-Biomaterial Interface*, ed. Davies JE, University of Toronto Press, Toronto. 1991 b; 214-228

DAVIES JE, SHAPIRO G, LOWENBERG BF. Osteoclastic resorption of calcium phosphate ceramic thin films. *Cells and Materials.* 1993; 3(3):245-256.

DE BRUIJN JD, KLEIN CPAT, DE GROOT K, VAN BLITTERSWIJK CA. Influence of crystal structure on the establishment of the bone-calcium phosphate interface in vitro. In: *Calcium Phosphate Biomaterials: Bone-bonding and Biodegradation Properties*, Ph.D. thesis. de Bruijn JD 1993 a; chapter 4, 63-78.

DE BRUIJN JD, BOVELL YP, VAN BLITTERSWIJK CA. Structural arrangements at the interface between plasma-sprayed calcium phosphate and bone. In: *Calcium Phosphate Biomaterials: Bone-bonding and Biodegradation Properties*, Ph.D. thesis. de Bruijn JD 1993 b, chapter 5, 79-92.

DE GROOT K, GEESINK RGT, KLEIN CPAT, SEREKIAN P. Plasma-Sprayed Coatings of Hydroxyapatite. *J Biomed Mater Res.* 1987; 21:1375-1381

DE GROOT K, KLEIN CPAT, WOLKE JGC, DE BLIECK-HOGERVORST JMA. Plasma sprayed coatings of calcium phosphate. In: *CRC Handbook of Bioactive Ceramics*, Volume II. Yamamuro T, Hench LL, Wilson J (Eds), CRC Press, Boca Raton, FL, USA. 1990; 133-142.

DE GROOT K, WOLKE JGC, JENSEN JA. "State of the art: Hydroxyapatite coatings for dental implants". *J Oral Impl.* 1994; 20:232-234.

DELECRIN J, SZMUCKLER-MONCLER S, DACULSI G, RIEU J, DUQUET B. Ultrastructural, crystallographic and chemical analysis of different calcium phosphate plasma coatings. In: *Bioceramics*, Volume 4, Bonfield W, Hastings Janner KE (Eds). Butterworth-Heinemann, Ltd., London. 1991; 311-315.

DE LANGE GL, DE PUTTER C, BURGER EH, DE GROOT K. The bone-hydroxylapatite interface, In: *Biomaterials and Clinical Applications*, Pizzoferrato A *et al.* (Eds), Elsevier, Amsterdam, The Netherlands. 1987; 317-222.

DE LANGE GL, DONATH K. Interface between bone tissue and implants of solid hydroxyapatite or hydroxyapatite-coated titanium implants, *Biomaterials*. 1989; 10(3):121-125.

DE LANGE GL, DE PUTTER C, DE WIJS FLJA. Histological and ultrastructural appearance of the hydroxyapatite-bone interface. *J Biomed Mater Res*. 1990; 24:829-845.

DENISSEN HW, DE GROOT K, MAKKES PCH, VAN DEN HOOFF A, KLOPPER PJ. Tissue response to dense apatite implants in rats. *J Biomed Mater Res*. 1980; 14:713-721.

DEPORTER DA, WATSON PA, PILLIAR RM, MELCHER AH, WINSLOW J, HOWLEY TP, HANSEL P, MANIATOPOULOS C, RODRIGUEZ A, ABDULLA D, PARISIEN K, SMITH DC. A Histological Assessment of the Initial Healing Response Adjacent to Porous-surfaced Titanium Alloy Dental Implants in Dogs. *J Dent Res.* 1986 a; 65(8):1064-1070.

DEPORTER DA, FRIEDLAND B, WATSON PA, PILLIAR RM, HOWLEY TP, ABDULLA D, MELCHER AH, SMITH DC. A Clinical and Radiographic Assessment of a Porous-surfaced Titanium Alloy Dental Implant System in Dogs. *J Dent Res.* 1986 b; 65(8):1071-1077.

DEPORTER DA, WATSON PA, PILLIAR RM, HOWLEY TP, WINSLOW J. A histological Evaluation of a Functional Endosseous, Porous-surfaced, Titanium Alloy Dental Implant System in the Dog. *J Dent Res.* 1988; 67(9):1190-1195.

DEPORTER DA, WATSON PA, PILLIAR RM, CHIPMAN ML, VALIQUETTE N. A Histological Comparison in the Dog of Porous-surfaced vs Threaded Dental Implants. *J Dent Res.* 1990; 69(5):1138-1145.

DEPORTER DA, WATSON PA, PILLIAR RM, PHAROAH M, CHIPMAN M, SMITH DC. A Clinical Trial of a Partially Porous-surfaced Endosseous Dental Implant in Humans: Protocol and 6-month Results. In: *Tissue Integration in Oral Orthopedic and Maxillofacial Reconstruction.* Laney WR & Tolman DE (Eds). Quintessence Books, Chicago, Illinois. 1992; 250-258.

DEPORTER DA, WATSON PA, PILLIAR RM, PHAROAH M, SMITH DC, CHIPMAN M. A Clinical Trial in Humans of a Partially Porous-surfaced Endosseous Dental Implant: Three to Four Year Results. *Int J Oral Maxillofac Implants*. 1996; 11:83-91.

DISLICH H. Thin films from the sol-gel process. In: *Sol-Gel Technology for thin films, fibers, preforms, electronics, and specialty shapes*. Klein LC (Ed). Noyes Publications, Park Ridge, NJ, USA. 1988; 50-79.

DRISKELL T, HASSLER C, McCOY L. "The significance of resorbable bioceramic in the repair of bone defects" - *26th Annual Conf on Engineering in Medicine and Biology*. 1973; p. 199.

DUCHEYNE P, HENCH LL, KOGAN A, MARTENS M, BURSENS A, MULIER JC. Effect of Hydroxyapatite Impregnation on Skeletal Bonding of Porous-surfaced Implants. *J Biomed Mater Res*. 1980; 14:225-237.

DUCHEYNE P, BEIGHT J, CUCKLER J, EVANS B, RADIN S. Effect of calcium phosphate coating characteristics on early post-operative bone tissue ingrowth. *Biomaterials*. 1990 a; 11:531-540.

DUCHEYNE P, RADIN S, HEUGHEBAERT M, HEUGHEBAERT JC. Calcium phosphate ceramic coatings on porous titanium: effect of structure and composition on electrophoretic deposition, vacuum sintering and in vitro dissolution. *Biomaterials*. 1990 b; 11(4): 244-254.

DUCHEYNE P, CUCKLER JM. Bioactive ceramic prosthetic coatings. *Clin Orthop*. 1992; Mar(276):102-114.

DZIEDZIC DM, DAVIES JE. Effects of implant surface topography on osteoconduction. *Proceedings of the 20th meeting of the Society of Biomaterials*. Society of Biomaterials, Boston, MA, USA. 1994; 298.

FABES BD, ZELINSKI BJJ, UHLMANN DR. Sol-gel derived ceramic coatings. In: *Ceramic films and coatings*. Wachtman JB, Haber RA (Eds). Noyes Publications, Park Ridge, NJ, USA. 1993; 224-283.

FILIAGGI MJ, PILLIAR RM, COOMBS NA. Charaterization of the interface in the plasma-sprayed HA coating / Ti-6Al-4V implant system, *J Biomed Mater Res*. 1991; 25:1211-1229.

FILIAGGI MJ, PILLIAR RM, COOMBS NA. Post-plasma spraying heat treatment of the HA coating / Ti-6Al-4V implant system. *J Biomed Mater Res*. 1993; 27:191-198.

FILIAGGI MJ. Evaluating sol-gel ceramic thin films for metal implant applications. A study on the processing and mechanical properties of Zirconia films on $_{Ti\text{-}6Al\text{-}4V}$. University of Toronto, Ph.D. thesis, 1995.

FILIAGGI MJ, PILLIAR RM, YAKUBOVICH R, SHAPIRO G. Evaluating sol-gel ceramic thin films for metal implant applications. I: Processing and structure of zirconia films on Ti-6Al-4V. *J of Biomed Mater Res*. 1996 a; 33: 225-238

FILIAGGI MJ, PILLIAR RM, ABDULLA D. Evaluating sol-gel ceramic thin films for metal implant applications. II: Adhesion and fatigue properties of zirconia films on Ti-6Al-4V. *J of Biomed Mater Res*. 1996 b; 33: 239-256.

FRANK RM, KLEWANSKY P, HEMMERLE J, TENENBAUM H. Ultrastructural demonstration of the importance of crystal size of bioceramic powders implanted into human periodontal lesions. *J Clin Periodontol*. 1991; 18:669-680.

FRIBERG B, IVANOFF CJ, LEKHOLM U. Inferior alveolar nerve transposition in combination with Branemark implant placement. *Int J Periodont Rest Dent*. 1992; 12:441.

GANELES J, LISGARTEN MA, EVIAN CI. Ultrastructure of durapatite-periodontal tissue interface in human infrabony defects. *J Periodontol.* 1985; 57:133-139.

GEESINK RGT, DE GROOT K, KLEIN CPA. Chemical Implant Fixation Using Hydroxyl-apatite Coatings. *Clin Orthop Rel Res.* 1987; 225:147-170.

GOMEZ-ROMAN G, SCHULTE W, D'HOEDT B, AXMAN-KRCMAR D. The Frialit-2 implant system: Five year clinical experience in single-tooth and immediately loaded postextraction application. *Int J Oral Maxillofac Implants.* 1997; 12:299-309.

GOTTLANDER M, ALBREKTSSON T. Histomorphometric Studies of Hydroxyapatite-Coated and Uncoated CP Titanium Threaded Implants in Bone. *Int J Oral Maxillofac Implants.* 1991; 6:399-404.

GUGLIEMI M, COLOMBO P, FERON F, MANCINELLI DEGLI ESPOSTI L. Dependence of thickness on the withdrawal speed for SiO_2 and TiO_2 coatings obtained by the dipping method. *J Mater Science.* 1992; 27:5052-5056.

HAAS R, MENSDORFF-POUILLY N, MAILATH G, WATZEK G. Survival of 1,920 IMZ implants followed for up to 100 months. *Int J Oral Maxillofac Implants.* 1996; 11(5):581-588.

HENCH LL, SPLINTER RJ, ALLEN WC, GREENLEE TK. Bonding mechanisms at the interface of ceramic prosthetic materials. *J Biomed Mat Res.* 1971; 2:117-141.

HENCH LL, PASCHALL HC. Direct chemical bond of bioactive glass-ceramic materials to bone and muscle. J Biomed Mater Symposium. *J Biomed Mater Res.* 1973; 4:25-42.

HENCH LL, ETHBRIDGE EC. Biomaterials: An interfacial approach. Academic Press, New York, NY. 1982.

HENCH LL, WILSON J. Surface-active biomaterials, *Science.* 1984; 226:630-636.

HULBERT SF, BOKROS JC, HENCH LL,. WILSON J, HEIMKE G. Ceramics in clinical applications, past, present, future. In: *High Tech Ceramics.* Vincenzini P (Ed). Elsevier, Amsterdam. 1987; 3-27.

JANSEN JA VAN DE WAERDEN JPCM WOLKE JGC DE GROOT K. Histologic evaluation of the osseous adaptation to titanium and hydroxyapatite-coated titanium implants. *J Biomed Mater Res.* 1991; 25:973-989.

JANSEN JA, VAN DER WAERDEN JPCM, WOLKE JGC. Histologic investigation of the biologic behaviour of different hydroxyapatite plasma-sprayed coatings in rabbits. *J Biomed Mater Res.* 1993; 27:603-610.

JARCHO M, KAY JF, KENNETH I, GUMAER KI, DOREMUS RH, DROBECK HP. Tissue, cellular and subcellular events at a bone-hydroxylapatite interface. *J Bioeng.* 1977; 1:79-92.

JARCHO M. Calcium phosphate ceramics as hard tissue prosthetics. *Clin Orthop Res.* 1981; 157:259-278.

JASTY M, RUBASH H, PAIEMENT GD, BRAGDON CR, PARR J, HARRIS W. Porous-surfaced Uncemented Components in Experimental Total Hip Arthroplasty in Dogs. Effect of Plasma-Sprayed Calcium Phosphate Coatings on Bone Ingrowth. *Clin Orthopaedics & Related Res.* 1992; 280:300-309.

JENSEN OT, NOCK D. Inferior alveolar nerve repositioning in conjunction with placement of osseointegrated implants: A case report. *Oral Surg Oral Med Oral Pathol.* 1987; 63:263.

KASEMO B, LAUSMAA J. The bone-tissue interface and its analogues in surface science and technology. In: *The Bone-Biomaterial Interface*. Davies JE (Ed). University of Toronto Press, Toronto, 1991: 19-32

KAY JF, JARCHO M, LOGAN G, LIU S-T. The structure and properties of hydroxyapatite coatings on metal. *Transactions of the Annual Meeting of the Society Biomaterials*. Minneapolis, Minnesota. 1986; 14: 9.

KENT JN, BLOCK MS. Simultaneous maxillary sinus floor bone grafting and placement of hydroxylapatite coated implants. *J Oral Maxillofac Surg*. 1989; 47:238.

KLEIN CPAT, DRIESSEN A, de GROOT K. Biodegradable behaviour of various calcium phosphate materials in bone tissue. *J Biomed Mater Res*. 1983; 17:769.

KLEIN CPAT, DRIESSEN A, de GROOT K. Relationship between the degradation behaviour of calcium phosphate ceramics and their physical-chemical characteristics and ultrastructural geometry. *Biomaterials*. 1989; 5:157.

KLEIN LC. Sol-gel coatings. In: *Thin film processes II*. Vossen JL, Kern W (Eds). Academic Press Inc. Boston, MA, USA. 1991; 501-522.

KOHN DH. Overview of Factors Important in Implant Design. *J Oral Implantol*. 1992; 28:204-219.

LACEFIELD WR. "Hydroxyapatite Coatings" in Bioceramics: Material Characteristics Versus In Vivo Behaviour, *Annals of New York Academy of Science*. 1988; 523:72-80.

LEGEROS RZ, ORLY I, GREGOIRE M, DACULSI G. Substrate surface dissolution and interfacial biological mineralization. In: *The Bone-Biomaterial Interface*. Davies JE (Ed). University of Toronto Press, Toronto. 1991; 76-88.

LEGEROS RZ, DACULSI G, ORLY I, GREGOIRE M, HEUGHEBAERT M, GINESTE M, KIJKOWSKA. Formation of carbonate apatite on calcium phosphate materials: Dissolution / precipitation processes. In: *Bone-bonding Biomaterials*. Ducheyne P et al. (Eds), Reed Healthcare Communications, Leiderdorp, The Netherlands. 1992; 201-212.

LEKHOLM U, ZARB GA. Patient selection and preparation. In: *Tissue-Integrated Prostheses: Osseointegration in Clinical Dentistry*. Branemark P-I, Zarb GA, Albrektsson T (Eds). Chicago, Quintessence. 1985; 199-209.

LEVY D, DEPORTER DA, PILLIAR RM, WATSON PA, VALIQUETTE N. Initial healing in the dog of submerged versus non-submerged porous-surfaced endosseous dental implants. *Clin Oral Impl Res*. 1996; 7:101-110.

MANIATOPOULOS C, PILLIAR RM, SMITH DC. Threaded versus Porous-surfaced Designs for Implant Stabilization in Bone-endodontic Implant Model *J Biomed Mater Res*. 1986; 20:1309-1333.

MANLEY MT. Calcium phosphate biomaterials: A review of the literature. In: *Hydroxyapatite Coatings in Orthopaedic Surgery*. Geesink RGT, Manley MT (Eds). Raven Press, Ltd., New York. 1993; 1-23.

MAXIAN SH ZAWADSKY JP DUNN MG. Effect of Ca /P coating resorption and surgical fit on the bone implant interface. *J Biomed Mater Res*. 1994; 28:1311-1319

MEFFERT RM BLOCK MS KENT JN. "What is osseointegration?". *Int J Periodont Rest Dent*. 1987; 4:9-21.

NORDSTROM EG, SODERGARD BE, KUKKONEN L. Thin sol-gel-derived silica-coatings on CP-Titania and bioactivity thereupon. *Bio-med Mater and Engineering*. 1994; 4(3):187-192.

OGISO M, TABATA T, ICHIJO T, BORGESE D. Bone calcification on the hydroxy apatite dental implant and the bone-hydroxyapatite interface. *J of Long Term Effects of Med Imp.* 1992; 2(23):137-148.

ORR RD, DE BRUIJN JD, DAVIES. Scanning electron microscopy of the bone interface with titanium, titanium alloy and hydroxyapatite. *Cells and Materials.* 1992; 2(3):241-251.

OSBORN JF. Bonding Osteogenesis under Loaded Conditions - The Histological Evaluation of a Human Autopsy Specimen of a Hydroxyapatite Ceramic Coated Stem of a Titanium Hip Prosthesis In: *Bioceramics.* Ooislie H, Aoki H, Sawai R (Eds). Ishiyaku EuroAmerica Inc., Tokyo. 1989; 388-399.

PIATTELLI A, SCARANO A, PAOLANTONIO M. Immediately loaded screw implant removed for fracture after a 15-year loading period: Histological and histochemical analysis. *J Oral Implantol.* 1997; 23(1&2):75-79.

PILLIAR RM, CAMERON HU, MacNAB I. Porous surfaced layered prosthetic devices. *Biomed Eng.* 1975; 10:126-131.

PILLIAR RM. Implant Stabilization by Tissue Ingrowth. In: *Tissue Integration in Oral and Maxillo-Facial Reconstruction.* Van Steenberghe D (Ed). Excerpta Medica, Amsterdam. 1986; 60-76.

PILLIAR RM, LEE JM, MANIATOPOULOS C. Observations on the Effect of Movement on Bone Ingrowth into Porous-surfaced implants. *Clin Orthol Rel Res.* 1986; 208:108-113.

PILLIAR RM. Porous-surfaced Metallic Implants for Orthopedic Applications *J Biomed Mater Res.* 1987; 21:1-33.

PILLIAR RM. Quantitative evaluation of the effect of movement at the porous-surfaced implant-bone interface. In: *Bone-Biomaterial Interface Workshop in Toronto.* Davies JD (Ed). Dec 1990 a.

PILLIAR RM. Dental implants: materials and design. *J Can Dent Assoc.* 1990 b Sept; 56(9):857-861.

PILLIAR RM, DEPORTER DA, WATSON PA, VALIQUETTE N. Dental Implant Design - Effect on Bone Remodeling. *J Biomed Mater Res.* 1991 a; 25:467-483

PILLIAR RM, DEPORTER PA, WATSON PA, PHAROAH M, CHIPMAN M, VALIQUETTE N, CARTER S, DE GROOT K. The Effect of Partial Coating with Hydroxyapatite on Bone Remodeling in Relation to Porous-surfaced Titanium-alloy Dental Implants in the Dog. *J Dent Res.* 1991 b; 70(10):1338-1345.

PILLIAR RM, LEE JM, DAVIES JE. Interface zone: factors influencing its structure for cementless implants. In: *Biological material and mechanical considerations of joint replacement.* Morrey BD (Ed). Raven Press Ltd., New York. 1993 a: 225.

PILLIAR RM, FILIAGGI MJ. New calcium phosphate coating methods. *Bioceramics* 6, Philadelphia, PA. November. 1993 b: 165-171

PILLIAR RM, DEPORTER DA, WATSON PA. Tissue-implant interface: micromovement effects. In: *Clinical applications.* Vincenzini P (Ed). Techna, Srl., 1995: 569.

QIU Q, VINCENT P, LOWENBERG B, SAYER M, DAVIES JE. Bone growth on sol-gel calcium phosphate thin films *in vitro. Cells and Materials.* 1993; 3(4):351-360.

QUIRYNEN M, NAERT I, VAN STEENBERGHE D, DEKEYSER C, CALLEN A. Periodontal aspects of osseointegrated fixtures supporting a partial bridge. An up to 6-years retrospective study. *J Clin Periodontol.* 1992; 19(2): 118-126.

RADIN SR, DUCHEYNE P. Plasma spraying induced changes of calcium phosphate ceramic characteristics and the effects on in vitro stability *J Mater Sci: Mater in Medicine.* 1992; 3:33-42.

RICCI JL, SPIVAK JM, ALEXANDER H, BLUMENTHAL NC, PARSONS R. Hydroxyapatite ceramics and the nature of the bone-ceramic interface. *Bulletin of the Hospital for Joint Diseases Orthopaedic Institute.* 1989; 49(2):178-191.

RICCI JL, SPIVAK JM, BLUMENTHAL NC, ALEXANDER H. Modulation of bone ingrowth by surface chemistry and roughness. In: *The Bone-Biomaterial Interface.* Ed. Davies JE. University of Toronto Press, Toronto. 1991; pp. 334-349.

RIVERO DP, FOX J, SKIPOR AK, URBAN RM, GALANTE JO. Calcium Phosphate-coated Porous Titanium Implants for Enhanced Skeletal Fixation. *J Biomed Mater Res.* 1988; 22:191-201.

SELLA C, MARTIN JC, LECHANU A, LECOEUR J, BELLIER JP, HARMAND MF, NAJI A, DAVIDAS JP. Corrosion potential of metal implants by sputter-deposited biocompatible ceramic coatings. *Surf Coat Technol.* 1991; 45:129-135.

SHIRKHANZADEH M. Electrochemical preparation of protective oxide coatings on titanium surgical alloys, *J Mater Sci. : Mat. in Med.*, 1992; 3:322-325.

SCHNITMAN PA, WOHRLE PS, RUBENSTEIN JE, DASILVA JD, WANG NH. Ten year results for Branemark implants immediately loaded with fixed prostheses at implant placement. *Int J Maxillofac Impl.* 1997; 12:495-503.

SCHROEDER A, VAN DER ZYPEN E, STICH H, SUTTER F. The reaction of bone, connective tissue and epithelium to endosteal implants with sprayed titanium surfaces. *J Maxillofac Surg.* 1981; 9:15.

SCHROEDER A, SUTTER F, KREKELER G (Eds). Oral implantology. The ITI Hollow-Cylinder System (English Ed). Stuttgart: Georg Thieme Verlag, 1991.

SOLAR RJ, POLLACK SR, KOROSTOFF E. In vitro corrosion testing of titanium surgical implant alloys: an approach to understanding titanium release from implant. *J Biomed Mater Res.* 1979; 13(2):217-250.

SPIEKERMANN H, JANSEN VK, RICHTER EJ. A 10-year follow-up study of IMZ and TPS implants in the edentulous mandible using bar-retained overdentures. *Int J Oral Maxillofac Implants.* 1995; 10(2):231-243.

STRAWBRIDGE I, JAMES PF. The factors affecting the thickness of sol-gel derived silica coatings prepared by dipping. *J Non-Crystal Solids.* 1986; 86:381-393.

TARNOW DP, EMTIAZ S, CLASSI A. Immediate loading of threaded implants at stage 1 surgery in edentulous arches: Ten consecutive case reports with 1- to 5-year data. *Int J Oral Maxillofac Implants.* 1997; 12: 319-324.

TEIXEIRA ER, SATO Y, AKAGAWA Y, KIMOTO T. Correlation between mucosal inflammation and marginal bone loss around hydroxyapatite-coated implants: A 3-year cross-sectional study. *Int J Oral Maxillofac Implants.* 1997; 12:74-81.

THOMAS KA, COOK SD, ANDERSON RC, HADDAD RJ, KAY JF, JARCHO M. Biological response to HA coated porous titanium hips. *12th Annual Meeting of the Society of Biomaterials.* May 29 - June 1, 1986 a; Minneapolis, MN:15.

THOMAS KA, COOK SD, KAY JF, JARCHO M, ANDERSON RC, HARDING AF, REYNOLDS MC. Attachment strength and histology of HA coated implants. In: Saha S, ed. *Biomedical Engineering V. Recent Developments. Proceedings of the Fifth Southern Biomedical Engineering Conference.* New York, NY: Pergamon Press. 1986 b; 205-211.

THOMAS KA, KAY JF, COOK SD, JARCHO M. The Effect of Surface Macrotexture and Hydroxylapatite Coating on the Mechanical Strengths and Histologic Profiles of Titanium Implant Materials. *J Biomed Mater Res.* 1987; 21:1395-1414.

THOMAS KA, COOK SD, HADDAD RJ, KAY JF, JARCHO M. Biologic response to HA-coated titanium hips. A preliminary study in dogs. *J of Arthroplasty.* March 1989; 4(1):43-53

VAILLANCOURT H. Finite Element Analysis of Bone Remodeling Around Porous-surfaced Dental Implants. Ph.D. thesis 1994, University of Toronto.

VAN BLITTERSWIJK CA, GROTE JJ, KUIJPERS W, BLOK-VAN HOEK CJG, DAEMS WTH. Bioreactions at the tissue/hydroxyapatite interface. *Biomaterials.* 1985; 6:243-251.

VAN BLITTERSWIJK CA, GROTE JJ, KOERTEN HK, KUIJPERS W. Biological performance of ß-whitlockite. A study in the non-infected and infected rat middle ear. *J Biomed Mater Res.* 1986; 20:1197-1217.

VAN BLITTERSWIJK CA, HESSELING SC, GROTE JJ, KOERTEN HK, DE GROOT K. The biocompatibility of hydroxyapatite ceramic: A study of retrieved human middle ear implants. *J Biomed Mater Res.* 1990 a; 24:433-443.

VAN STEENBERGHE D, LEKHOLM U, BOENDER C, FOLMER T, HENRY P, HERRMANN I. The applicability of osseointegrated oral implants in the rehabilitation of partial edentulism: A prospective multicenter study on 558 fixtures. *Int J Oral Maxillofac Implants.* 1990 b;5:272-281.

WHEELER SL. Eight-year clinical retrospective study of titanium plasma-sprayed and hydroxyapatite-coated cylinder implants. *Int J Oral Maxillofac Implants.* 1996; 11:340-350.

WHITEHEAD RY, LACEFIELD WR, LUCAS LC, LEMONS JE. Structural and bond strength evaluations of plasma sprayed HA coatings, *Proc. 4th World Biomat Congress*, Berlin, 1992; 503.

WILLIAMS DF, BLACK J, DOHERTY PJ. Second consensus conference on definitions in biomaterials. In: *Biomaterial-Tissue Interfaces, Advances in Biomaterials 10.* Doherty PJ, Williams RL, Williams DF and Lee AJC (Eds). Elsevier Science Publishers, Amsterdam. 1992; 525-533.

WISBEY A, GREGSON PJ, TUKE M. Application of PVD TiN coating to Co-Cr-Mo based surgical implants, *Biomaterials.* 1987; 8:477-480.

WOOD RM, MOORE DL. Grafting of the maxillary sinus with introrally harvested autogenous bone prior to implant placement. *Int J Oral Maxillofac Implants.* 1988; 3:209.

YI G, SAYER M. Sol-gel processing of complex oxide films. *Am Ceram Soc Bull.* 1991; 70(7):1173-1179.

IMAGE EVALUATION TEST TARGET (QA-3)

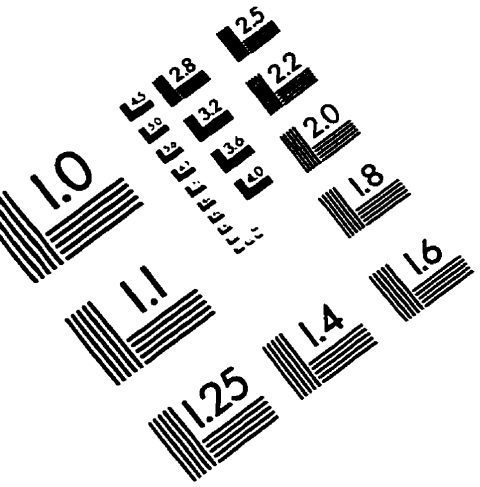

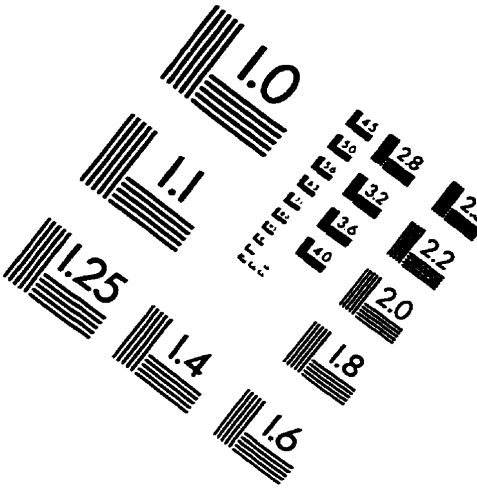

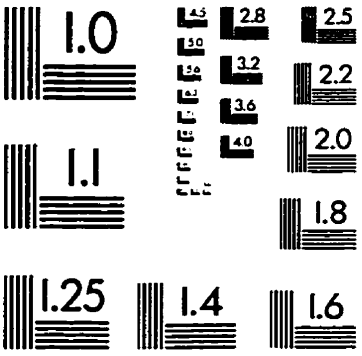

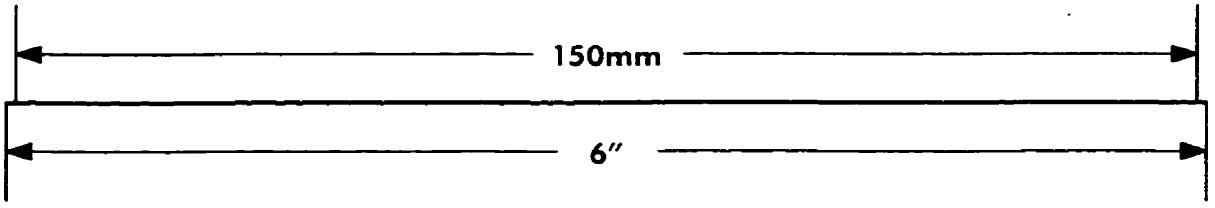

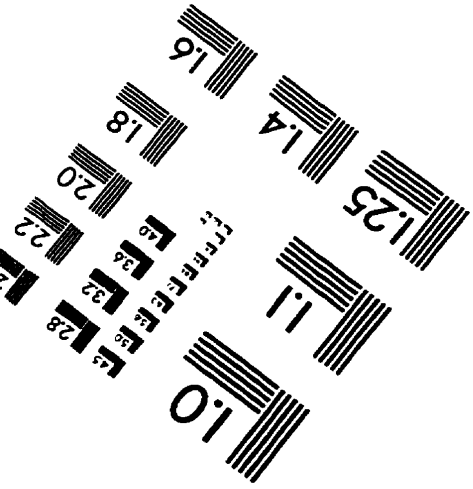

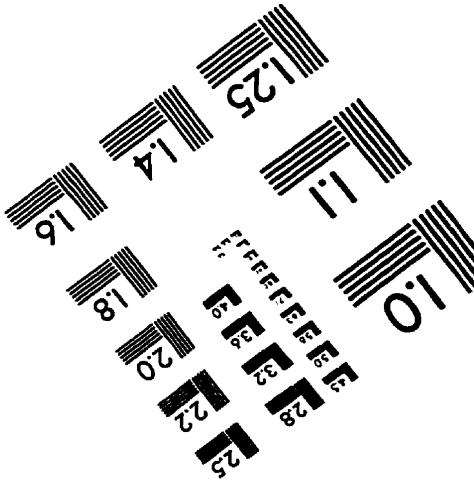

APPLIED IMAGE, Inc
1653 East Main Street
Rochester, NY 14609 USA
Phone: 716/482-0300
Fax: 716/288-5989